Bacterial Toxicity of Oxide Nanoparticles and Their Effects on Bacterial Surface Biomolecules

BACTERIAL TOXICITY OF OXIDE NANOPARTICLES AND THEIR EFFECTS ON BACTERIAL SURFACE BIOMOLECULES

A Dissertation Presented

by

WEI JIANG

Submitted to the Graduate School of the
University of Massachusetts Amherst in partial fulfillment
of the requirements for the degree of

DOCTOR OF PHILOSOPHY

May 2011

Department of Plant, Soil, and Insect Sciences

BACTERIAL TOXICITY OF OXIDE NANOPARTICLES AND THEIR EFFECTS ON BACTERIAL SURFACE BIOMOLECULES

A Dissertation Presented

by

WEI JIANG

Approved as to style and content by:

_____
Baoshan Xing, Chair

_____
Stephen Simkins, Member

_____
Richard W Vachet, Member

_____
Stephen Rich, Department Head
Department of Plant, Soil, and Insect Sciences

ACKNOWLEDGEMENTS

I am exceedingly grateful for the leadership and direction of Dr. Baoshan Xing throughout my graduate program. His wisdom, vision, and experience greatly benefit me in my study. His guidance and support for the past six years have been invaluable, and he deserves much of the credit for my growth as a scientist and as an individual. I highly appreciate his never-ending kindness and encouragement, and I am fortunate to have worked with him.

I thank Dr. Stephen Simkins and Dr. Richard Vachet for serving on my doctoral committee. They are sincerely acknowledged for giving me constructive suggestions and always being supportive, have improved the quality and richness of my graduate experience.

I would like to thank all members in Dr. Xing's research group and my friends in the Department of Plant, Soil, and Insect Sciences for their friendship and valuable help: Hamid Mashayekhi, Saikat Ghosh, Lei Song, Kun Yang, Xilong Wang, Seunghun Kang, Yingchen Bai, Jian Zhao and many others. They have been very important to my life during my study.

Many friends have helped make my time in graduate school a distinct pleasure. In particular, thanks to Sally, Ruiwen, Luwei, Haoheng for being generally awesome, and for bringing out the best in me.

My special thanks go to my parents for their love, support, and endless encouragement. This work would not have been possible without them.

ABSTRACT

BACTERIAL TOXICITY OF OXIDE NANOPARTICLES AND THEIR EFFECTS ON BACTERIAL SURFACE BIOMOLECULES

MAY 2011

WEI JIANG, B.S., NANJING UNIVERSITY

M.S., RESEARCH CENTER FOR ECO-ENVIRONMENTAL SCIENCES, CHINESE ACADEMY OF SCIENCES

Ph.D., UNIVERSITY OF MASSACHUSETTS, AMHERST

Directed by: Professor Baoshan Xing

Toxicity of nano-scaled Al_2O_3, SiO_2, TiO_2 and ZnO to bacteria (*Bacillus subtilis*, *Escherichia coli* and *Pseudomonas fluorescens*) was examined and compared to that of their respective bulk (micro-scaled) counterparts. All nanoparticles (NPs) but TiO_2 showed higher toxicity than their bulk counterparts. Toxicity of released metal ions was differentiated from that of the oxide particles. ZnO was the most toxic among the three NPs, causing 100% mortality to the three tested bacteria. TEM images showed attachment of NPs to the bacteria, suggesting that the toxicity was affected by bacterial attachment.

The effects of oxide NPs on bacteria cells and bacterial surface biomolecules were studied by FTIR spectroscopy to provide a better understanding of their cytotoxicity. Lipopolysaccharide (LPS) and lipoteichoic acid could bind to oxide NPs through hydrogen bonding and ligand exchange, but the cytotoxicity of NPs seemed largely related to the function-involved or structural changes to proteins and phospholipids. The

three NPs decreased the intensity ratio of β-sheets/α-helices, indicating protein structure change, which may affect cell physiological activities. The phosphodiester bond of L-α-Phosphatidyl-ethanolamine (PE) was broken by ZnO NPs, forming phosphate monoesters and resulting in the highly disordered alkyl chain. Such damage to phospholipid molecular structure may lead to membrane rupture and cell leaking, which is consistent with the fact that ZnO is the most toxic of the three NPs.

LPS and PE are amphiphilic biomolecules that are major constituents of the outer membrane of Gram-negative bacteria. Their micelles and vesicles were studied as model cell membranes to evaluate NP effects on membrane construction. The adsorption of polysaccharides on Al_2O_3 and TiO_2 NPs dispersed LPS vesicles and micelles. LPS coated Al_2O_3 NPs, while it caused the aggregation of TiO_2 NPs according to atom force microscopy images. Desorption from the two NPs was slow due to the firm hydrogen bonding. For PE, Al_2O_3 NPs induced large multilamillar vesicles, while ZnO NP converted vesicles to tiny aggregates due to molecular structure breakup. PE stability in solution was disturbed by adding NPs, but its stability was enhanced by increasing pH. The electrostatic force was the determining factor for the vesicle stability.

TABLE OF CONTENTS

Page

LIST OF TABLES

LIST OF FIGURES

CHAPTER 1

GENERAL INTRODUCTION

1.1 Engineered Nanoparticles and Their Environmental Hazard

Engineered nanoparticles (NPs) are materials with at least one dimension of 100 nanometers or less. Engineered NPs mainly include metal NPs, oxide NPs, fullerene and carbon nanotubes. Nanotechnology is one of the fast growing sections of the high tech economy with more than 1000 products using NPs reported to date (www.nanotechproject.org). It is estimated that the annual value of nanotechnology-related products will be $1 trillion by 2011-2015 (Bainbridge and Mihail, 2001). Products using NPs can be found in different industrial, medical, personal and military applications.

The size of NPs, which are in the range of internal cell organelles, not only may enable their use in manipulating or sensing biological systems (Jaiswal and Simon, 2004), but have also raised concerns about their possible harmful interactions in the environment (Nel et al., 2006; Thill et al., 2006). Size is the main characteristic of NPs. As the size of a particle decreases, its surface area to volume ratio increases, allowing a greater proportion of its atoms or molecules to be displayed on the surface rather than the interior of the material. The increase in the percentage of atoms on the surface determines the potential reactive groups on the particles' surface (Nel et al, 2006). This can modify the physicochemical properties of the material and may increase the uptake and interaction with biological tissues, which could generate adverse biological effects in living cells that would not otherwise be possible with the same material in larger form. A review article by Nel et al. (2006) summarized the particles' surface properties and the possible

mechanisms by which NPs interact with biological tissues to produce reactive oxygen species (Fig. 1.1). The reactive oxygen species could be produced by UV activation, electron generation from structural defects, and by redox, catalytic and Fenton chemistry. The surface properties affecting interaction with biological tissues include surface dissolution, surface coating, catalytical activity or passivity, and hydrophobicity or hydrophilicity. In summary, the small particle size, large surface area of NPs and their ability to produce reactive oxygen species are considered to be related to their toxicity (Nowack and Bucheli, 2007).

The unique properties of NPs, such as high specific surface area, abundant surface reactive sites, charge, shape, and mobility, could potentially lead to unexpected health or environmental hazards. NP toxicities have been reported for mammalian cell lines (Hussain et al., 2005; Brunner et al. 2006), plants (Lin and Xing 2007, 2008), crustaceans (Roberts et al., 2007; Lovern et al., 2007; Baun et al., 2008; Zhu et al., 2009b), fish (Oberdorster 2004; Smith et al., 2007; Griffitt et al., 2007) and mice (Wang et al., 2007; Zhu et al., 2009a). They also present potential risks to human health because they have been shown to be toxic to human lung cells (Worle-Knirsch et al. 2007) and red blood cells (Rothen-Rutishauser et al. 2006). Human exposure is far from impossible because so many customer products have utilized NPs. Moreover, after NPs find their way into the environment, they may end up in the ecosystem food web through direct uptake of water or food, potentially leading to human exposure through food, drinking water, and/or recreational activities.

NP release into the environment is inevitable because of their increasing production and application. Many new types of nanomaterials have been released in great

amounts (Nowack and Bucheli, 2007), while their potential toxicity and harm to the organisms and ecosystems remains unknown. Both scientists and the public need a better understanding of behavior and effects of this new material group in the ecosystem. It is important to consider environmental, health and safety aspects at an early stage of nanomaterial development and use, in order to more effectively identify and manage potential human and environmental health impacts from nanomaterial exposure (Baun et al., 2008).

1.2 Oxide Nanoparticles and Their Toxicity to Organisms

Oxide NPs are the most widely produced and used nanomaterials. Aluminum oxide (Al_2O_3), silicon dioxide (SiO_2), titanium dioxide (TiO_2), and zinc oxide (ZnO) are among the most frequently used industrial additives with various applications. Aluminum oxide, since it has good dielectric and abrasive properties, is widely used as an abrasive agent or insulator. TiO_2 is an opacifier which has been used in paints, papers, toothpastes, plastics, sunscreen, and many cosmetic products. SiO_2 in crystalline form is widely used in electronics as a semiconductor. ZnO, which has ceramic properties, has applications in semiconductors and pigments (Adams et al. 2006), beauty products and textiles. Nano oxides have greater surface area and reactivity than their bulk counterparts, hence providing superior performance, but they may also bring higher environmental and health risks.

A new question for oxide NPs toxicity is whether the toxicity is size-related or component-related. Some researchers think the oxide NPs toxicity is from dissolved metal ions (Brunner et al., 2006). To figure out this problem, some researchers evaluated

the amount/toxicity of released metal ions. Zhu et al. (2009a) suggested that the Fe_2O_3 NPs, not Fe^{3+} caused toxicity to rats by studying the dissolution of Fe_2O_3, and systemic distribution of Fe^{3+} in rat body. Other researchers compared the NPs toxicities to their bulk particles (BPs) counterparts. In a study on toxicity of nano-sized and bulk ZnO, CuO and TiO_2 to bacteria and crustaceans, Heinlaan et al. (2008) reported nano-CuO showed more toxicity than bulk-CuO to the tested organisms. However, Adams et al. (2006) reported that there was no difference between TiO_2, SiO_2, ZnO NP and BP toxicity to bacteria because they formed similar size aggregates. Franklin et al. (2007) also reported similar toxicity between ZnO NPs and BPs to freshwater microalgae. Therefore, whether NP toxicity is caused by size or by composition should be further evaluated and probably should be examined case by case.

1.3 Potential Impact to Ecosystem and Human Health When Bacteria Are Exposed to NPs

Bacteria are prokaryotic cells, typically 0.5 to 5 μm in length. As an important component of the environmental system, they are found everywhere in water, soil and air, playing many critical roles required for normal ecosystem function and productivity. The most important job of bacteria is decomposition. By decomposing dead organic matter, the bacteria recycle carbon atoms and mineral nutrients (e.g., N, P) stored in organic matter to inorganic forms for primary producers to use. Without bacteria, primary productivity on the globe would stop. In addition, some bacterial species can generate oxygen into the atmosphere, or fix nitrogen from the atmosphere into a usable form, both of which are important chemical cycles in the environment.

NPs can kill bacteria according to the existing literature. Carbon-based NPs (Lyon et al, 2006; Kang et al. 2009), oxide NPs (Adams et al. 2006; Brayner et al, 2006; Thill et al., 2006; Huang et al. 2008) and metal NPs (Choi and Hu, 2008) are all reported to have microbial cytotoxicity. The unusual death of bacteria caused by NPs may affect the normal biological, chemical and nutrient cycles in the ecosystem, and may cause further detrimental impacts on other organisms.

Another problem is that when bacteria are exposed to NPs, NPs may enter the food web through bacteria. Bacteria are essential links in both the aquatic and soil food webs. In the aquatic food web, bacteria are the main food of protozoa, which will be fed on by fish. In the soil food web, bacteria are food of protozoa, nematodes, arthropods, which will feed birds and animals. Thus, the uptake and adhesion of NPs to bacteria will place NPs in food webs, potentially affecting human food safety.

Although we already know about the antibacterial activity of NPs, it is still not very clear how NPs approach bacteria in media and how they cause bacterial toxicity. This study will provide better understanding on interactions between bacteria and NPs and useful information about the impact of engineered NPs once released into environmental systems.

1.4 Components and Structure of Bacteria Cell Envelope

The bacteria cell wall provides structural integrity to the cell and contributes 60-70% of the total bacterial weight in a hydrated state. Bacterial cell walls differ from other organisms by the presence of peptidoglycan, which is located immediately outside of the cytoplasmic membrane and is responsible for the rigidity of the bacterial cell wall and

determines the cell's shape (Singleton, 1997). It is relatively porous and can be penetrated by particles of approximately 2 nm. While all bacterial cell walls contain peptidoglycan, Gram-positive and Gram-negative have different overall cell wall structures. The Gram-positive cell wall is characterized by the presence of a very thick peptidoglycan layer. Embedded in the thick peptidoglycan layer are polyalcohols called teichoic acid, some of which are lipid-linked to form lipoteichoic acid. A Gram-negative cell wall contains a thin peptidoglycan layer adjacent to the cytoplasm membrane. In addition to the peptidoglycan layer, the Gram-negative cell wall also contains an additional outer membrane composed of phospholipids and lipopolysaccharides which face into the external environment (Figure 1.2).

Peptidoglycans are polymers consisting of sugars and amino acids that form a mesh-like layer outside the plasma membrane of bacteria, forming the cell wall. The sugar component consists of alternating residues of β-(1,4) linked *N*-acetylglucosamine and *N*-acetylmuramic acid residues. Attached to the *N*-acetylmuramic acid is a peptide chain of three to five amino acids. The peptide chain can be cross-linked to the peptide chain of another strand forming the 20-80 nm thick 3D mesh-like layer completely surrounding the cell (Ghuysen and Hakenbeck, 1994). The thick layer of peptidoglycan provides both a physical barrier for protection from the environment and a scaffold for the attachment of secondary cell wall polymers (including teichoic and teichuronic acids) and surface proteins (Scott and Barnett, 2006).

Teichoic acids (TAs) may be either covalently bonded to the *N*-acetylmuramic acid of the peptidoglycan layer, or linked to a glycolipid associated with the cell membrane (lipoteichoic acids, LTAs) (Araki and Ito, 1989). Because LTAs are

covalently linked to lipids within the cytoplasmic membrane, they are responsible for connecting the peptidoglycan to the cytoplasmic membrane. TAs give the Gram-positive cell wall an overall negative charge due to the presence of phosphodiester bonds between TA monomers. The functions of TAs include cation homeostasis, trafficking of various ions and nutrients, and the display of surface proteins (Scott and Barnett, 2006).

Lipopolysaccharides (LPS) are a major component of the outer membrane of Gram-negative bacteria, contributing greatly to the structural integrity of the bacteria and protecting the membrane from certain kinds of chemical attack. LPS molecules are composed of repeating monosaccharides joined by glycosidic linkages, attached to the cell surface via covalent bonds to lipid components, named lipid A (Roberts, 1996). The polysaccharide core is bound to lipid A through a specific sugar called 2-keto-3-deoxyoctulosonic acid (KDO) (Rietschel E.T., 1982). LPS molecules increase the negative charge of the cell membrane and helps stabilize the overall membrane structure. LPS molecules are of crucial importance to Gram-negative bacterial cells.

Phospholipids are a class of lipids and are a major component of all cell membranes. PLs have three essential parts: a three-carbon backbone of glycerol, two long-chain fatty acid esterified to carbons 1 and 2 of the glycerol, and phosphoric acid esterified to carbon 3 (Pollard and Earnshaw, 2004). The hydrophobic fatty acid chains line up and the hydrophilic head groups are exposed to water to form the lamellar bilayer, establishing a permeability barrier and providing a matrix with which membrane proteins are associated (D. E. Vance and J. Vance, 1991).

The Protein composition of the outer membrane of gram-negative bacteria is relatively simple. The outer membrane of gram-negative bacteria contains porins,

murein-lipoprotein, OmpA, and minor proteins. OmpA and lipoprotein have no pore functions. The minor proteins have important roles, in the uptake of iron and vitamins. Porin proteins are very important for Gram-negative bacteria because all hydrophilic nutrients passing through the outer membrane go through them (Benz, 1988).

The Periplasmic space or periplasm is a space between the inner cytoplasmic membrane and outer membrane of Gram-negative bacteria. Such additional cellular compartment occupies between 5 and 20% of the total cell volume. It plays important roles in the physiology of Gram-negative bacteria. The periplasmic space is almost isoosmotic with the cytoplasm; thus osmotic pressure is maintained across the outer membrane and not across the inner membrane (Ghuysen and Hakenbeck, 1994). The periplasmic space is strongly anionic compared to the external medium because of anionic groups attached to the outer membrane and because of anionic membrane-derived oligosaccharides present in the periplasmic space that maintain part of the osmolarity (Benz, 1988). The periplasm provides an oxidizing environment, which is required for proper protein folding (Scott and Barnett, 2006).

1.5 Bacterial Adhesion to Particles

In nature bacteria usually attach on a mineral surface and form biofilms, a process is critical to the survival and transport of bacteria cells. The adherence of bacteria cells to a large flat mineral surfaces in nature, or the attraction of tiny NPs to bacteria under lab conditions, are both interactions between the biological surface of bacteria and a solid surface. These interactions can be controlled by long-range electrostatic forces and short-range interactions, including chemical bonding, van der Waals forces and hydrophobic

effects (Parikh and Chorover, 2006), and are also influenced by steric effects (Neu and Marshall, 1990). Previous studies have indicated that bacterial adhesion may be dominated by bacterial surface biopolymers (Jucker et al., 1998; Omoike and Chorover, 2004). These biopolymers are involved in nearly every type of interaction through their highly-charged structure, functional groups, and bridging effect to the surface.

The shape and size of particles also play a role in bacterial adhesion. The adsorption of microorganisms onto surfaces can happen in three ways: (1) a number of microbial cells can become attached to a single larger surface; (2) adsorbent particles and microbial cells of equal size can mutually interact; or (3) several adsorbent particles of dimensions smaller than the microbial cells can adhere to a single cell. The mechanism of sorption, rates of transport, and equilibrium capacities can differ in all three cases (Bitton and Marshall, 1980). Therefore, bacteria can grow very well on the flat surface of some minerals, while nano-sized particles of the same mineral may have totally different effects on the same bacteria.

1.5.1 Lipopolysacchrides (LPS) and Teichoic Acid (TA) Adsorption on Oxides

LTA and LPS exist on Gram-positive cell walls and Gram-negative cell walls, respectively, but they have similar properties. They both cause the bacterial cell to be overall negatively charged due to the phosphoesters in their structure. They are both amphiphilic biopolymers with the hydrophobic side embedding in the membrane and the hydrophilic side extending from the intact cell into aqueous solution. When bacteria approach a surface, or small particles are attracted to bacteria, LTA or LPS are most likely the first in contact with the surface/particle.

LPS molecules cover approximately 45% of the surface of Gram-negative bacteria. LPS molecules are amphiphilic with a hydrophobic lipid A region anchored in the outer membrane and a hydrophilic O-antigen extending into aqueous solution. Between the lipid A region and O-antigen chain is the core oligosaccharide part, which often carries phosphate and carboxylic acid groups. LPS molecules play complex roles in bacteria adhesion to surfaces. They may promote bacterial adhesion by sorption of either free LPS molecules to surfaces during conditional film formation or through cell adhesion mediated by membrane-bound LPS (Parikh and Chorover, 2008). The O-antigen part is most likely responsible for the polymer interactions with surfaces for Gram-negative bacteria. LPS can bond to GeO_2, α-Fe_2O_3 and α-Al_2O_3 surfaces via O-antigen function groups (Parikh and Chorover, 2008). Cells with primarily long O-antigen preferentially adhere to hydrophilic surfaces, whereas cells with shorter O-antigen have a higher affinity for hydrophobic surfaces (Makin and Beveridge, 1996). During cell adhesion to negatively charged surfaces, the O-antigen may extend beyond the electrostatic energy barrier and become adsorbed in a secondary minimum in close proximity to the surface (Jucker et al., 1997). The bridging between cells and surface leads to irreversible adhesion due to strong short-range interactions, such as hydrogen bonds, which were detected when LPS absorbed on TiO_2, Al_2O_3 and SiO_2 particles (Jucker et al., 1997). However, LPS molecules also cause repulsion of bacteria from a surface due to the resistance of the polymer layer against compression. The polymer layer hinders the cells from reaching the energy minimum (Jucker et al., 1998), which is the requirement for DLVO (Derjaguin, Landau, Verwey and Overbeek) interaction theory. It seems at first LPS could anchor cells to the surface, but the rigidity of the long chain maintains a

distance between the cell surface and solid surface and prevents the outer membrane from really making contact with the solid surface.

Lipoteichoic acid (LTA) is a primary adhesion molecule for Gram-positive bacteria. LTA is a long chain of phosphodiesters (anionic) with glucosamine (neutral) and D-alanine branches (cationic). Charge neutralization is incomplete, allowing LTA to form ionic bonds with surrounding fluids, dissolved ions and the substrate. In the studies of LTA adhesion on TiO_2 by ^{31}P solid-state NMR spectroscopy, it was suggested that the alanine and glucosamine groups interact with the surface (Wickham and Rice, 2008). The glucosamine side chain can participate in hydrogen binding, while the alanine side chain can have ionic bonds (Rice and Wickham, 2004). The D-alanine groups carry a positive charge (NH_3^+) to be attracted to the negatively charged TiO_2 surface. D-alanine deficient LTA bacterial mutants lose their ability to adhere to polystyrene, glass, and metal oxide surfaces, which is evidence of the vital role of D-alanine in LTA mediated bacterial adhesion (Abachin et al., 2002; Neuhaus and Baddiley, 2003). On the TiO_2 surface LTA has two separate chemical environments, suggesting that roughly half of the LTA backbone is in close proximity to the TiO_2 surface (Wickham and Rice, 2008). In another study through high-resolution magic-angle-spinning nuclear magnetic resonance (HRMAS-NMR) spectroscopy, the chemical environment was also altered by LTA-surface interactions when LTA adhered to silica and hydroxyapatite (Cravatt, 2005). In FTIR studies, P-O-Fe bonding peaks were detected when Gram-positive *Bacillus subtilis* or its extracellular polymeric substance adsorbed on α-Fe_2O_3 and α-FeOOH. This suggested that the phosphodiester forms an innersphere complex with the iron (hydr)oxides (Omoike and Chorover, 2004; Parikh and Chorover, 2006).

1.5.2 Protein Interaction with Solid Surface

It is hard to summarize the role of proteins in bacterial adhesion because there are different types of proteins on the outer membrane and cell surface. For the study of bacterial adhesion to particles, we mainly consider the roles of extracellular proteins and outer membrane proteins. Extracellular proteins are secreted by bacteria, released into the medium around cells, and remain in close proximity to the cell surface (Glenn, 1976). They are not included in the composition of cell wall structures. Extracellular proteins can increase bacterial adhesion to solid surfaces (Gomez-Suarez et al., 2002). Outer membrane proteins are found in the outer cell membrane and are involved in specialized functions. Jucker et al. (1997) suggested the outer membrane proteins are unlikely to interact with the solid surface since they are hidden behind the O-antigen layer of the LPS. The rigidity of LPS would prevent the solid surface from approaching the membrane protein. However, when the outer membrane protein exposure was increased by removing of LPS from *T. ferrooxidans*, cell adhesion to a hydrophobic sulfuric surface was higher due to an increased cell hydrophobicity (Arredondo et al., 1994). This suggests that the outer membrane proteins are also good adhesins when they are exposed to the extracellular environment. When we change the bulk material to nano-sized particles, the chance of outer membrane protein exposure to particles could be increased. The protection due to LPS may be ineffective because the small size of NPs may enable them to enter the gaps between the long biopolymer chains. In those conditions, the outer membrane protein may be damaged by contact with NPs and the physiological activities of the cell may be affected as well.

Adsorption-induced protein structure changes have been reported in some previous studies. Buijs et al. (1996) observed that the amount of β-sheet decreased when the β-sheet dominated protein immunoglobulin G adsorbed on silica or methylated silica surfaces. The reduction in the β-sheet content was larger on hydrophobic methylated surfaces than on the hydrophilic silica surfaces. Loss of the α-helical structure was reported when the protein lysozyme adsorbed on silica NPs (Vertegel et al., 2004). In another study utilizing Raman spectroscopy, an increased content of β-sheet and a decreased content of α-helical structure were found after fibrinogen adsorbed on TiO_2 NPs. Likewise, an increase of β-sheet structure and a decrease in random coil structure were found after fibronectin adsorbed on TiO_2 NPs (Strehle et al., 2004). According to these studies, the structure of outer membrane protein may also be rearranged when these proteins adhere to NPs, however, the structural changes vary for different proteins and different particles.

In the adsorption process, the secondary structure of the protein also plays a crucial role. In an α-helical structure, less than 25% of the side-chains are in the same plane, and they are orientated in the same direction. For a β-sheet structure, 50% of the side-chains point into the same direction and are therefore available for the adsorption process (Creighton, 1993). Hence, for an adsorption process, it would be preferable if the protein exhibits a β-sheet rather than an α-helix structure (Strehle et al., 2004).

1.5.3 Phospholipid (PL) Interaction with Solid Surfaces

Phospholipids consist of a long hydrophobic hydrocarbon chain attached to a hydrophilic polar head group. The polar head group contains a phosphodiester moiety

and, often, a secondary or quaternary amine moiety. The phospholipid can form bilayer vesicles in solution. Bacteria cell membranes are made of the PL bilayers as well. Adsorption to oxides can cause the rupture of the PL membrane. A popular theory for the membranolytic action of certain oxides is that the surface interacts with portions of membrane proteins or with the phosphate or amine moeities of the PLs' polar head group (Sahai, 2002). The interactions supposedly result in conformational changes to the PL bilayer, ultimately leading to disruption of the membrane. Although there are many applications of coating oxide surfaces through PL vesicle fusion and deposition on the surface, forming supported lipid bilayer membranes, the mechanism of how the PL is adsorbed on the oxides remains unclear.

The first question is about the interaction between oxide and PL. Oxide–PL interactions fundamentally depend on electrostatic (including charge and dipole), polarization, and H-bonding forces (Israelachvili, 1992). Electrostatic attraction may occur first. In some studies on dipalmitoylphosphatidylcholine (DPPC) adsorption on quartz, rutile and corundum, there was a greater adsorption to the positively charged surface, suggesting the phosphate ester (—R—PO_4^-—R'—) moiety of the headgroup to dominate the electrostatic interaction between the phospholipid and the charged surface site (Oleson and Sahai, 2008; Xu et al., 2009). The electrostatic interactions between oxide surface and the positively charged alkylammonium moiety (—R—$N(CH_3)_3^+$) in the DPPC headgroup could be negligible because of the lower positive charge density associated with the relatively bulky choline group compared to the negative charge density associated with the smaller phosphoester moiety (Oleson and Sahai, 2008; Xu et al., 2009). But, unlike to the principal animal phospholipid DPPC which contains the

bulky (—R—$N(CH_3)_3^+$), the principal bacterial PL phosphatidylethanolamine (PE) contains the much smaller (—R—NH_3^+) moiety in its headgroup. The positive charge density is also high, and the moiety dominating the electrostatic interaction needs to be rejudged. Electrostatic attraction alone cannot explain the adsorption to the neutral or negatively charged surfaces. Under such condition van der Waals force (Reimhult et al., 2002; Oleson and Sahai, 2008) or H-bonding (Yuan et al., 1995; Rapuano and Carmona-Ribeiro, 1997) were suggested to be the responsible forces. The theory is that the primary amine (—NH_3^+) group or the PO_4^- moiety can H-bond to the neutral sites on oxide surfaces such as SiOH, AlOH, FeOH, TiOH, while quaternary ammonium (—R—$N(CH_3)_3^+$) cannot H-bond. Other researchers do not agree that H-bonding is one of the interactions. They found that there was an interfacial water layer of 0.4-1.5 nm thickness between solid substrates and PL bilayers (Kim et al., 2001; Mornet et al., 2005). The thickness of the intermediate water layer precluded the covalent bond or H-bond formation between PL headgroups and oxide surface sites, which would require closer proximity of the two (Oleson and Sahai, 2008).

The second question is about the rupture of cell membrane. The PL bilayer vesicle could be a simple model for a cell membrane (Figure 1.3). The overall adsorption, fusion, and rupture of vesicles on an oxide surface depend on PL-oxide adhesion energy, vesicle bending energy, and water-oxide adhesion energy (Seifert and Lipowsky, 1990; Zhdanov and Kasemo, 2001). The driving force for the rupture of adsorbed vesicles is the PL-oxide interaction, which causes adhesion-induced stretching to the membrane. When the adhesion energy can no longer be balanced by the elastic energy (PL-PL interaction), the membrane ruptures (Seifert, 1997). Therefore, the stronger the PL-oxide interaction, the

more the vesicles are deformed, and the more possible the PL membrane is ruptured by the adhesion. For example, deformation is larger for adhesion on SiO_2 than on TiO_2 for a given vesicle size, indicating a stronger vesicle-surface interaction on SiO_2 (Reimhult et al., 2002; 2003). Larger vesicles are more deformed by the surface interaction than smaller ones on same surfaces (Reimhult et al., 2003). Another interesting study on cell adhesion onto highly curved surfaces discussed the effect of an oxide surface curvature on cell membrane rupture (Kaufmann and Tanaka, 2003). They observed cell membrane ruptured after cells adhering to 3 μm spherical silica beads, while there was no adhesion or rupture of cells on the planar silica surface. The explanation was that the adhesion energy between cells and silica beads was larger than between cells and planar substrates, probably due to the larger local contact angle near the three-phase contact. Such results suggest that nano-sized oxide particles in our proposed study may be more dangerous to cell phospholipid membranes due to the increased chance of rupture. PL vesicle rupture was reported on the silica NPs, forming lipid bilayer coated on NPs (Mornet et al., 2005). However, a complete understanding of membrane rupture is still not available.

1.6 Imaging Techniques Used to Probe the Nano-Bio Interface

Imaging with scanning electron microscopy (SEM), transmission electron microscopy (TEM) and fluorescence microscopy has aided our understanding of cellular uptake, attachment and processing of NPs. Standard SEM and TEM are not good at imaging soft materials (such as dendrimers and liposomes), and a drying process is required for sample preparation. Cryo-TEM makes it possible to look at the specimen in a

fully hydrated state, and has been used for imaging of supported lipid bilayer (Mornet et al., 2005) and NP transmigration into liposomes (Bihan et al., 2009).

Fluorescently labeled NPs and corresponding techniques have several potential problems: label instability, altered physicochemical properties and photo bleaching from laser exposure (Nel et al., 2009). Live cell confocal microscopy has been developed to visualize NP at nanometer resolution in real time within cells without structural damage, which is ideal for imaging NP movement through intracellular environments, including vesicle tracking, particle transport and membrane mechanisms (Stephens and Allan, 2003). Another way is to label phospholipid membrane using fluorescent lipid or fluorescent dyes to record the NP-induced membrane deformation, rupture, reconstruction, gelation and fluidization (Wang et al., 2008; Laurencin et al., 2010).

Atomic force microscopy (AFM) is a very high-resolution type of scanning probe microscopy with demonstrated resolution on the order of fractions of a nanometer and has developed into a powerful tool in structural biology. The AFM tips can scan the bio-structure in liquids. Individual proteins and cell membrane structures can be studied in situ (Scheuring et al., 2005), making this technique another good way to reveal the influences of NPs on cell membrane.

Surface-enhanced Raman scattering (SERS) measures the enhanced Raman scattering of molecules adsorbed on metal surfaces (which may be nanotextured), being used increasingly for bioimaging of cells and intact animals (Qian et al., 2008). This technique is sensitive enough to detect single molecules and has been successfully used in tumor imaging through single wall carbon nanotubes (Keren et al., 2008).

1.7 FTIR in the Study of Bacterial Surface Biomolecules

Very little molecular-level information is available for the initial adhesion of bacteria to solid surfaces, because this interface is very challenging to study with most analytical techniques. FTIR spectroscopy provides molecular-scale information for both organic and inorganic constituents involved in bacterial adhesion. Furthermore, infrared spectroscopy allows studies in a variety of environments, including optically turbid media, rendering this technique uniquely well suited to probe the bacteria-oxide interface.

1.7.1 ATR-FTIR Spectroscopy and its Advantage on Studying Bacterial Cell Envelope Structure Damage

Attenuated total reflection (ATR) offers a further possibility to directly investigate the chemical composition of smooth surfaces of various materials (Harrick, 1967). ATR spectra can be obtained with practically no sample preparation, which offers the significant advantage that the sample can be investigated in a relatively undisturbed state (Schmitt and Flemming, 1998). Such an advantage is important in our proposed study on NPs toxicology to bacteria, because we seek to know the damage caused by NPs. We will not want the results confused with cell damage from the sample preparation process.

For ATR-FTIR technique, penetration depth of the evanescent wave into the sample (d_p) is given by

$$d_p = \frac{\lambda}{2\pi(n_c^2 \sin^2\theta - n_s^2)^{1/2}}$$

where θ is the angle of incidence, λ is the wavelength of the infrared radiation, and n_s and n_c are refractive indices of sample and ATR crystal. An increasing incident angle and a high refractive index of the internal reflection element (IRE) will decrease the depth of penetration. For bacteria cells, $n_s \approx 1.39$, while n_c value is 2.4 for diamond/ZnSe ATR

crystal, which is the IRE crystal in our instrument. Therefore the penetration depth of incidence beam at 45º is 2040 nm at 1000 cm^{-1}, and 908 nm at 1800cm^{-1}. Since this penetration depth is comparable to the size of bacterial cells, ATR-FTIR spectroscopy methods have been applied in different aspects of microbiology, including bacterial cell wall chemistry (Ojeda, et al., 2008), bacterial swarming (Gue et al., 2001), characterization of extracellular polymeric substances (Omoike and Chorover, 2004; Badireddy et al., 2008), elucidation of cell surface functional groups (Jiang et al., 2004), adhesion of bacteria to polymers (Branan and Wells, 2007) and minerals (Omoike et al., 2004; Parikh and Chorover, 2006).

However, for our proposed study of NPs adhesion on/damage to bacterial cell wall, the ATR-FTIR technique still has its own limits. The average thickness of the bacterial cell wall ranges from 20 to 50 nm (Berveridge, 1981). Based on the penetration depth calculation, the evanescent wave should also penetrate the interior of the bacteria cells, provided the cells are attached to the IRE crystal surface. The signal from the cytoplasm contents will mix with the signal from the cell wall/surface components, which may cause trouble in revealing NPs interactions on the bacterial cell wall surface. Therefore, the IR spectra for individual bacteria cell wall components should also be collected and compared to the spectra of whole cells.

We propose to apply the ATR-FTIR technique in this study with two intentions. The first is to reveal the NPs adhesion mechanism on the bacteria surface. Some studies have already successfully detected bond formation or other changes by ATR-FTIR spectroscopy between bacteria cell surface polymeric substances and mineral surfaces. An inner-sphere P-O-Fe bond was detected when bacteria adhered to hematite, which

showed an intense and sharp peak at 1016 cm^{-1} (Parikh and Chorover, 2006). In other research on LPS adhesion, ν (C-O, C-O-C) and ν_{as} (PO_4^-) absorbances decreased with increasing pH on hydrophilic surfaces (GeO_2, α-Fe_2O_3, α-Al_2O_3), showing charge properties are significant for LPS interactions with hydrophilic surfaces, while hydrophobic interactions dominate the LPS adsorption on hydrophobic surfaces (Parikh and Chorover, 2008). The H-bonding between oxides and LPS was reported by Jucker et al. (1997) when they studied the LPS adsorption on TiO_2, Al_2O_3 and SiO_2. The O-H stretching band (3600-3750 cm^{-1}) of the surface hydroxyl diminished with increasing adsorbed LPS concentration.

The second intention, to detect the cell wall structure change/damage after NPs exposure, may be more important in determining the NP toxicity mechanism. Bond breaking and structural damage in bacterial cell walls have been reflected on ATR-FTIR spectra during photocatalytic oxidation process by TiO_2 (Kiwi and Nadtochenko, 2005; Nadtochenko, et al., 2005). For the toxicology of oxide NPs, if bacterial cell walls are damaged by NPs, we may find a difference in the IR spectra. According to the literature, proteins are most susceptible to changes in IR spectra when exposed to oxides. The intensity ratio of amide Ⅱ (1540 cm^{-1})/amide Ⅰ (1650 cm^{-1}) was reported to be altered when MnO_X bound to *Pseudomonas putida* surface (Parikh and Chorover, 2005), and also when *bacillus subtilis* extracellular polymeric substances adsorbed on SiO_2 and goethite (Omoike and Chorover, 2004), reflecting an adsorption-induced variation in the secondary and tertiary structures of the protein. Amide Ⅰ band shifts were also reported when proteins interact with minerals (Omoike and Chorover, 2004). Since amide Ⅰ bands are most widely used in studies of protein secondary structure by IR spectroscopy

(Surewicz et al., 1993), we will discuss the application of the second derivative to the amide Ⅰ band to extract information of the secondary structure of proteins.

1.7.2 DRIFT-FTIR on NP Surface Analysis

Diffuse Reflectance Fourier Transform Infrared Spectroscopy (DRIFT-FTIR) is a technique that collects and analyzes scattered IR energy. When the IR beam enters the sample, it can either be reflected off the surface of a particle or be transmitted through a particle. The IR energy reflecting off the surface is typically lost. The IR beam that passes through a particle can either reflect off the next particle or be transmitted through the next particle. This transmission-reflectance event can occur many times in the sample. Finally, such scattered IR energy is collected by a spherical mirror that is focused onto the detector. The detected IR light is partially absorbed by particles of the sample, bringing the sample information.

The DRIFT mode offers some important advantages, such as the ability to assess both mineral and organic structures in particles, good sensitivity, and high throughput (Galle et al., 2004). So, it is a technique better adapted to the analysis of fine particles and powders, as well as rough surfaces (e.g., the interaction of a surfactant with the inner particle, the adsorption of molecules on the particle surface) and has been shown to be more sensitive to surface species than transmission measurements (Mitchell, 1993). This technique has been used as a powerful tool in the study of biofilm and pollutant binding on river sediment particles (Galle et al., 2004), dicarboxylic acid adsorption on clay minerals (Kang and Xing, 2007), and humic acid adsorption on goethite (Kang and Xing, 2008) and NPs oxides (Yang et al., 2009). Therefore, DRIFT-FTIR can be used to study

the biopolymers/biomolecules adsorption on NP surfaces when the sample can be ground to 5 microns or less.

1.8 Current Queries on NPs Bacterial Toxicity

Although many studies have reported the antibacterial activity of NPs, some queries on NPs bacteria toxicity are still not answered very well.

First, are the toxicities of NPs due to their size-related properties or just because of their composition? Such a query is mainly asked about the metal NPs and soluble oxide NPs. Some researchers have attributed the NPs' toxicity to the dissolved toxic ions (Brunner et al., 2006; Heilaan et al., 2008). However, limited studies have addressed the toxicity of metal ions in previous investigations.

A second question would be about the surface reactivity in relation to bacterial toxicity. The most popular mechanistic explanation is generation of ROS-causing membrane damage (Nel et al., 2006; Neal, 2008). However some studies have reported that TiO_2, SiO_2 and ZnO NPs still show antibacterial activity under dark conditions (Daoud et al., 2005; Adams et al., 2006), which may be attributed to as yet undetermined mechanisms. Some other researchers have hypothesized that free radicals may be produced from CdSe/ZnS quantum dots under dark conditions (Green and Howman, 2005). But, for the antibacterial activity of NPs, the possibility of ROS generation in the absence of photons has not been studied.

A third question would be about the damage to cell envelope structures in NP-cell surface interactions. Outer membrane disruption has been repeatedly observed (Pal et al., 2007; Lok et al., 2007) and is considered to be the reason for NPs' toxicity. But how the

disruption happens is not clear. It may be caused by chemical damage to membrane biomolecules (Fang et al., 2007), or may be caused by NPs robbing lipid molecules from fluid PL bilayer membrane through adsorption (Kaufmann and Tanaka, 2003), or may be caused by membrane gelation or fluidization after NP attachment (Wang et al., 2008). The NPs' effects to outer membrane proteins have not been addressed because only few studies have worked on the protein adsorption on NPs (Strehle et al., 2004; Vertegel et al., 2004).

1.9. Objectives

This work seeks to evaluate the toxicity of several engineered oxide NPs to common bacterial species and the influences of NPs on the bacteria surface biomolecules. The specific objectives of the proposed research are**:**

(1) to evaluate the bacterial toxicity of nano- and bulk-particles and their released metal ions, and to determine whether the toxicity is composition-related or size-related;

(2) to probe the NP-induced molecular structural change/damage to bacterial surfaces using FTIR technique and to better understand the mechanism of NP toxicity to bacteria

(3) to examine NP-induced membrane constructional and morphological changes

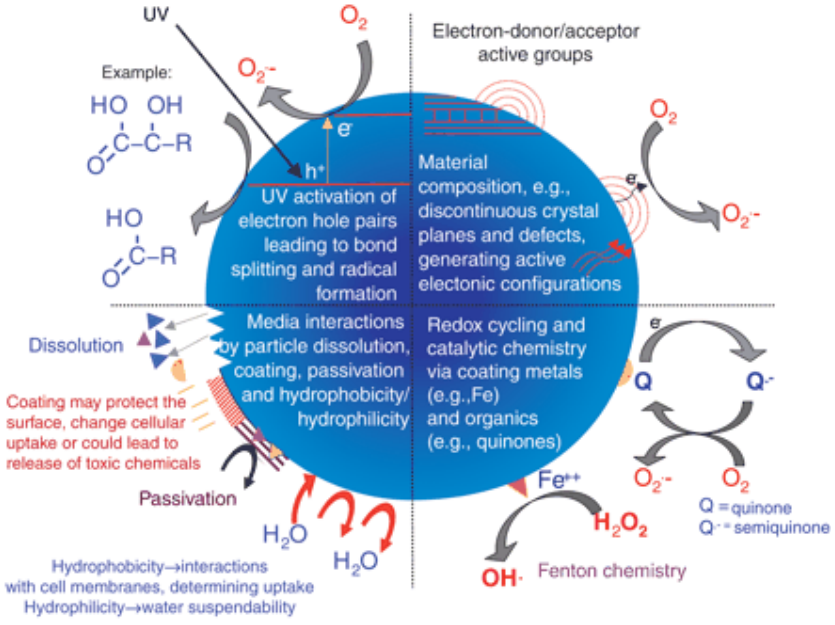

Figure 1.1. Possible mechanisms by which nanoparticles interact with biological tissue (Nel et al, 2006).

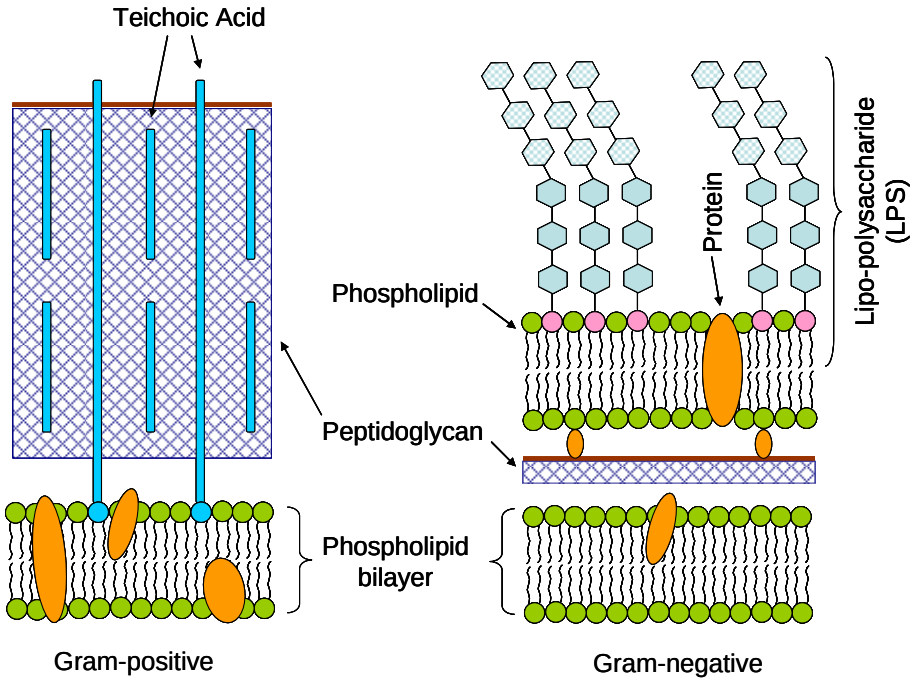

Figure 1.2. Bacterial cell envelope structure.

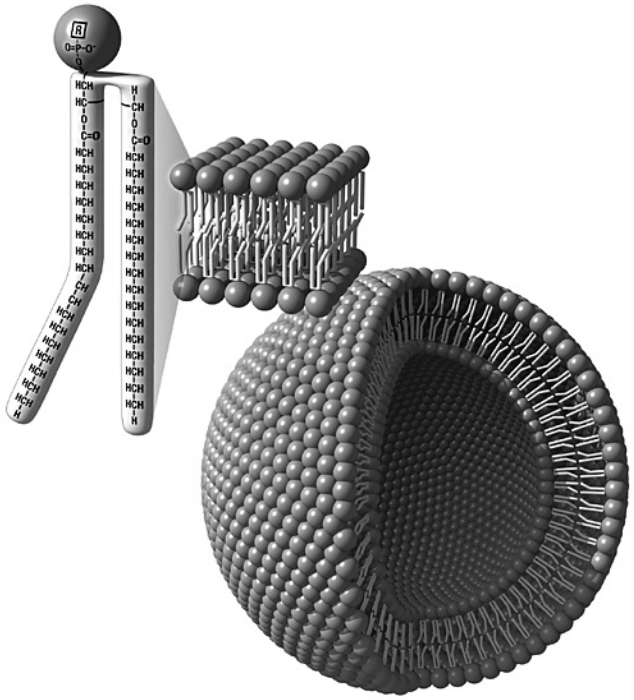

Figure 1.3. Phospholipid molecule, bilayer and vesicle (www.nai.nasa.gov)

CHAPTER 2

BACTERIAL TOXICITY COMPARISON BETWEEN NANO- AND MICRO-SCALED OXIDE PARTICLES

2.1 Abstract

The Toxicity of nano-scaled aluminum, silicon, titanium and zinc oxides to bacteria (*Bacillus subtilis*, *Escherichia coli* and *Pseudomonas fluorescens*) was examined and compared to that of their respective bulk (micro-scaled) counterparts. All nanoparticles but titanium oxide showed higher toxicity (at 20 mg/L) than their bulk counterparts. Toxicity of released metal ions was differentiated from that of the oxide particles. ZnO was the most toxic among the three nanoparticles, causing 100% mortality to the three tested bacteria. Al_2O_3 nanoparticles had a mortality rate of 57% to *B. subtilis*, 36% to *E. coli*, and 70% to *P. fluorescens*. SiO_2 nanoparticles killed 40% of *B. subtilis*, 58% of *E. coli*, and 70% of *P. fluorescens*. TEM images showed attachment of nanoparticles to the bacteria, suggesting that the toxicity was affected by bacterial attachment. Bacterial responses to nanoparticles were different from their bulk counterparts; hence nanoparticle toxicity mechanisms need to be studied thooughly.

2.2 Introduction

Nanotechnology is one of the fast growing sections of high tech economy. Products

using nanoparticles (NPs, less than 100 nm) can be found in different industrial, medical, personal and military applications. NPs, which are in the range of internal cell organs, not only may enable their use in manipulating or sensing biological systems (Jaiswal and Simon, 2004), but have also raised concerns about their possible harmful interactions in the environment (Nel et al., 2006; Thill et al., 2006). Their small particle size, large surface area and ability to produce reactive oxygen species are considered to be related to their toxicity (Nowack and Bucheli, 2007). Because of increasing production and application of NPs, their release into the environment is inevitable, which requires a better understanding of their fate and behavior in the environment.

Aluminum oxide (Al_2O_3), silicon dioxide (SiO_2), titanium dioxide (TiO_2), and zinc oxide (ZnO) are among frequent industrial additives with various applications. Aluminum oxide, having good dielectric and abrasive properties, is widely used as an abrasive agent or insulator. TiO_2 is an opacifier which is used in paints, paper, plastic, and many cosmetics products. SiO_2 in crystalline form is widely used in electronics as semiconductors. ZnO showing ceramic properties have applications as semiconductors or pigments (Adams et al., 2006). Nano metal oxides having greater surface area than their bulk counterparts provide superior performance in their applications.

The toxicities of oxide NPs have been reported for mammalian cell lines (Brunner et al., 2006; Chang et al., 2007), bacteria (Adams et al., 2006; Huang et al., 2008), plants (Lin and Xing, 2007, 2008), and crustaceans (Lovern et al., 2007; Heinlaan et al., 2008). But few studies have compared the NPs toxicities to their bulk particles (BPs)

counterparts. In a study on toxicity of nanosized and bulk ZnO, CuO and TiO_2 to bacteria and crustanceans, Heinlaan et al. (2008) reported nano CuO showed more toxicity than bulk CuO to the tested organisms. However, Adams et al. (2006) reported no difference between TiO_2, SiO_2, ZnO NPs and BPs toxicity to bacteria because they formed similar size aggregates. Franklin et al. (2007) also reported similar toxicity between ZnO NPs and BPs to freshwater microalgae. Therefore, NP toxicity caused by size or by composition should be further evaluated and probably should be examined case by case.

The role of released metal ions in NPs toxicity needs to be taken into account for NP toxicological studies. Limited studies addressed the toxicity of metal ions in previous investigations, mainly on ZnO (Franklin et al., 2007; Lin and Xing, 2007; Heinlaan et al., 2008), Ag (Lok et al., 2007), and CdSe (Derfus et al., 2004). Some of the researchers attributed the NPs toxicity to the dissolved toxic ions, rather than NPs themselves, thus the importance of the particle solubility is worth careful examinations.

Bacteria perform many critical roles in the ecosystem function and productivity. The toxicity of nanomaterials to bacteria has caused many concerns. Interactions between bacteria and NPs may provide us with more information about the impact of NPs once released to the ecosystem. At the same time, bacteria as single cell organisms are good test models to study the NPs toxicity and to know how the NPs affect cell/organism function. Hence, NPs toxicity at the cellular level should be examined in a medium whose ionic strength is close to real natural fresh water, which may help understand if NPs are harmful to the microbes in the environment, particularly in aquatic systems.

This research was, therefore, performed to better understand if the bacteria toxicity of NPs was size- or composition-related by comparing the NPs to their bulk counterparts and by evaluating the contribution of dissolved metal ions to the overall toxicity. In addition, the interactions between NPs and bacteria and their surface properties were examined. All toxicity assessments in this work were done using three model bacteria species: gram-positive *Bacillus subtilis*; gram-negtive *Escherichia coli* and *Pseudomonas fluorescens*.

2.3 Materials and Methods

2.3.1 Preparing Nanoparticles Suspensions

Aluminum (60 nm), titanium (50 nm) and zinc (20 nm) oxide nanoparticles were purchased from Zhejiang Hongsheng Material Technology Co., China. Silicon oxide NPs (20 nm, Ludox CL) suspension was purchased from Sigma Aldrich. Micro-sized particles of the same composition were purchased from Fisher Scientific Co. Nanoparticles and their micro counterpart powders were sterilized in an oven at 160 °C for 3 hours, then dispersed in filter-sterilized DI water (Millipore, resistivity =18.3 MΩ/cm) to make stock suspensions of 2000 mg/L (Brunner, et al., 2006). The suspensions were placed in an ultra-sound water bath for 30 min to break aggregates before diluting them to the exposure concentrations. Colloidal SiO_2 suspension was diluted to 4000 mg/L, and autoclaved for 20 min at 120 °C.

2.3.2 Metal Ion Concentration Measurement in Suspension

Each oxide particle (NPs or BPs) suspension at 20 mg/L was centrifuged at 12,000 RPM for 10 min. Clear supernatant was carefully collected and filtered through a 0.22 μm sterilized filter. The ion concentrations were measured by an ICP-OES after acidification by 1% nitric acid (Lin and Xing, 2008; Wang et al., 2009).

2.3.3 Toxicity Assessment

Bacillus subtilis, *Escherichia coli* and *Pseudomonas fluorescens* used in this study were obtained from the Department of Food Sciences, University of Massachusetts, Amherst. Bacteria were maintained in Tryptic Soy (TS) agar slants in a 4 °C refrigerator. For all experiments, the bacteria were grown in 50 mL Tryptic Soy (TS) medium for one day at 30 °C in an incubation shaker. Bacteria were separated from the broth by centrifugation at 5,000 RPM for 5 minutes, then washed by 9 g/L sodium chloride solution. Bacteria were finally resuspended in 1 g/L NaCl for use in toxicity tests, which is in the range of natural fresh waters. Then bacterial suspensions were diluted to 2×10^8 cells/mL for the toxicity treatments. Initial bacteria cell populations were determined using its turbidity measured at 500 nm by a UV-visible spectrometer (Agilent 8453).

For the NP treatments, 10 mL of bacteria suspension was added to a test tube. Then, 100 μL of a NP stock suspension was added to achieve the exposure concentration of 20 mg/L. Such amount of NPs did not affect the pH value of bacteria suspension (pH=6.5). The tubes without NPs were used as control. Bacteria and NPs were mixed

fully by vortexing. Then the tubes were incubated for 2 hours at 30 °C in a dark shaker. The toxicity was evaluated by comparing the number of colony forming units on TS agar plates to the control after 24 h incubation. All treatments were prepared in duplicate and each set of the experiments was repeated at least three times to ensure data reproducibility.

2.3.4 Zeta Potential Measurements

Zeta potentials of all the samples were measured by a Zetasizer (Malvern Instruments Ltd.) at 25 °C. NPs stock suspension was diluted to 200 mg/L in 1g/L NaCl, divided into ten aliquots of 10 mL, and adjusted to various pH values from 4 to 10 by 0.01 *M* HCl or NaOH solution. The samples were stored for 2 hours to achieve equilibrium and put into an ultra-sound bath to disperse aggregates before zeta potential measurements. Their exact pH values were measured again after zeta potential measurements. Zeta potentials of three bacteria species were also measured at pH=6.5, 2×10^8 cells/mL in 1 g/L NaCl.

2.3.5 Transmission Electron Microscopy (TEM) Imaging

All the NP suspensions were diluted to 100 mg/L in distilled water, and bacteria suspensions were diluted to 1×10^7 cells/mL. To study the bacteria and NPs combination, equal volumes of bacteria and NP suspension were mixed. One drop of suspension was placed on a 400 mesh formvar coated grid and dried in a laminar flow hood. A JEOL 100CX Transmission Electron Microscope operated at 100 kV was used to obtain TEM

images.

2.3.6 Statistical Analysis

Two-tailed equal variance *t*-tests were used to evaluate the differences between controls and each treatment, as well as between different treatments. Microsoft Excel 2003's version was used for the *t*-test analysis.

2.4 Results and Discussion

2.4.1 Toxicity Measurement

Al_2O_3, SiO_2 and ZnO NPs showed highly significant ($p < 0.01$) toxicity to all three bacteria species (Figure 2.1). ZnO was the most toxic among the three NPs; all bacteria died at 20 mg/L. Al_2O_3 appeared to kill more *B. subtilis* (57% death rate) than SiO_2 (40%), while their mortality did not show significant differences at the 95% confidence level. SiO_2 caused a significantly higher ($p < 0.01$) death rate for *E. coli* (58%) than Al_2O_3 (36%). Their toxicities were similar to *P. fluorescens*, having a 70% death rate. TiO_2 NPs did not affect bacteria populations, which was different from the results of previous studies (Fu et al, 2005, Adams et al. 2006). They used much higher concentrations of nano TiO_2 suspension than we did in this research. They also tested TiO_2 toxicity in the presence of light to generate reactive oxygen species (ROS), which is one possible mechanism of TiO_2 toxicity (Neal, 2008). Our study was done in the absence of light, which may be another reason for not observing TiO_2 toxicity. *P. fluorescens* was sensitive

to Al_2O_3 and SiO_2 NPs among three bacteria species, showing the highest mortality rate.

Toxicity of Al_2O_3, SiO_2 and ZnO BPs was compared to their nano counterparts at the same concentration (Figure 2.1 A, B and C). The Al_2O_3 and SiO_2 BPs did not exhibit any negative effect on the three bacteria species. ZnO BPs were, however, toxic to the *E. coli* and *P. fuorescens*, but less toxic ($p < 0.05$) than ZnO NPs (Figure 2.1 B and C). *B. subtilis* was completely wiped out in the presence of ZnO BPs (Figure 2.1 A), but the other two species were more resistant (Figure 2.1 B and C). Therefore, our results indicate that Al_2O_3, SiO_2 and ZnO NPs were toxic to the tested bacteria, while their BPs however showed no or lower toxicity, which means that the particle size did cause a toxicity difference. We measured the particle size in suspension (Figure 2.2), showing the aggregation of NPs in the 1g/L NaCl, because the aggregate sizes were much bigger than their respective individual sizes. However, BPs had minimal aggregation because their individual sizes were similar to the corresponding aggregate sizes in solution (Figure 2.2 and 2.3). Therefore, we assume the toxicity of Al_2O_3, SiO_2 and ZnO should not come from their aggregates because NPs aggregate sizes were similar to BPs (Figure 2.2). Individual and small aggregate NPs were presented as on the surface of bacteria, except TiO_2 NPs (Figure 2.4), though large aggregates were observed in NPs suspension (Figure 2.2). A distribution equilibrium would exist between individual NPs and their aggregates.

Metal oxide toxicity could also be induced by dissolved metal ions from the oxides. Brunner et al. (2006) studied the toxicity of NPs to a human and a rodent cell line. They divided the tested NPs to soluble and insoluble NPs, suggesting the toxicity of soluble

NPs was from the soluble metal ions released from NP dissolution before or after the NPs enter the cell. In our study dissolved metal ions were not present in a measurable quantity in the supernatant of aluminum, titanium and silicon oxide (NPs and BPs) suspension. But 2 mg/L of Zn^{2+} was detected in the 20 mg/L ZnO suspension (for both NPs and BPs). Subsequently, toxicity of zinc ions at 2 mg/L to the bacteria was examined. *B. subtilis* was extremely sensitive to Zn^{2+} (Figure 2.1 A, 0% survival rate) while *E. coli* and *P. fluorescens* exhibited 86% and 100% survival rate respectively at 2 mg/L of Zn^{2+} (Figure 2.1 B and C). It may be difficult to tell the ZnO toxicity mechanism to *B. subtilis* because this species was too sensitive to dissolved Zn^{2+} ions. But *E. coli* and *P. fluorescens* could resist 2 mg/L Zn^{2+}, showing no or very low mortality (Figure 2.1 B and C), indicating that toxicity of ZnO NPs to these species was not due to only dissolved zinc ions. Another way to examine the effect of ions from the oxides is to compare the toxicity of ZnO NPs and BPs to *E. coli* or *P. fluorescens*. We noticed that ZnO NPs exhibited much higher toxicity than its BPs, but they both released the similar amount of zinc ions. Thus, the toxicity difference between ZnO NPs and BPs was likely due to the size-related properties. For Al_2O_3 and SiO_2 NPs, we did not detect any of the Al and Si released from the NPs, and their BPs were not toxic to the bacteria. Hence, the observed toxicity of Al_2O_3 and SiO_2 NPs would come from their nano-size related properties.

Mechanisms of NP antibacterial activity and the properties related to the toxicity are still not clearly understood. A majority of previous studies suggest that the mechanism of NP toxicity may relate to their photosensitivity and production of ROS under specific

wavelength high-intensity light. Cell membrane architecture could be impaired through lipid peroxidation by ROS. Damage and disorganization in the cell wall were observed in the bacteria exposed to MgO (Stoimenov et al., 2002) and ZnO (Brayner et al., 2006) NPs. In this study, Al_2O_3, SiO_2 and ZnO antibacterial activity was observed under dark condition, indicating possible production of free radicals under dark condition (Green and Howman, 2005) or other undetermined toxicity mechanisms additional to ROS.

2.4.2 Nanoparticle Attachment to the Bacteria as Examed by TEM

Oxide NPs can cause toxicity to the three bacteria species, thus they should have come into contact with the bacteria cells. High resolution TEM made it possible to visualize the NP adhesion on bacteria. Images of Al_2O_3, SiO_2, TiO_2 and ZnO NPs are shown in Figure 2.3. NP attachment to *P. fluorescens* is shown as an example (Figure 2.4) because the three bacteria species did not show differences in oxide attachment for a given type of oxide NP. From Figures 2.3 and 2.4, Al_2O_3, SiO_2 and ZnO NPs coated the whole bacteria cells. All SiO_2 NPs sizes were between 10 and 20 nm and SiO_2 NPs evenly coated on the bacteria cell wall (Figure 2.4 B). Al_2O_3 NPs were similar to the SiO_2, although they were not as uniform as SiO_2 NPs. Both SiO_2 and Al_2O_3 were rarely found in other area of the grid except on bacteria surface, showing a tendency for them to attach on the cell wall rather than aggregate together. However ZnO NPs attachment to the bacteria was different. They covered the bacterial cell but also scattered everywhere on TEM grid (Figure 2.4 D). Their attachment to the bacterial cell may be weaker than Al_2O_3

and SiO_2 NPs. But ZnO NPs were more toxic than Al_2O_3 and SiO_2. The possible reasons could be: 1) dissolved Zn^{2+} ions in the solution contributed to the overall toxicity; 2) Zn^{2+} would be released in the cytoplasm if ZnO NPs entered the bacterial cells; and 3) the attachment mode of ZnO NPs could cause more damage to the bacterial cell wall. Further study is needed to better understand the toxicity differences among NPs. The bacterial cells were rarely coated by TiO_2 (Figure 2.4 C). TiO_2 NPs formed aggregates as big as several hundred nanometers (Figure 2.4 C). The aggregates were composed of many single TiO_2 NPs because the size of a single TiO_2 NP is around 50 nm.

It was not clear if the NPs could pass through the bacterial cell wall, then reach or go through the cellular membrane in this study. TiO_2 NPs were found in mammalian cells after the treatment (Long et al., 2006; Rothen-Rutishauser et al., 2006). ZnO NPs were reported in bacterial cells (Brayner et al., 2006; Huang et al., 2008) and plant root cells (Lin and Xing, 2008). From another point of view, NPs were considered unlikely to enter the bacterial cell cytoplasm (Neal, 2008). NPs, found inside cytoplasm, could have entered due to the disruption of cell membrane. To date, there is still lack of definite knowledge regarding the interaction of oxide NPs with the bacterial cell wall and possible permeation of the NPs into the bacterial cells. In this study, TiO_2 NPs would be not likely to pass through the bacterial cell wall compared to the other three types of NPs, considering their aggregate size and exhibition of no bacterial toxicity, even though they were reported in mammalian cells (Hussain et al., 2005). The smaller bacterial cell size and cell wall structure compared to mammalian cells may make it easier for NPs to enter

mammalian cells than bacteria cells.

2.4.3 Surface Charge and NPs Attachment

There are several possible attachment mechanisms of oxide NPs to bacterial surface: Van der Waals forces, electrostatic, hydrophobic and receptor-ligand interactions (McWhirter et al., 2002; Parikh and Chorover, 2006). The bacterial surface is negatively charged. The surface charge of *B. subtilis* was -41.3 mV, *E. coli* -7.20 mV and *P. fluorescens* -32.3 mV in 1 g/L NaCl at pH 6.5. The Al_2O_3 (+30 mV) and SiO_2 (+35 mV) NPs were positively charged at pH 6.5, while TiO_2 (-21 mV) and ZnO (-5 mV) were negatively charged at the same pH (Figure 2.5). It was not possible to measure the zeta potential of ZnO suspension in over the entire pH range because it dissolved at acidic and alkali pHs. The differences in the NP zeta potential may help us to understand how they attach to bacteria. For the highly positively charged oxides, Al_2O_3 and SiO_2 NPs, the negatively charged bacteria surfaces would attract these NPs. In addition, the aggregate size on the bacteria surface was much smaller than that in the medium without the bacteria (Figure 2.3 and 2.4), showing that the bacteria could attract small aggregates and individual particles from the suspension, thereby moving the NPs aggregation-dispersion equilibrium towards the dispersion direction. For TiO_2 NPs, an electrostatic force would also play an important role in their repulsion from the bacteria cell wall as shown by clean cell surfaces.

Electrostatic forces should contribute greatly to the adhesion of positively charged

particles, but we cannot exclude other mechanisms. The ZnO NPs with a zeta potential of -5 mV attached to the bacteria surface (Figure 2.4 D). When the electrostatic repulsion between NPs and bacteria was weak, the receptor-ligand interactions may dominate interactions between the oxides and the bacteria. Such a bond formation was reported in bacteria adhesion to natural mineral surfaces (Deo et al., 2001; Omoike and Chorover, 2004). Carboxyl, amide, phosphate, hydroxyl groups and carbohydrate-related moieties in the bacteria cell wall may provide sites for the molecular-scale interactions with the oxide NPs (Omoike and Chorover, 2004; Leone, et al., 2007). Attachment of a few large TiO_2 aggregates to the bacterial cell may be due to the drying process required for TEM observation.

The Al_2O_3 and SiO_2 NPs in our study could flocculate bacterial cell suspensions soon after their mixing (Figure 2.6). However, there was no clear change after adding TiO_2 and ZnO NPs to the bacterial suspension. Flocculation can be explained by the charges of NPs. Because Al_2O_3 and SiO_2 NPs are much smaller than the bacterial cells, they coated around the bacteria cell by electrostatic attractive forces, neutralizing the bacteria surface charge and creating large aggregates. The large aggregates of NPs-bacteria complex would settle quickly out of the suspension. However, no flocculation occurred after adding BPs (Figure 2.6 B). This indicates a particle size-dependant phenomenon. For negatively charged bacterial cells (a few μm in size), they could readily capture NPs by electrostatic attractive forces, while it would be difficult to attract BPs by moving them. Even if BPs could attach to the bacteria, they would only affect a few cells

because of the lower particle numbers in solution.

2.5 Conclusions

All nanoparticles except TiO_2 exhibited signs of toxicity to the tested bacteria, compared to the control. The Al_2O_3, SiO_2 and ZnO NPs showed higher toxicity than their BPs counterparts. Toxicity of NPs was not only from the dissolved metal ions, but also was from their tendency to attach on the cell walls rather than aggregate together. Sensitivity of bacteria to each type of NP varied with bacterial species. The ZnO NPs were most toxic among the studied NPs. TEM images confirmed the attachment of Al_2O_3, SiO_2 and ZnO NPs to the surface of bacteria. Further work is needed to study the effect of natural environmental parameters on NP toxicity and exact toxicity mechanisms. This study signifies environmental and health implications of manufactured nanoparticles relative to bulk particles.

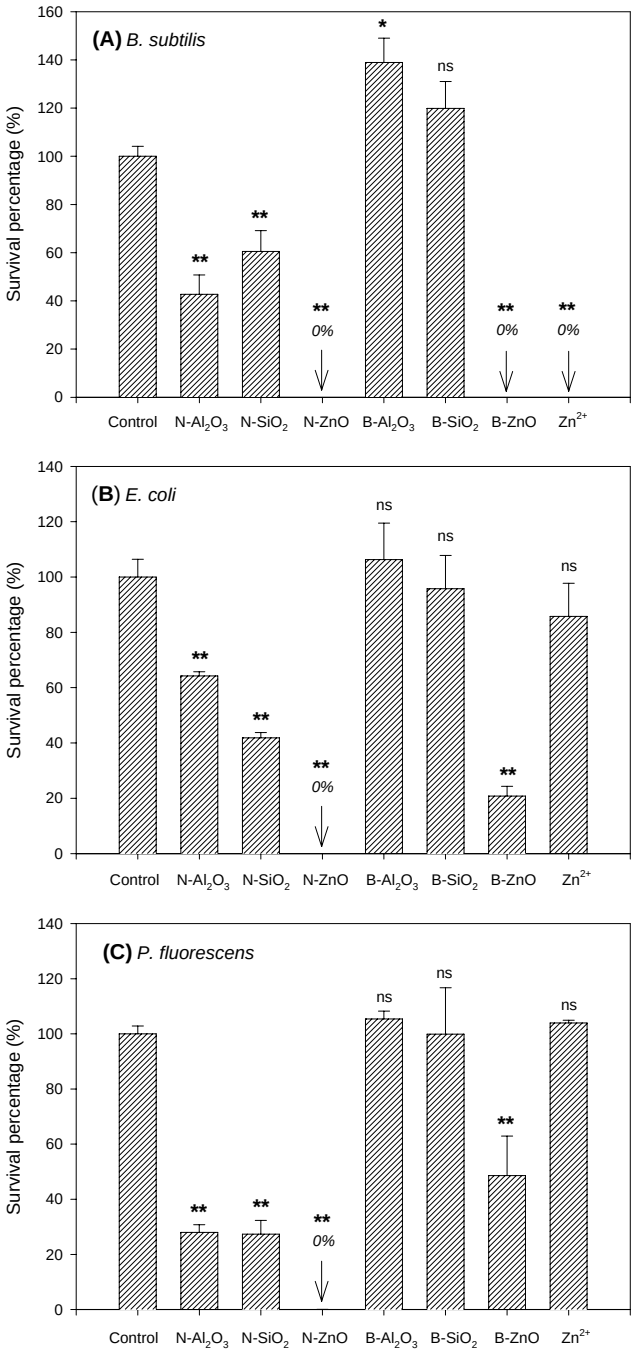

Figure 2.1. Toxicity of 20 mg/L nano-scaled oxide particles (N-), micro-scaled bulk oxide particles (B-) and 2 mg/L Zn^{2+} to *B. subtilis* (A), *E. coli* (B) and *P. fluorescens* (C). Oxide NPs showed higher toxicity than their BPs counterparts. ZnO NPs were most toxic, indicated by 0% survival. Zn^{2+} was less toxic than ZnO NPs and BPs to *E. coli* and *P. fluorescens*.

**Highly significantly different to control at $p < 0.01$ level; *significantly different to control at $p < 0.05$ level; ^{ns}not significantly different to control

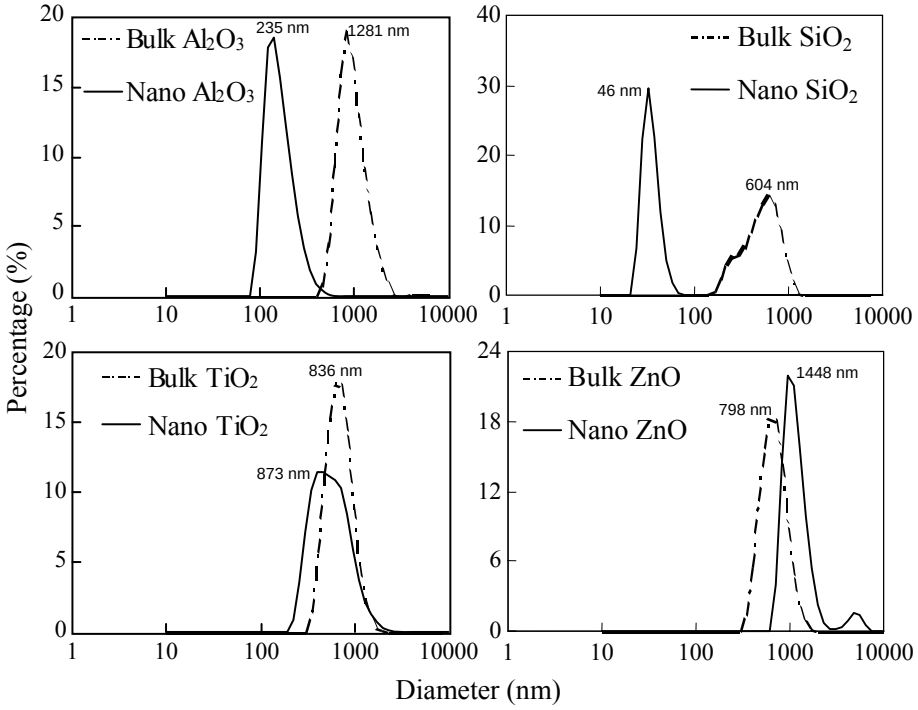

Figure 2.2. Size distribution of NPs and BPs (diameter in nm). All measurements were done in 1 g/L NaCl at pH= 6.5.

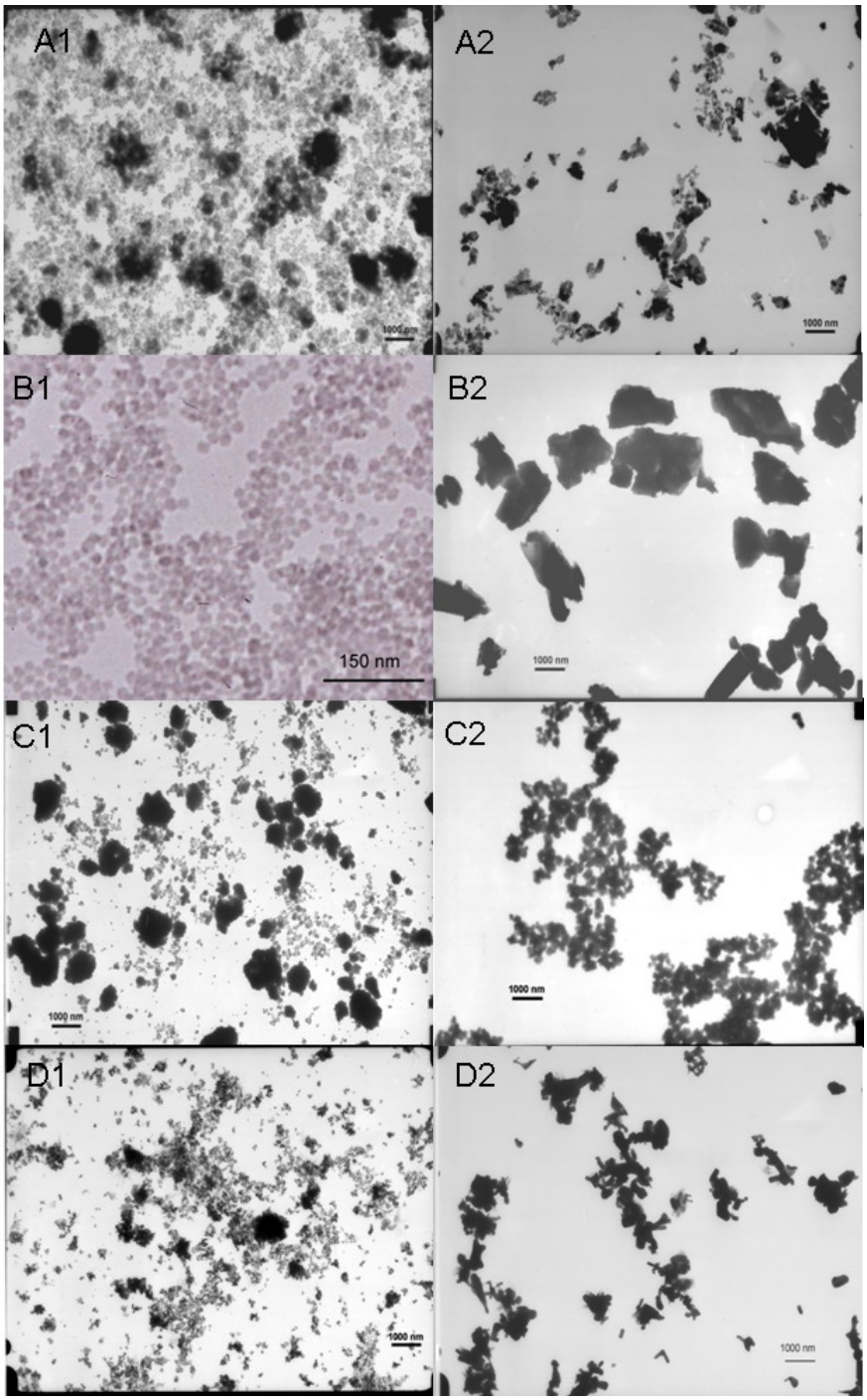

Figure 2.3. TEM images of oxide nanoparticles Al_2O_3 (A1), SiO_2 (B1), TiO_2 (C1), ZnO (D1); and bulk particles Al_2O_3 (A2), SiO_2 (B2), TiO_2 (C2), ZnO (D2). Both the NPs and BPs could aggregate to large particles. TiO_2 and ZnO NPs even formed larger aggregates than their BPs counterparts.

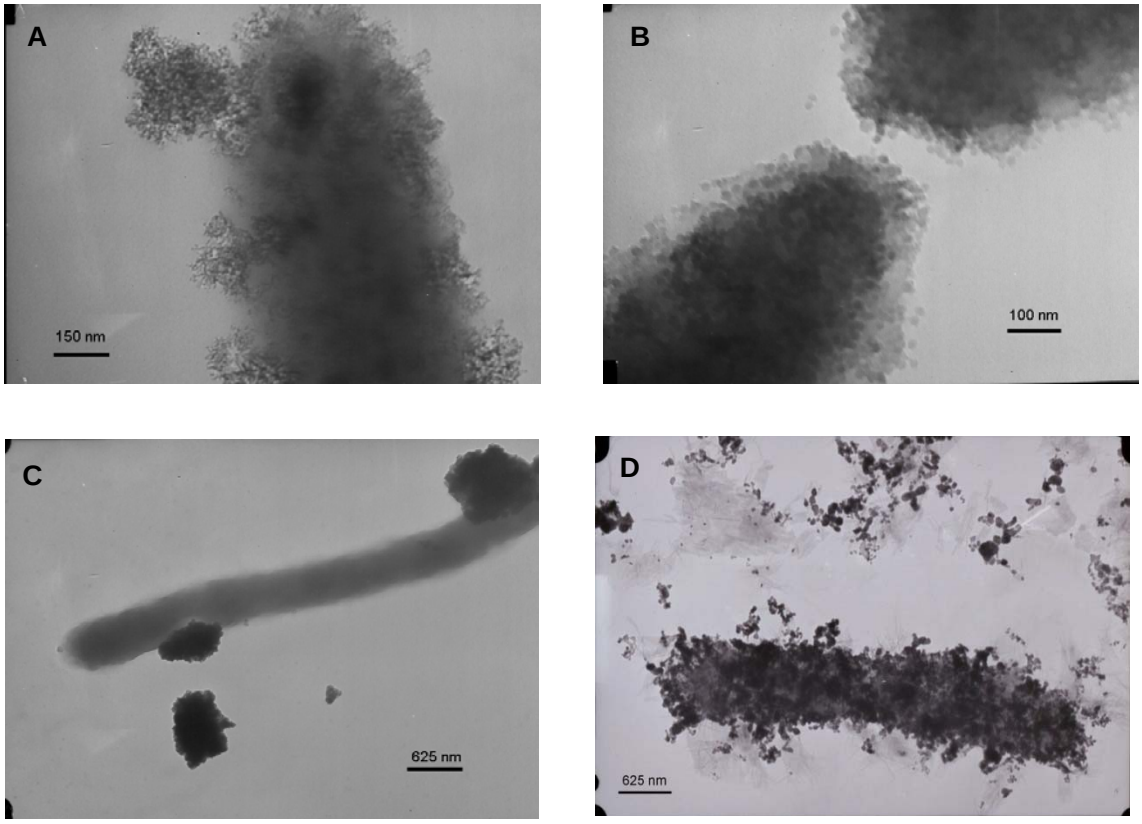

Figure 2.4. TEM images revealing attachment of nanoparticles to the surface of *P. fluorescens*: Al_2O_3 (A), SiO_2 (B), TiO_2 (C), ZnO (D).

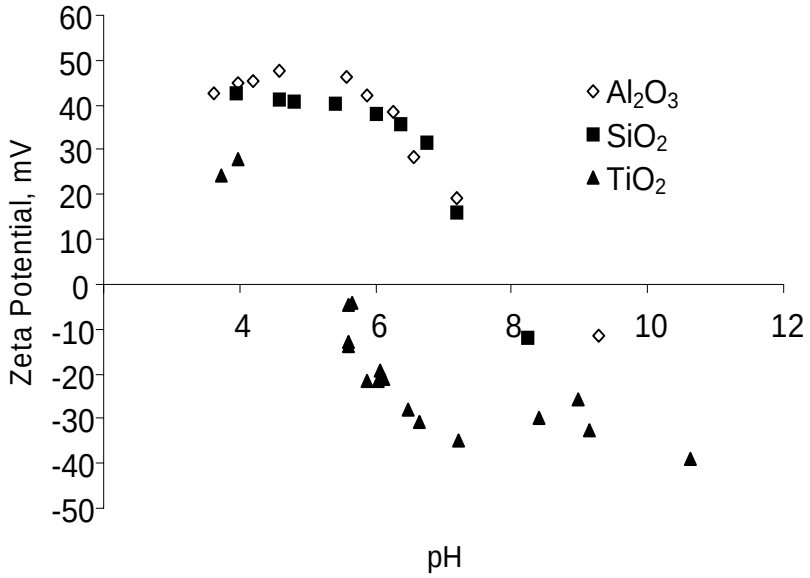

Figure 2.5. Zeta potential of oxide nanoparticles measured in 1 g/L NaCl solution.

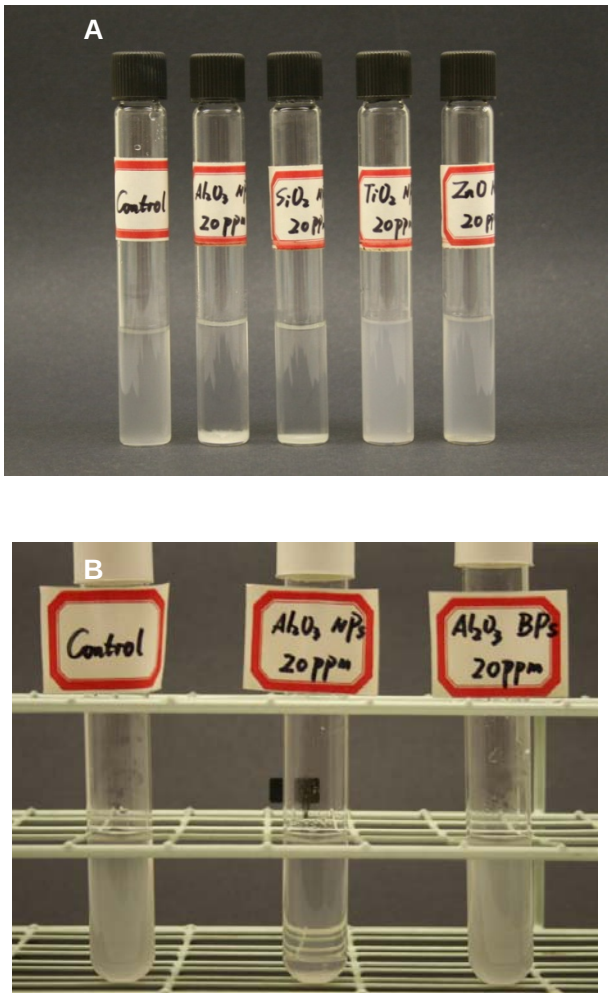

Figure 2.6. Flocculation of *P. fluorescens* suspension after its mixing with four nano-scaled particles (A), and the flocculation differences in nano-scaled and micro-scaled Al_2O_3 (B). In (A), Al_2O_3 and SiO_2 NPs caused the bacteria suspension to flocculate. In (B), Al_2O_3 NPs caused flocculation, while Al_2O_3 BPs did not.

CHAPTER 3

INTERACTION BETWEEN OXIDE NANOPARTICLES AND BIOMOLECULES OF BACTERIAL CELL ENVELOPE AS EXAMINED BY INFRARED SPECTROSCOPY

3.1 Abstract

The effects of Al_2O_3, TiO_2 and ZnO nanoparticles (NPs) on bacteria cells and bacterial surface biomolecules were studied by Fourier transform infrared spectroscopy (FTIR). All the examined biomolecules showed IR spectral changes after NP exposure. Lipopolysaccharide and lipoteichoic acid could bind to oxide NPs through hydrogen bonding and ligand exchange, but the cytotoxicity of NPs seemed largely related to the function-involved or devastating changes to proteins and phospholipids of bacteria. The three NPs decreased the intensity ratio of β-sheets/α-helices, indicating protein structure change, which may affect cell physiological activities. The phosphodiester bond of L-α-Phosphatidyl-ethanolamine was broken by ZnO NPs, forming phosphate monoesters and resulting in the highly disordered alkyl chain. Such damage to phospholipid molecular structure may lead to membrane rupture and cell leaking, which is consistent with the fact that ZnO is the most toxic of the three NPs. The cell surface biomolecular changes revealed by FTIR spectra provide a better understanding of the cytotoxicity of oxide NPs.

3.2 Introduction

Nanoparticles (NPs) are a new group of materials with rapidly growing production and application. The unique properties of NPs, such as high specific surface area, and abundant surface reactive sites, could potentially lead to unexpected health or environmental hazards (Nel et al., 2006). The toxicity of NPs to bacteria is one area of concern because bacteria are an essential link of food web and play many critical roles required for normal ecosystem function and productivity. Moreover, bacteria are a good test model as single cell organisms. The study of the uptake and adhesion of NPs to bacteria will help to understand how NPs interact with cells structures in the environment.

Microbial cytotoxicity of NPs has already been reported by the previous studies (Adams et al., 2006; Brayner et al., 2006; Thill et al., 2006; Huang et al., 2008). The location of NP toxicity, whether it occurs inside the bacterial cells or on the cell surface, is a key point for understanding toxicity mechanisms. Although NPs have been reported inside the bacterial cells,[3] passage of NPs across intact membranes appears to be unlikely (Neal, 2008). NP accumulation in the cytoplasm is most likely after membrane disruption, which is often observed (Brayner et al., 2006; Huang et al., 2008). In addition, the adsorption of NPs to bacterial surfaces was reported to associate with significant bacterial cytotoxicity (Thill et al., 2006). NP attachment to the cell envelope appeared necessary to cause their bacterial cytotoxicity in Chapter 2 (Figure 2.1 and Figure 2.4). Therefore, the NP adhesion process to bacterial surface is very important in the discussion of NP bacterial cytotoxicity. For this reason, the way in which NPs attach to bacterial surface and affect cell surface biomolecules is of interest.

Biomolecules on the bacterial envelope dominate cell adhesion through their highly-charged structure, functional groups, and/or the bridging effect to the surface (Jucker et al., 1998; Omoike and Chorover, 2004; Parikh and Chorover, 2006). In bacterial cells, lipopolysaccharide (LPS), lipoteichoic acid (LTA), protein and phospholipid are the major biomolecules possibly interacting with NPs when NPs attach to cell surface (Figure 1.2). Their chemical structures are presented in Figure 3.1. They not only work as adhesins, but also play important roles in maintaining normal cell physiological activities. Because NP toxicity relates to their adhesion onto bacteria, damage to the structure and change in the physio/chemical properties of surface biomolecules may be possible reasons of NP microbial toxicity.

The interactions between these biomolecules and oxide particle/surface have been studied in the areas of bacterial adhesion and biofilm formation (Jucker et al., 1997 &1998; Omoike and Chorover, 2004; Parikh and Chorover, 2006; Rice and Wickham, 2008), protein adsorption (Buijs et al., 1996; Wu and Narsimhan, 2008), phospholipid adsorption and supported membrane making (Mornet et al., 2005; Oleson and Sahai, 2008; Xu et al., 2009). However most of these studies either focused on the sorption process, rather than on change to the biomolecules and bacterial cell envelope structure, or did not link the changes in cell surface biomolecules to cytotoxicity. Therefore, the overall goal of this study was to better understand NP bacterial toxicity through NP adhesion-induced biomolecular change or even damage.

In identifying the damage to biomolecular structure and the bacterial envelope, it is very challenging to examine the interface between biomolecules and oxides using most analytical techniques. However FTIR technique has the advantages of providing

molecular-scale information for both organic and inorganic constituents involved in bacterial adhesion in a variety of environments, rendering it uniquely suited to probe the bacteria-oxide interface. The NPs on which we focused in this study were the oxide NPs Al_2O_3, TiO_2 and ZnO. They are among the most commonly engineered nanomaterials, and widely used in the electronic, cosmetic, automotive and medical products. Therefore, the specific objectives of this study were: (1) to compare the IR spectra of the NP-exposed biomolecules and intact cells with unexposed ones; (2) to figure out which molecule or functional groups may be changed or damaged by the NPs; and (3) to provide clues on structural damage of the cell envelope, and on possible reasons for NP bacterial cytotoxicity.

3.3. Materials and Methods

3.3.1 Chemicals and Materials

Aluminum oxide (with the mean diameter of 60 nm), titanium oxide (50 nm) and zinc oxide (20 nm) NPs were purchased from Zhejiang Hongsheng Material Technology Co., China. The NP powder was dispersed in distilled deionized (DI) water (Millipore, resistivity =18.3 MΩ/cm) to make stock suspensions of 2,000 mg/L. The pH of the Al_2O_3 and TiO_2 suspensions were adjusted to 6.5 and pH of the ZnO suspension adjusted to 7.

Bacterial cells used in the experiment were Gram-positive *B. subtilis*, and Gram-negative *E. coli* and *P. fluorescens*. The bacteria were grown in Tryptic Soy (TS) medium for one day at 30°C in an incubation shaker. Then the cells were separated from the broth by centrifugation at 5,000 RPM for 5 minutes, and washed twice using 1 g/L sodium

chloride solution. The harvested cell pellets were freeze-dried and kept at -20°C for future use.

The LPS from *E. coli* O55:B5 (code L4005), LTA from *B. subtilis* (code L3265), L-α-Phosphatidyl-ethanolamine (PE) from *E. coli* (code P8068), and lyophilized bovine serum albumin (BSA) powder were bought from Sigma Aldrich and used without further purification. The protein G recombinant from *E. coli* (Sigma Aldrich, code 19459) was dialyzed to get rid of the phosphate buffered saline in the lyophilized powder.

3.3.2 FTIR Sample Preparation

A Perkin-Elmer Spectrum One FTIR spectrometer, equipped with a lithium tantalate ($LiTaO_3$) detector and a one-reflection horizontal attenuated total reflectance (ATR) accessory with a diamond/ZnSe internal reflection element (IRE) crystal (Shelton, CT), was used to collect all ATR-FTIR spectra. The bacterial sample was made by mixing 5 mg bacteria lyophilized powder with 1 mL 2,000 mg/L NP suspension in 25 mL DI water, and shaking the samples for 2 hrs. Then a mixture of wet paste was obtained by centrifugation. After air-drying the wet paste on the top of IRE, a spectrum was obtained by collecting more than 200 scans with a spectral resolution of 2 cm^{-1} and a scan speed of 0.5 cm/sec. The biomolecule samples (i.e. lipopolysaccharide (LPS), lipoteichoic acid (LTA), protein or phospholipids) were made by mixing 20 μL of 2,000 mg/L biomolecule solution with 20 μL of 2,000 mg/L NP suspension in a 96 cell wall plate. After a 2 hr exposure in the 4°C refrigerator, the mixture was dropped on the top of IRE, air-dried, and scanned. The diffuse reflectance infrared Fourier transform (DRIFT) technique was used to study the biomolecules adsorbed on the oxide NPs. For the sample

preparation, 1 mL 2,000 mg/L biomolecule solution was mixed with 1 mL 2,000 mg/L NPs suspension, then the final volume was adjusted to 5 mL. The sample was kept in a 4°C refrigerator for 24 hrs. The particles were separated from the supernatant through centrifugation and washed twice with DI water. Then the wet paste was freeze-dried, and ground with 95 mg KBr for DRIFT analysis (Kang and Xing, 2008).

Bacterial and biomolecule samples without NP treatment and pure NP samples were also scanned to compare with the NP-exposed samples. To isolate the spectra of the bacteria and of the biomolecules from the mixtures, the NP spectra were subtracted from the spectra of their mixtures. The IR bands below 1000 cm^{-1} are not discussed for samples treated with Al_2O_3 and TiO_2 NPs because the strong oxide absorbance in this region. To identify the effects of zinc ions on PE, an equal volume of 3,300 mg/L $ZnCl_2$ (the concentration if all the ZnO NPs are dissolved) solution was mixed with 2,000 mg/L PE, which led to the precipitation of PE. The solid substance was collected for IR study after a 24 hr equilibrium at 4°C.

3.3.3 Second Derivative of IR Spectra

Bacterial and protein IR spectra were further analyzed in the amide I region (1600-1700 cm^{-1}) to extract information on protein secondary structure and potential changes due to exposure to NPs. Data collections and spectral calculations were performed using the Spectrum software package (Perkin-Elmer). The 2^{nd} derivatives of the original amide I spectra were obtained after nine-point Savitzky-Golay smoothing (Branan and Wells, 2007; Badireddy et al., 2008). During the 2^{nd} derivative process, the amide I band was decomposed to separate overlapping peaks by enhancing spectral resolution. Water vapor

peaks were removed by subtracting the water vapor spectra obtained in blank experiment. Maximum absorption intensity, band frequency, and band width were obtained from the 2nd derivative spectra to determine the protein structural changes (Buijs et al., 1996; Badireddy et al., 2008).

3.4. Results and Discussion

3.4.1 ATR-FTIR Spectra of Bacterial Cells Exposed to NPs

Three bacterial species, Gram-positive *B. subtilis*, and Gram-negative *E. coli* and *P. fluorescens*, showed similar FTIR spectra (Figure 3.2). The intense bands around 1638 cm^{-1} and 1540 cm^{-1} corresponded to the amide I and amide II bands respectively (Buijs et al., 1996; Naumann et al., 1996). The amide I primarily represented the carbonyl stretching vibration ν (C=O) in the peptide bond groups, while amide II band was assigned to the bending vibration δ of N-H and ν of C-N in amide (Jiang et al., 2004). Oxide NPs caused a slight shift and shape change in the amide I band, shown more clearly in the 2nd derivative spectra (Figure 3.3), indicating the changes to protein structure. A small peak at 1745 cm^{-1} in *B. subtilis* spectrum was from the ester ν (C=O) (Naumann et al, 1996), which was not seen in the spectra of *E. coli* and *P. fluorescens*. This peak diminished after mixing with ZnO NPs (Figure 3.2a). The infrared absorption from 1425 cm^{-1} to 1475 cm^{-1} consisted of at least two bands at 1468 cm^{-1} and 1454 cm^{-1}, corresponding to the CH_2 scissoring and CH_3 asymmetric bending δ_{as} (Kinder et al., 1997; Kiwi and Nadtochenko, 2005). The symmetric bending δ_s of CH_3 was comparably weak and hided by the band of symmetric vibration ν_s (COO^-) at 1398 cm^{-1} (Naumann et al., 1996; Kiwi and Nadtochenko, 2005). The band around 1230 cm^{-1} was assigned to the

asymmetric vibration ν_{as} of PO_2^- in phosphodiesters (Wong et al., 1991; Omoike and Chorover, 2004). A combination of ν (C-O, C-O-C, C-O-P) was centered at 1059 cm^{-1} for *B. subtilis* (Naumann et al., 1996; Parikh et al., 2006; Branan and Wells, 2007), and at 1079 cm^{-1} for gram-negative *E. coli* and *P. fluorescens*. Since the peak at 1079 cm^{-1} was the sugar vibration for intact bacterial cells (Naumann et al., 1996), the sugar content of Gram-negative species appeared to be higher. In the *B. subtilis* spectra (Figure 3.2a), Al_2O_3 and ZnO NPs shifted the band around 1059 cm^{-1} to the lower wavenumber. The shift may be caused by the binding of the functional groups on the bacterial surface to the oxides, because this IR absorbance region is related to the hydroxyl, carbonyl, carboxylic acid and phosphate groups (Naumann et al., 1996, Jiang et al., 2004). However, the intact bacterial cells are such a complex system, from the bacterial cell IR spectra alone, it is hard to tell which biomolecules or which functional groups are affected by the NP treatment. Further understanding of NP-induced bacterial cell changes need to be based on the bacterial cell envelope structure and the IR spectra of the extracted cell envelope components.

3.4.2 NP-induced Changes to Protein Secondary Structure Revealed by ATR-FTIR

The amide I bands are the most intense bands in all the three bacterial spectra (Figure 3.2). This region reflects quantitative and qualitative relationships between the various secondary structures present in protein (Naumann et al., 1996; Torii and Tasumi, 1996). There are certain cell constituents other than protein that can give rise to IR absorbance in the amide region, such as DNA and RNA. However, since the relative amounts per cell mass of these constituents and their absorbance intensities are much

lower than for protein, the IR features observed in this spectral region are almost completely defined by the protein amide I band (Naumann et al., 1996). By comparing the bacterial spectra with the spectra of pure protein, the protein structural changes in the intact bacterial cells can be determined.

The amide I band is not a pure C=O stretching mode, because it coupled appreciably with the C-N stretch and in-plate N-H bending (Bellamy, 1975). The frequency of this vibration, therefore, depends on the nature of the hydrogen bonding in which the C=O group is involved (Figure 3.1) and the transition dipole coupling (Surewicz et al., 1993; Buijs et al., 1996). Thus the amide I frequency is highly sensitive to the secondary structure adopted by the polypeptide chain. The amide I band of the protein BSA has a high α-helix content (Peters, 1996) and was centered at 1653 cm^{-1}; while the amide I band of protein G contains more β-sheets than α-helix (Goward et al., 1991) and was centered at 1638 cm^{-1} (Figure 3.5).

The 2^{nd} derivative of the amide I band can enhance the spectral resolution. In the 2^{nd} derivative spectra of bacteria (Figure 3.3a), BSA and protein G (Figure 3.3b), the bands around 1653 cm^{-1} were associated with α-helix; the bands at 1632-1636 cm^{-1} were ascribed to β-sheet; and the small band at 1645 cm^{-1} was assigned to unordered segments as is generally done (Giacomelli et al., 1999; Vedantham et al., 2000). In the 2^{nd} derivative spectra the protein BSA only exhibited α-helix bands because it has 54-68% α-helix but very little β-sheet (Carter and Ho, 1993; Peters, 1996). In the 2^{nd} derivative spectra, the band intensity of the β-sheet region was higher than the α-helix for all the three bacteria (Figure 3.3a), indicating the high content of β-sheet structure in the overall cell proteins. Exposure to oxide NPs changed the β-sheet band of the bacteria and protein

G, shifting the whole band to a lower frequency and forming of new peaks at 1630 and 1627 cm^{-1} (Figure 3.3). For most proteins, several components are included in the β-sheet region. This multiplicity reflects differences in β hydrogen-bonding strength and in transition dipole coupling in different β-stands (interstrand interactions) (Surewicz et al., 1993). The major peak around 1636 cm^{-1} is generally ascribed to antiparallel β-sheet (Surewicz et al., 1993). The new peaks, or the splitting of "β-bands" induced by NPs, indicated that NP attachment to the proteins can cause variation in hydrogen bond strength and the interaction between β-strands. The low-frequency shift indicated stronger hydrogen bonds, which could result from either intermolecular or intramolecular bonding (Jackson et al., 1991; Giacomelli et al., 1999). The α-helix bands contained at least two components around 1653 cm^{-1} and 1659 cm^{-1} (Figure 3.3). NP exposure to bacteria and protein G did not cause any shape or position changes in the α-helix bands. However a new peak at 1650 cm^{-1} emerged when BSA was exposed to NPs.

Another remarkable change caused by NP exposure was the intensity ratio of β-sheet to α-helix (Table 3.1). This ratio decreased after mixing the bacteria with the NPs (Table 3.1). It is possible that the β-sheet structure in the protein molecule was diminished by unfolding; or the hydrogen-bonding environment of the carbonyl group changed, thereby decreasing the sensitivity of β-sheet structure to infrared light. In contrast, after NP exposure, the β-sheet/α-helix intensity ratio was more stable in protein G than bacterial cells (Table 3.1). The proteins on the bacterial cell surface may not be as stable as the protein G, or the proteins on cell surface have higher β-sheet content than in the cell as a whole, resulting in a greater impact on the β-sheet than on the α-helix structure.

3.4.3 LTA Adsorption on Oxide NPs Studied by FTIR

LTA is a primary adhesion molecule for Gram-positive bacteria (Figure 1.2). It is a long chain of phosphodiesters (anionic) with glucosamine (neutral) and D-alanine branches (cationic) (Figure 3.1a). The peak of the ester carbonyl group at 1743 cm^{-1} (Naumann et al, 1996) diminished after exposure to Al_2O_3 and TiO_2 NPs, and disappeared when exposed to ZnO NPs (Figure 3.6). The peak at about 1696 cm^{-1}, which indicates the ν (C=O) of protonated carboxylic acid (Brandenburg and Seydel, 1996), disappeared after LTA was mixed with or adsorbed on each of the NPs. In the ATR spectra (Fig. 3a), the Al_2O_3 and ZnO NPs increased the absorbance at 1600 cm^{-1} and 1408 cm^{-1}. These two peaks were from the asymmetric and symmetric stretching (ν_{as} and ν_s) of COO^- respectively (Naumann et al., 1996; Omoike and Chorover, 2004; Jiang et al., 2004). It is possible that the ester bond of the D-alanine branch connected to the LTA was broken to form D-alanine acid when LTA attached to the NPs. Another possibility is that the carboxylic groups form inner-sphere complex with oxide metal center, enhancing ν_{as} and ν_s of COO^- (Gao et al., 2009). The increase in pH due to LTA adsorption on NPs (Table 3.2), and the similar decrease in ester carbonyl caused by NaOH (Figure 3.7), indicated that the hydroxyl groups may break the D-alanine off from the LTA chain. Free hydroxyl groups in solution can be produced by ligand exchange of LTA with surface hydroxyl groups of oxides, leading to the increase of pH. The amide bands in LTA spectra should be from the CH_3CONH^- group in the glucosamine branch. The IR absorbance band around 1220 cm^{-1} was from ν_{as} of phosphodiesters in the LTA long chain (Omoike and Chorover, 2004). The shoulder band at 1091 cm^{-1} was the ν_s of phosphodiester (Wong et al., 1991; Omoike and Chorover, 2004). We did not find any

obvious changes to the phosphodiester bond before and after NPs treatment. The intense peak at 1043 cm^{-1} were the combination of C-O, C-O-C and C-O-P stretching vibration (Omoike and Chorover, 2004; Badireddy et al., 2008).

There are several speculations on how LTA attaches to the oxide surface. The alanine and glucosamine groups (Figure 3.1a) were suggested to interact with the TiO_2 surface from a ^{31}P solid-state NMR study on LTA adhesion (Wickham and Rice, 2008). The glucosamine side chain may participate in hydrogen bonding, while the alanine side chain may have ionic bonds (Rice and Wickham, 2004). In FTIR studies on Gram-positive *Bacillus subtilis* or its extracellular polymeric, the phosphodiester was suggested to form an innersphere complex with the iron (hydr)oxides (Omoike and Chorover, 2004; Parikh and Chorover, 2006). In this work, the increase of pH (Table 3.2) and the possible hydrolysis of the alanine ester after mixing with NPs suggest the ligand exchange with the oxide surface hydroxyl groups. The phosphodiester groups are most likely the ligands exchanging with the surface hydroxyl groups and forming the P-O-metal bond, which was reported on the bacterial adhesion study on iron oxides (Omoike and Chorover, 2004; Parikh and Chorover, 2006), but was not detected in our study. However the current study cannot exclude the possibility of hydrogen bonding, ionic bonds, hydrophobic interaction, electrostatic force, and water bridging (Parikh and Chorover, 2006), which may be not IR sensitive.

3.4.4 LPS Adsorption on Oxide NPs Studied by FTIR

LPS are amphiphilic molecules with a hydrophobic lipid A region anchored in the outer membrane of Gram-negative bacteria and hydrophilic O-antigen extending into

aqueous solution (Figure 1.2 and Figure 3.1b). Between the lipid A region and O-antigen chain is the core oligosaccharide part, which often carries phosphate and carboxylic acid groups (Figure 3.1b). The shoulder peak at 1724 cm^{-1} (Figure 3.8) was the ν of COOH (Brandenburg and Seydel, 1996; Jiang, 2004). Absorbance at amide area from 1500 cm^{-1} to 1700 cm^{-1} was from the protein in the LPS sample (the sample contains up to 10% of protein). The sugar bands at 1074 cm^{-1} (Brandenburg and Seydel, 1996) shifted to lower wavenumber after attaching to ZnO NPs (Figure 3.8a). This is due to the weakening of the C-O bond caused by an increase in the degree or strength of hydrogen bonding with oxides (Brandenburg and Seydel, 1996). In the DRIFT spectra, Al_2O_3 and TiO_2 NPs increased the IR absorbance around 1456 and 1148 cm^{-1} (Figure 3.8b), which are the C-H deformation and sugar C-O, C-C vibrations, respectively (Bellamy, 1975; Brandenburg and Seydel, 1996). Thus, the chemical environment of the O-antigen sugar chain is likely changed after LPS attaches to oxide NPs. Our IR observation was supported by previous studies that showed binding of LPS to oxide surfaces via O-antigen function groups (Jucker et al., 1997; Parikh and Chorover, 2008). Hydrogen bonds were detected when LPS adsorbed on TiO_2, Al_2O_3 and SiO_2 particles (Jucker et al., 1997). Most likely the O-antigen part was responsible for the interactions with oxides through hydrogen bonding.

3.4.5 NP-induced PE Chemical Structural Damage

PE is the principal bacterial phospholipid. In Figure 3.9a and b, the strong absorption at 1740 cm^{-1} was from the ν (C=O) of ester carbonyl (Lewis and McElhaney, 1996). The observed PE C=O stretching band has been shown to be a summation of at least two major components that are usually near 1738-1742 cm^{-1} and 1724-1729 cm^{-1},

reflecting the differences in the degrees of hydration or hydrogen bonding to the ester carbonyl groups (Lewis et al., 1998; Greenhall et al., 1998). ZnO NPs slightly shifted ν (C=O) from 1740 to 1736 cm^{-1}, whereas zinc ions caused no shift (Figure 3.9b). The shift may be due to the hydrogen-bonding of the ester carbonyl group to ZnO NP surface (Greenhall et al., 1998). The ν (C=O) remained in the ester frequency region (Bellamy, 1975; Socrates, 2001) and ν (COO^-) bands did not show after NP exposure (Figure 3.9a and b), indicating that the ester bond was not broken by the NPs.

The bands at 1636 and 1533 cm^{-1} (Figure 3.9) were due to deformation of RNH_3^+ or RNH_2 (Bellamy, 1975; Socrates, 2001). The band at 1636 cm^{-1} disappeared when PE adsorbed on the three NPs, due perhaps to the interaction of the PE amine moiety with the oxide surface. The new peak formed at 1616 cm^{-1} when PE adsorbed on ZnO NPs (Figure 3.9b) was the N-H deformation band from hydrochlorides of simple amine (Bellamy, 1975), indicating that the PE amine moiety may interact with the ZnO surface hydroxyl groups. The region from 980 to 1050 cm^{-1} should be from NH_3^+ rocking (Socrates, 2001). All these bands did not shown on the IR spectra of phospholipids with $R\text{-}N(CH_3)_3^+$ moieties (Kinder et al., 1997; Greenhall et al., 1998). ZnO also caused the disappearance of band of 980-1050 cm^{-1}. Adding NaOH to the PE film reduced the peak at 980-1050 cm^{-1}, 1636 and 1533 cm^{-1} (Figure 3.10), supporting that they were all related to amine moiety.

The IR band between 1300 and 1500 cm^{-1} was mainly due to C-H deformation (Bellamy, 1975; Socrates, 2001). The peak at 1468 cm^{-1} was assigned to the CH_2 scissoring; peak at 1416 cm^{-1} was from α-CH_2 (attached to CO or PO) scissoring (Kiwi and Nadtochenko, 2005). The asymmetric and symmetric bending vibration (δ_{as} and δ_s)

of CH_3 had two peaks at 1457 and 1378 cm^{-1} (Kinder et al., 1997; Kiwi and Nadtochenko, 2005). The bands near 1367, 1354, and 1341 cm^{-1} were especially useful for conformational analysis (Maroncelli et al., 1982; Lewis et al., 1994; Cieslik-Boczula et al., 2008). These bands were assigned to the wagging vibrations of methylene fragments in the kink (gauche-trans-gauche (gtg)), double-gauche (gg), and end-gauche (eg) conformations, respectively (Figure 3.9c). The 1378 cm^{-1} (CH_3 umbrella) vibration was not sensitive to conformational order changes. After PE sorbed on the ZnO NPs, the band at 1341 cm^{-1} disappeared (Figure 3.9c), suggesting a low concentration of end-gauche (eg) conformers. The intensive bands at 1362 cm^{-1} were a combination of gtg and gg bands (Figure 3.9c), revealing increases in the gtg and gg populations. Compared to the untreated PE sample, PE adsorbed on ZnO NPs showed highly disordered states, due to the wagging vibration of the gauche-rich alkyl chains (Cieslik-Boczula et al., 2008).

Absorption bands between 1200 and 1250 cm^{-1} (Figure 3.9a and b) resulted from the ν_{as} of PO_2^- in phosphodiester (Omoike and Chorover, 2004). The frequency is at about 1220 cm^{-1} when the phosphodiester group is fully hydrogen-bonded, and at 1240 cm^{-1} and above when the phosphodiester group is nonhydrogen-bonded (Wong et al., 1991). Adding NaOH to PE reduced nonhydrogen-bonded phosphodiester at 1248 cm^{-1} (Figure 3.10a). In Figure 3.9b, the nonhydrogen-bonded phosphodiester increased after adsorbing onto ZnO, splitting the peak. It was reported that after binding with metal cations, hydration of PO_2^- diminished due to the replacement of water molecules (Brandenburg et al., 1997), PO_2^- frequency shifted upwards for Mg^{2+} (Brandenburg et al., 1997), and a doublet peak formed for Ca^{2+} (Parikh and Chorover, 2007). In the current research, the Zn^{2+} caused a more obvious increase of nonhydrogen-bonded phosphodiester (Figure

3.9b). ZnO NP dissolution and release of Zn^{2+} has been widely reported (Franklin et al., 2007). Therefore, Zn^{2+} dissolved from ZnO NPs likely bonded to the phosphodiester and hindered the hydrogen bond formation between phosphodiester and water molecules. The ν_s of PO_2^- at 1094-1084 cm^{-1} (Lewis and McElhaney, 1996; Kinder et al., 1997) overlapped with the bands arising from C-N, C-O, C-O-C, and C-O-P stretching modes (Socrates, 2001; Parikh and Chorover, 2006), but had a shoulder peak at 1091 cm^{-1} (Figure 3.9b). Due to the diminishing peak at 1078 cm^{-1} after PE adsorbing on ZnO, a sharp ν_s (PO_2^-) peak emerged at 1091 cm^{-1} (Figure 3.9b). The formation of two new peaks at 1111 and 976 cm^{-1} on both ATR and DRIFT spectra after ZnO NP exposure corresponded to the ν_{as} and ν_s of deprotonated PO_3^{2-} groups, respectively (Bartl et al., 1998; Socrates, 2001; Jiang et al., 2004; Parikh and Chorover, 2006), indicating part of the PO_2^- group in phosphodiester was converted into terminal phosphoryl PO_3^{2-} groups (Figure 3.9d). After acidification these two peaks disappeared due to the protonation (Figure 10b). Since Zn^{2+} ions did not induce two such peaks (Figure 3.9b), ZnO NPs were responsible for breaking the phosphate ester bond. The new peak at 1030 cm^{-1} could be assigned to ν (C-C-O) of $R_1R_2CHCH_2OH$ after the phosphodiester group breaks between glycerol and phosphate moiety (Socrates, 2001). The ν_s (P-O-C) at 756 cm^{-1} (Socrates, 2001) decreased substantially after adsorbing on ZnO NPs (Fig. 5b). Another new peak at 937 cm^{-1} may be assigned to the ν_s of PO_4^{3-} (Persson et al., 1996; Jiang et al., 2004), which may form from the fall-off of terminal phosphoryl groups. The breaking of the phosphodiester bond and fall-off phosphate groups would change the amphiphilic character of the PE molecule, which may lead to the disorder of alkyl chains reflected by the CH_2 wagging spectra (Figure 3.9c). The absorbance at 1171 cm^{-1} was from ν_{as} of C-

O-C in esters (Socrates, 2001), mixing with the ZnO increased the intensity of this band (Figure 3.9). The absorbance at 1063 cm^{-1} was assigned to the ν_s of C-O-C (Greenhall et al., 1998; Kiwi and Nadtochenko, 2005) and emerged due to the diminishment of absorbance at 1078 cm^{-1}. The peak at 1078 cm^{-1} was assigned to ν (P=O) (Badireddy et al., 2008) and its reducing may be from the phosphodiester breaking or phosphate moiety adsorption on ZnO.

3.4.6 Biomolecular Structural Changes and the Bacterial Cytotoxicity

In the bacterial structure (Figure 1.2), LPS and LTA are both amphiphilic biopolymers with the hydrophobic side embedding in the membrane and the hydrophilic side extending from the intact cell into aqueous solution. When bacteria approach a surface, or small particles are attracted to bacteria, LTA or LPS are most likely the first contact with the surface/particles. These two biopolymers did adsorb on the NPs in this study. LTA adsorbed on the NPs by ligand exchange, and LPS adsorbed on the NPs via hydrogen bonding. Such bonding did not seem to damage the biomolecules or cause direct cytotoxicity because this is similar to the way in which bacteria adhere to surfaces through LPS or LTA polymers in the natural environment (Neu and Marshall, 1990). The D-alanin branch may fall off from the LTA chain during NP exposure. The effect of this structural change in LTA on bacterial cells is unclear because the function of the D-alanin branch is largely unknown. D-alanine deficient LTA bacterial mutants were reported to lose the ability to adhere to polystyrene, glass, and metal oxide surfaces (Neuhaus and Baddiley, 2003). Thus, the break-off of the D-alanin branch may have long-term effects on bacterial activities but not cause acute toxicity. However, the small size and large

surface area of NPs may increase their interaction with cell surface biopolymers comparing to the large surfaces in nature (Nel et al., 2006).

The cytotoxicity-related changes most probably depend on damage to proteins and phospholipids. The different types of proteins on the outer membrane and cell surface have important roles in cell physiological activities. The outer membrane proteins and some cell surface proteins are unlikely to interact with the large surface of large particles, because they are hidden behind the O-antigen layer of the LPS (Jucker et al., 1997). Their chances of exposure to NPs may be increased, however, because the small size of the NPs enable them to enter the gaps between the long biopolymer chains. When proteins adhere to particles or solid surfaces, their secondary structures may change (Buijs et al., 1996; Vertegel et al., 2004; Strehle et al., 2004) and partial protein unfolding may occur (Wu and Narsimhan, 2008). In this study, bacterial proteins showed a decrease in β-sheet content after exposure to the NPs. In these conditions, outer membrane proteins or surface proteins may be damaged and cell physiological activities may be affected as well, which may be a possible reason for NP cytotoxicity. The phospholipid membrane is also protected by cell surface biopolymers and usually does not attach to the particles or surfaces during normal bacterial adhesion processes in the environment. All three of the NPs changed the spectra of PE, with the ZnO NPs causing the most significant change, a result consistent with the toxicity assessment data in Chaper 2, which showed the higher toxicity of ZnO NPs than Al_2O_3, TiO_2, SiO_2 NPs and zinc ions (Figure 2.1). ZnO NPs might break PE chemical structure, leading to the highly disordered conformation of the alkane chain as revealed by the IR spectra. Our results also indicate changes in PE molecular hydrophobicity and loss of membrane integrity, possibly causing the rupture of

the membrane and the leakage of the periplasm. Because many important cell physiological activities occur in the periplasm, damage to phospholipid structure may lead to bacterial cell death.

3.5. Conclusions

Exposure to Al_2O_3, TiO_2 and ZnO NPs changed the IR spectra of bacterial cells, LTA, LPS, proteins and PE. Important bacterial biomolecules can adsorb on oxide NP surfaces during NPs exposure. LTA and LPS were good adhesins, binding to the oxide NPs in a manner that is similar to the way that these two biomolecules allow bacterial cells to bind to a solid surface in the environment. However, protein structural changes and phospholipid molecular damage, which were evident from the FTIR spectra of these biomolecules, were more likely reasons for NP bacterial toxicity. ZnO NPs, the most toxic in the three NPs, caused the most serious molecular damage to PE. If similar types of binding occur between NPs and mammalian cells, such interactions may represent another mode by which NPs could cause toxicity. In future work, imaging techniques will be needed to more carefully and directly probe cellular structural damage associated with NP exposure.

Table 3.1. Intensity ratio of β-sheets/α-helices

	Control	Al_2O_3	TiO_2	ZnO
B. subtilis	1.437	1.404	0.901	0.912
E. coli	1.427	0.823	0.824	1.207
P. fluorescens	1.700	1.048	1.106	1.164
Protein G	1.476	1.432	1.409	1.400

The intensity ratio of β-sheets/α-helices in the 2nd derivative spectra can represent the intensity ratio of original spectra (Figure 3.4).

Table 3.2. The pH changes after LTA exposed to NPs

	Before exposure		pH of NP and LTA mixture (After 2 hrs exposure)
	pH of NP suspension	pH of LTA solution	
Al_2O_3	6.52	6.59	7.43
TiO_2	6.43		7.02
ZnO	7.04		7.65

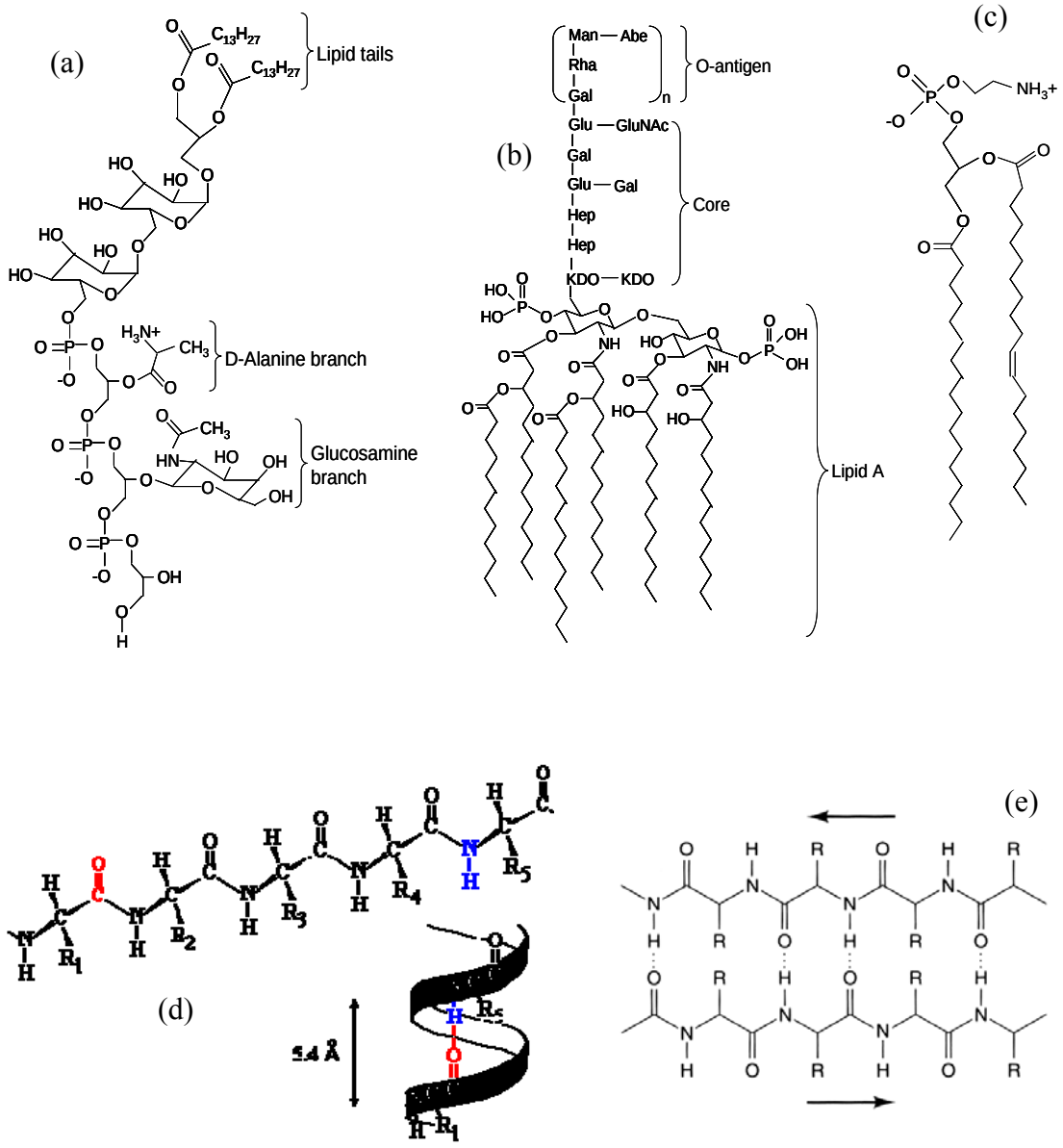

Figure 3.1. Chemical structures of lipoteichoic acid (a), lipopolysaccharide (b), phosphatidyl-ethanolamine (c), protein α-helix (d) and β-sheet (e).

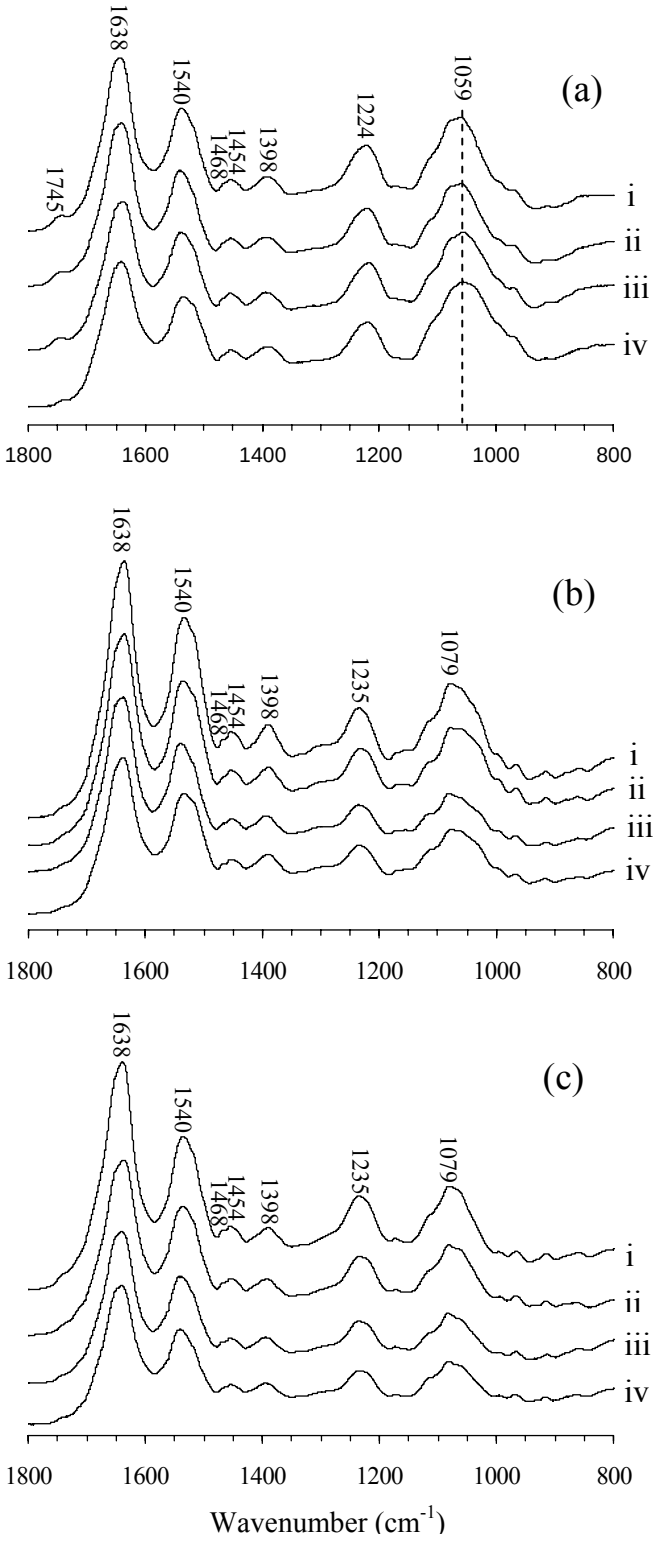

Figure 3.2. ATR-FTIR spectra of *B.subtilis* (a), *E.coli* (b) and *P. fluorescens* (c). (i) Bacterial cells only; (ii) bacterial cell and TiO_2 NPs mixture; (iii) bacterial cells and Al_2O_3 NPs mixture; (iv) bacterial cells and ZnO NPs mixture.

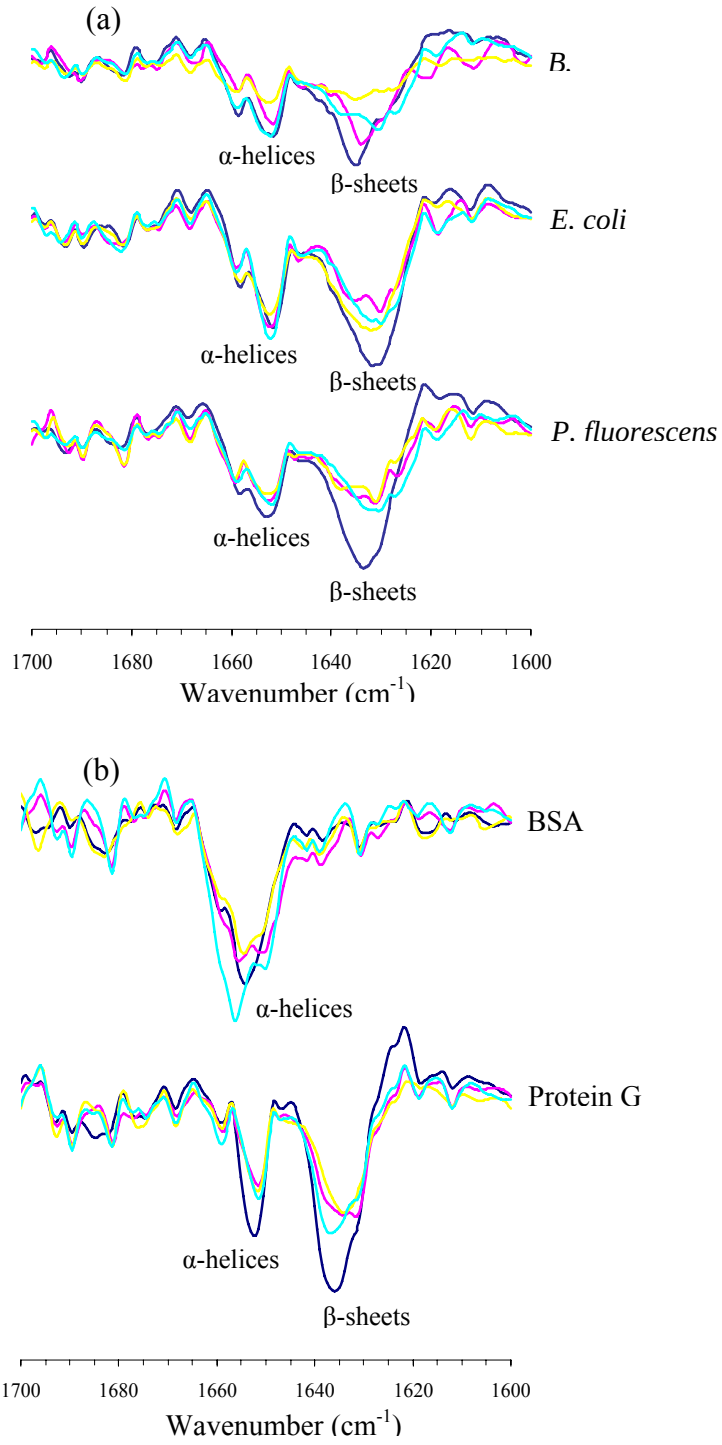

Figure 3.3. Second derivative to the amide I band of bacteria (a) and protein (b).
— Bacteria or protein only; — Mix with TiO_2 NPs;
— Mix with Al_2O_3 NPs; — Mix with ZnO NPs;

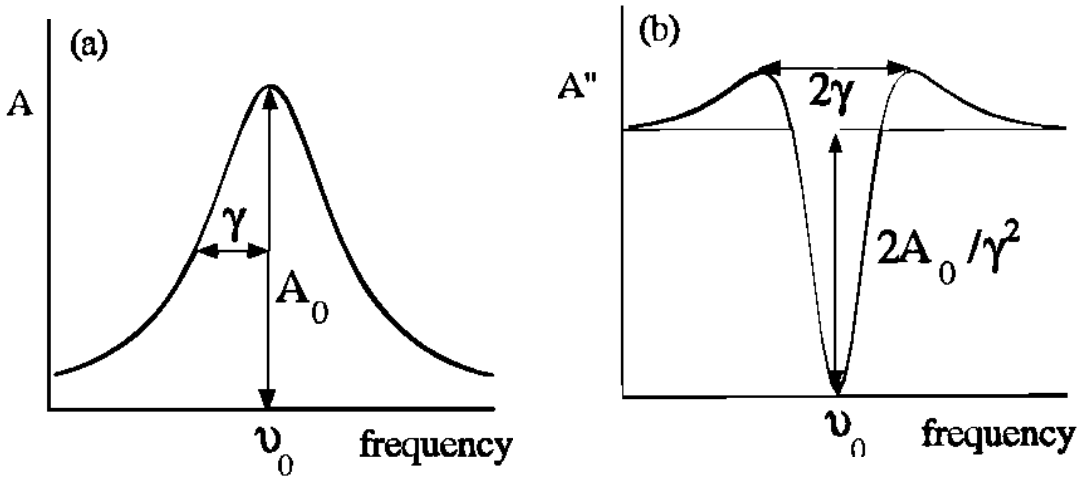

Figure 3.4. Lorentz shape of (a) original IR spectrum and (b) 2nd derivative spectrum (Buijs et al., 1996).

Assuming IR bands have a Lorentz shape, the intensity of an infrared absorption peak $A(\nu)$ can be expressed as $A(\nu) = A_0\gamma^2/[\gamma^2 + (\nu - \nu_0)^2]$, where A_0 is the maximum absorbance of the band, ν_0 is the frequency of the maximum, and γ is the half-width at half-height. h is the peak intensity on the 2nd derivative spectra, $h = 2A_0/\gamma^2$.[14] When peak width is consistent, the intensity ratio of β-sheet/α-helices can be presented as $\frac{A_{0(\beta)}}{A_{0(\alpha)}} = k\frac{h_{(\beta)}}{h_{(\alpha)}}$. Therefore the intensity ratio on the 2nd derivative spectra can represent the intensity ratio of original spectra.

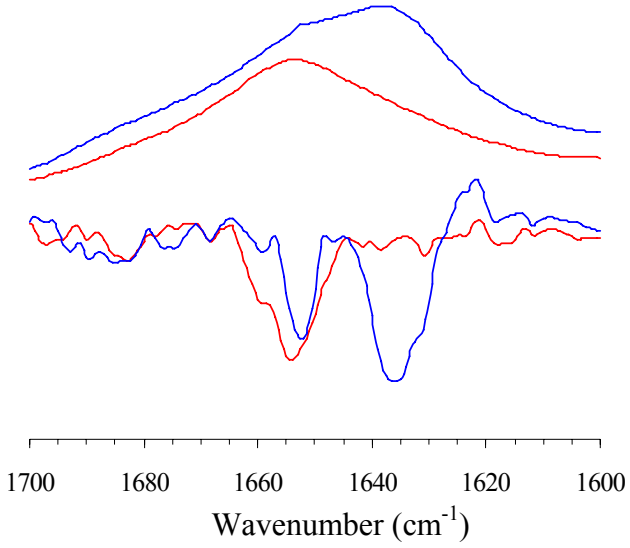

Figure 3.5. Amide I band of BSA (red) and protein G (blue). The upper traces are the original spectra, and the lower traces are the 2nd derivative spectra.

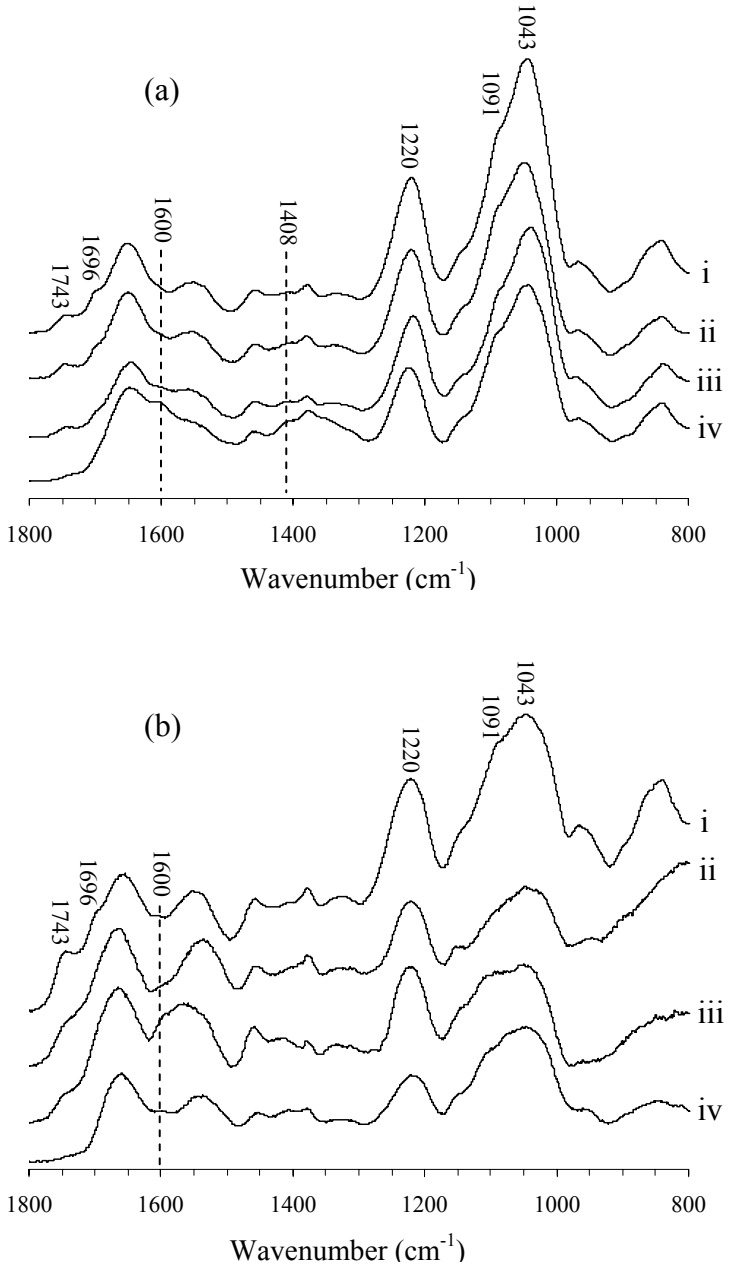

Figure 3.6. ATR-FTIR (a) and DRIFT (b) spectra of LTA. (i) LTA only; (ii) LTA mix with/adsorbed on TiO_2 NPs; (iii) LTA mix with/adsorbed on Al_2O_3 NPs; (iv) LTA mix with/adsorbed on ZnO NPs.

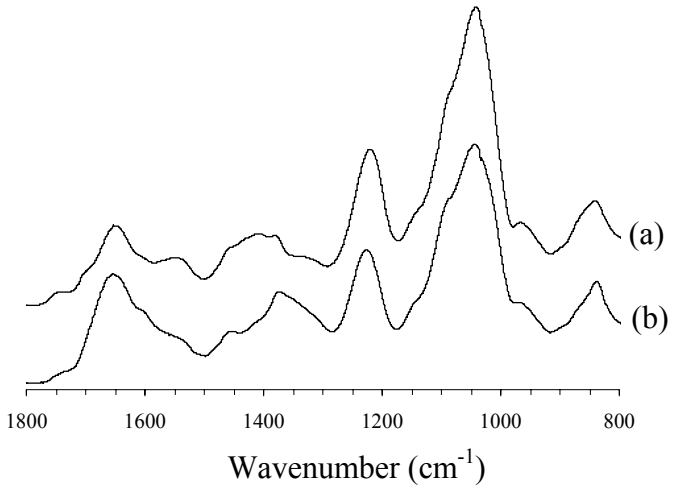

Figure 3.7. ATR-FTIR spectra of LTA (a) and adding 0.01 *M* NaOH to LTA (b) film.

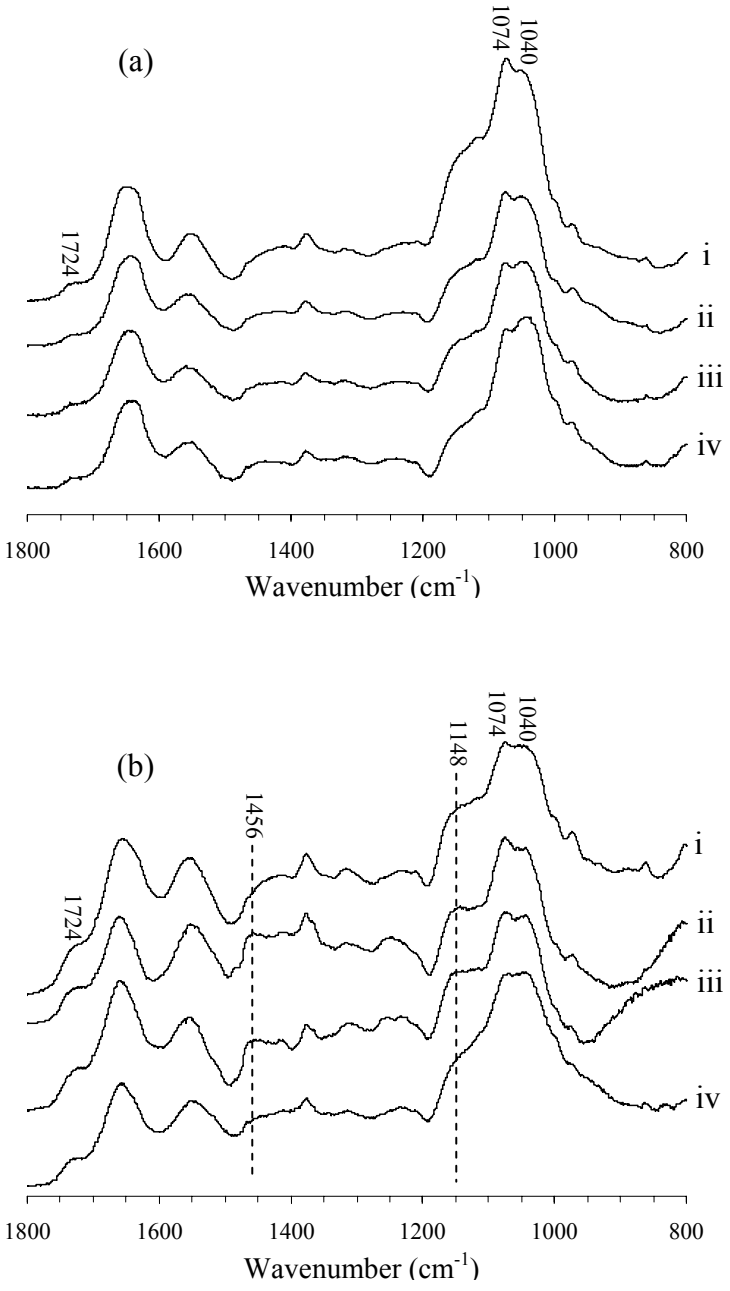

Figure 3.8. ATR-FTIR (a) and DRIFT (b) spectra of LPS. (i) LPS only; (ii) LPS mix with/adsorbed on TiO_2 NPs; (iii) LPS mix with/adsorbed on Al_2O_3 NPs; (iv) LPS mix with/adsorbed on ZnO NPs.

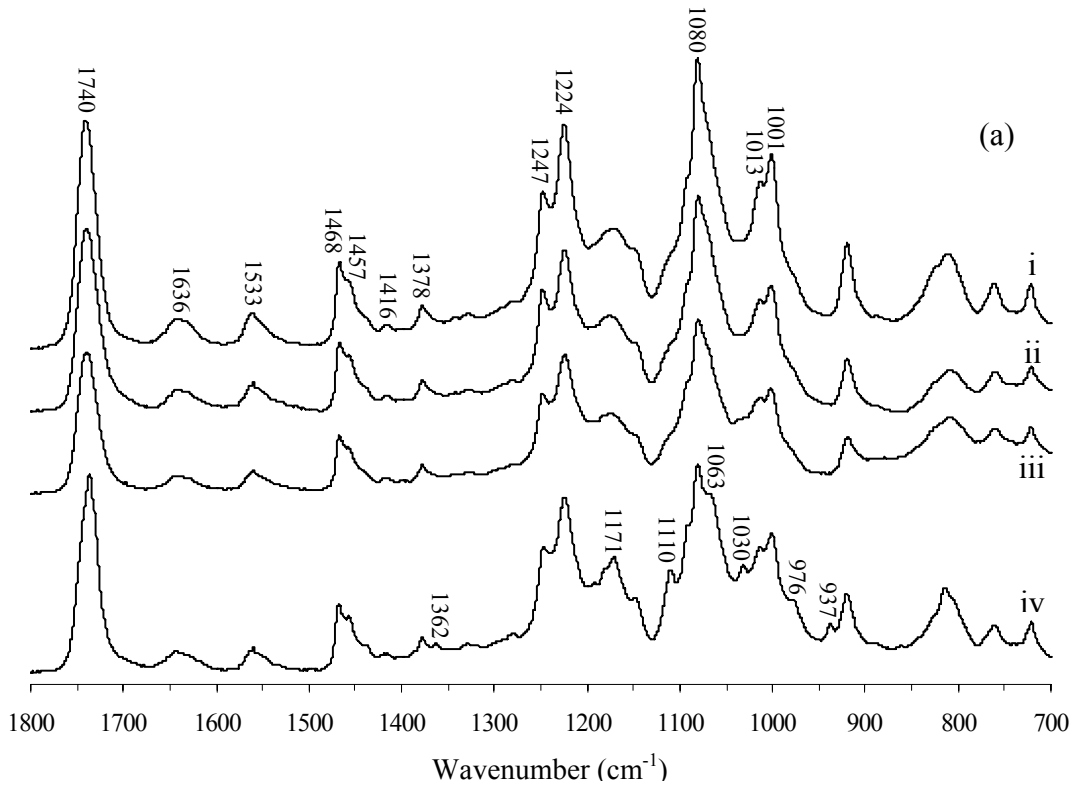
(a)
1740
1636
1533
1468
1457
1416
1378
1247
1224
1080
1013
1001
1063
1030
1171
1110
976
937
1362
i
ii
iii
iv
1800
1700
1600
1500
1400
1300
1200
1100
1000
900
800
700
Wavenumber (cm-1)

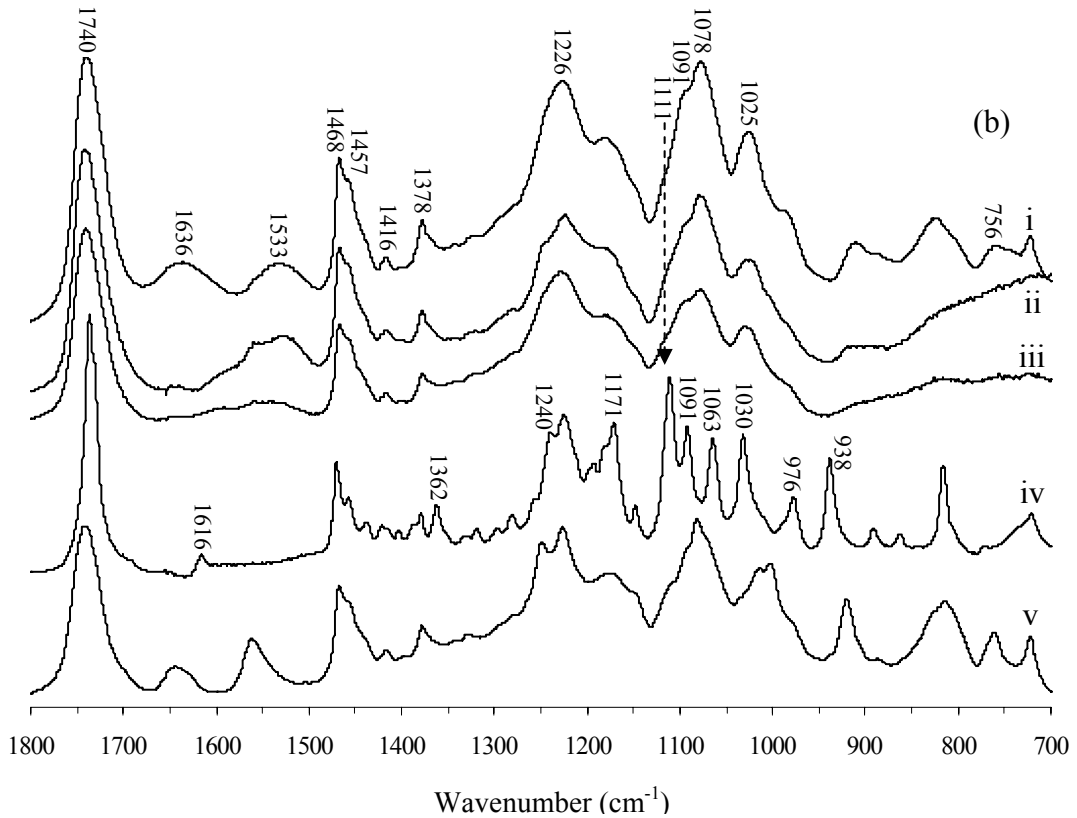
(b)
1740
1636
1533
1468
1457
1416
1378
1226
1111
1091
1078
1025
756
1240
1171
1091
1063
1030
976
938
1362
1616
i
ii
iii
iv
v
1800
1700
1600
1500
1400
1300
1200
1100
1000
900
800
700
Wavenumber (cm-1)

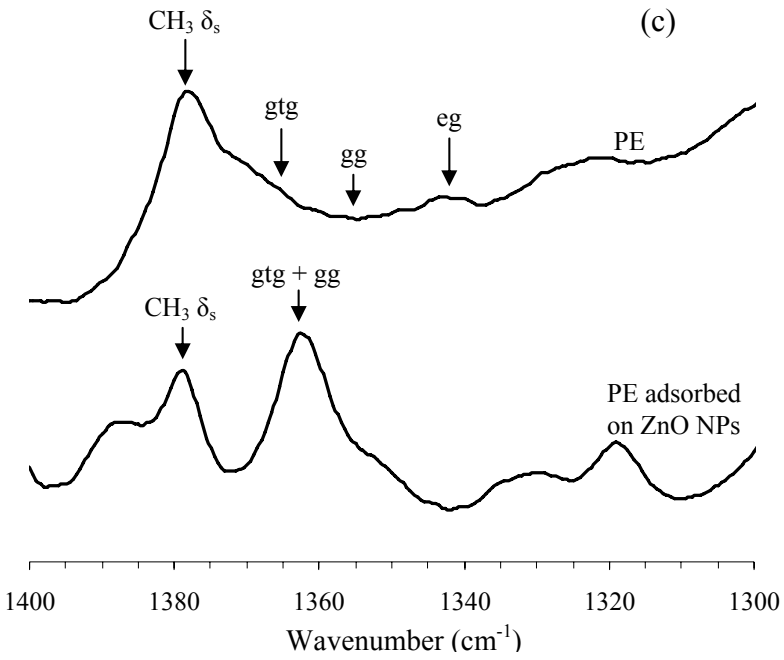

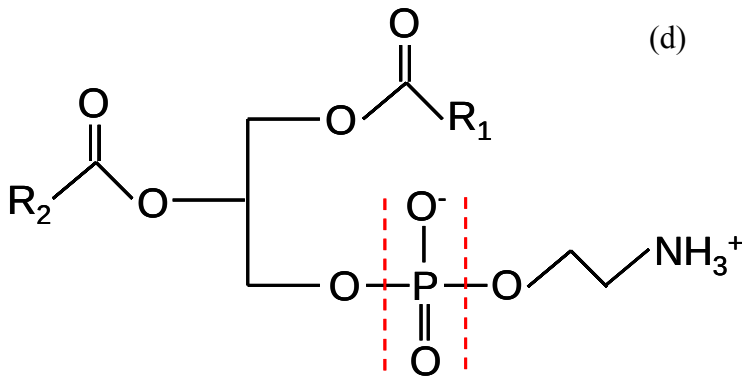

Figure 3.9. ATR-FTIR (a) and DRIFT (b) spectra of PE. (i) PE only; (ii) PE mix with/adsorbed on TiO_2 NPs; (iii) PE mix with/adsorbed on Al_2O_3 NPs; (iv) PE mix with/adsorbed on ZnO NPs; (v) PE mix with $ZnCl_2$. DRIFT spectra of CH_2 wagging region was enlarged to show the disorder of alkyl chain (c) after adsorbed on ZnO NPs. ZnO NPs may break the bond of phosphodiester (d).

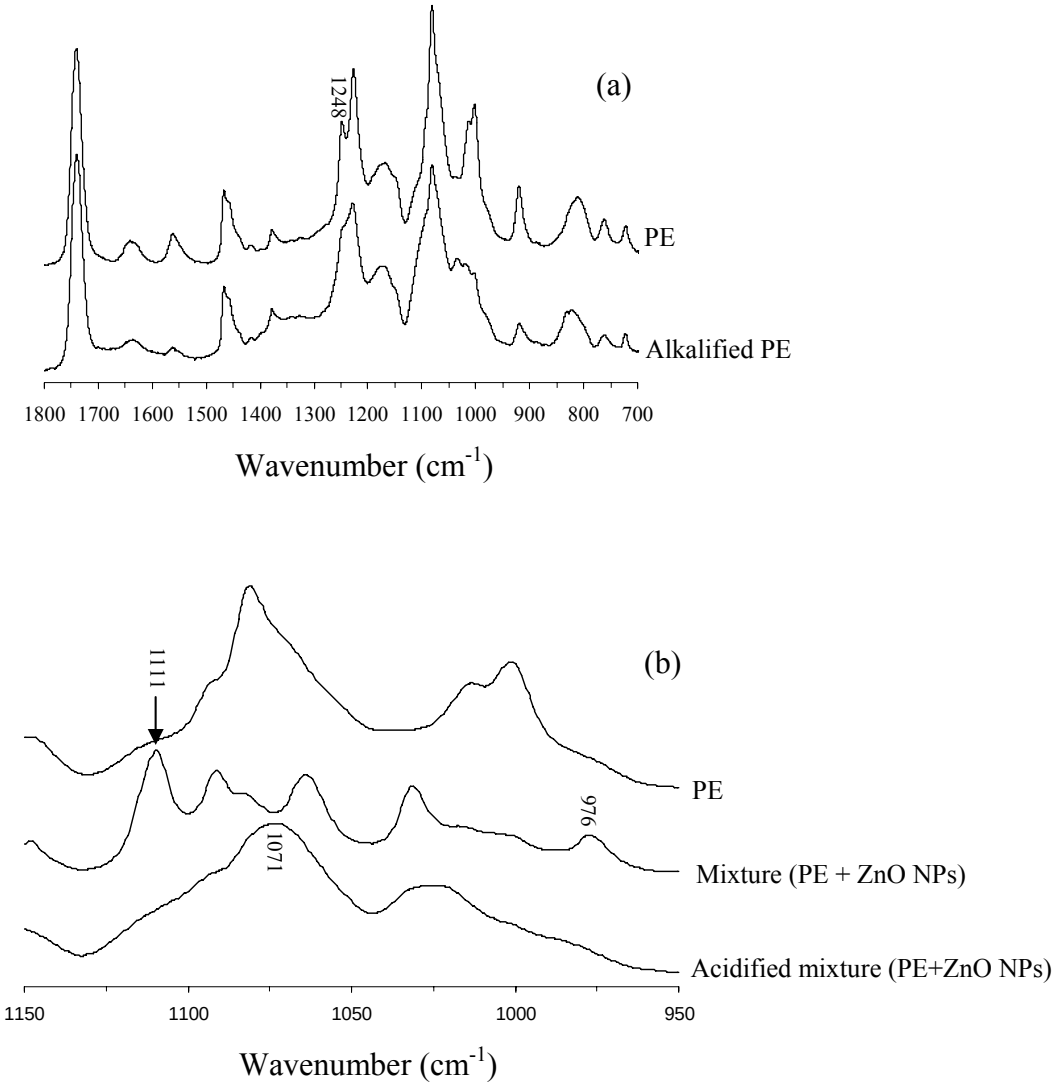

Figure 3.10. ATR-FTIR spectra of PE and alkalified PE by adding 0.01 *M* NaOH to PE film (a). Phosphoryl group region of PE, PE mixed with ZnO NPs and the acidified mixture by adding 0.01 *M* HCl (b). The deprotonated PO_3^{2-} band (1111 cm^{-1} and 976 cm^{-1}) disappeared after acidification due to full protonation.

CHAPTER 4

EFFECTS OF OXIDE NANOPARTICLES ON MICELLES AND VESICLES OF BACTERIAL MEMBRANE AMPHIPHILIC BIOMOLECULES

4.1 Abstract

Lipopolysaccharide (LPS) and L-α-Phosphatidyl-ethanolamine (PE) are amphiphilic biomolecules that are key constituents in the outer cell membranes of Gram-negative bacteria. Here, LPS and PE micelles and vesicles are studied as cell membrane models to evaluate nanoparticle (NP) effects on membrane structure. Using atomic force microscopy (AFM) and sorption experiments, we find that LPS vesicles are dispersed by Al_2O_3 and TiO_2 NPs because of the strong adsorption of LPS polysaccharide chains on oxide surfaces. LPS molecules coat on the Al_2O_3 NPs as a 40-100 nm layer, while aggregate together with TiO_2 NPs on AFM images. The increases of pH, ionic strength and sulfate concentration inhibit the adsorption of LPS molecules on NPs. The features of PE vesicles are changed after exposing to NPs. Al_2O_3 NPs induce large multilamellar vesicles, while ZnO NPs convert vesicles to small spots due to PE molecular breakup. The aqueous stability of PE is disturbed when adding NPs, but is enhanced by increasing pH. The interaction between NPs and membrane amphiphilic biomolicules may affect membrane fluidity, integrity and lateral organization, which is important for NP safety evaluation and for new NP designs in biological and biomedical applications.

4.2 Introduction

The interactions of nanomaterials with cells and lipid bilayers are an important research area because such interactions are critical in many applications such as medical imaging, drug delivery, disease diagnostics, DNA/protein structure probing (Salata, 2004; Verma and Stelacci, 2010). More and more nanomaterials are designed for biological applications, and this raises new concerns about the safety of nanotechnology (Nel et al., 2009). The small size, high surface curvature, large surface area, and abundant surface reactive sites may induce special reactions on the bio-surface (Kaufmann and Tanaka, 2003; Nel et al., 2006). The effect of NPs on microbes in the environment is one area of concern because of the crucial roles of microbes for ecosystem function and productivity. Cell membranes are the most important biological surfaces that nanomaterials interact with whether for nanomaterial applications or for safety assessments. Membranes make life possible by allowing cells to create an internal environmental different from that outside (Pollard and Earnshaw, 2004). All biological membranes are bilayers of lipids, and details of the interactions of NPs with such lipids are important to understand. In this work, lipopolysaccharide (PE) and L-α-phosphatidyl-ethanolamine are used as the model lipids to investigate NP-membrane interactions. These lipids have been chosen because they are the major components of the Gram-negative bacterial outer membrane. Chapter 2 and 3 have shown that NP attachment to the outer membrane of bacteria can led to changes in chemical structures of lipid molecules and in some case cell death. In this current study we seek to further understand the NP-induced structural changes caused to lipid bilayers.

LPS and PE are both amphiphilic biomolecules with hydrophobic tails and hydrophilic polysaccharide or phosphate-amine head groups (Figure 4.1, A&B). These molecules form micelles and vesicles in aqueous solutions (Figure 4.1). In comparison to the real cell membrane, the vesicles contain simpler components, but have similar properties such as lateral fluidity, bending rigidity, and a hydrophilic-hydrophobic-hydrophilic sandwich structure. Such vesicles have been used as model systems to better understand cell membranes (Laurencin et al., 2010). In addition, the interactions of intact vesicles with NPs and the associated vesicle stability have their specific research importance. Intracellular vesicular membranes and membrane-containing organelles are throughout eukaryotic cells. Vesicle-NP interactions are thus important for understanding not only extracellular events but also intracellular events that might be trigged when NPs penetrate into or are engulfed by cells.

Interactions between lipids and oxide surfaces have been explored in several studies on solid-supported lipid bilayers. The stability of the adsorbate and strength of the attachment are related to the nature of both the lipid and surface (Fortunelli and Monti, 2008). Phosphate and carbonyl oxygens are reported to bond to the rutile TiO_2 surfaces by very stable oxygen-bearing moieties (Fortunelli and Monti, 2008). Strong bonding to the substrate surfaces is likely to cause lipid bilayers to lose lateral fluidity. Some other support materials, however, retain a 1-2 nm water gap between lipid head groups and the substrate surface. For example, the mobile fraction of lipids on alumina is 85%, and there is a more tightly bound water layer at the alumina surface compared to silica (Morgan et al., 2008). The balance between adhesion energy and a vesicle's curvature energy is determinant for adsorption, deformation, and rupture of the vesicle (Richter et al., 2006).

While these previous studies provide insight into lipid interactions with a variety of materials, the small size of NPs adds additional complexity to the interactions. The curvature of NP surfaces are likely to be involved in the energy balance of adhesion and bilayer bending/tension. Curved supported substrates surface are reported to induce vesicle rupture more easily than flat oxide surfaces (Kaufmann and Tanaka, 2003). Also, the small NPs can enable them to be engulfed by vesicles (Bihan et al., 2009), or coat the vesicle surface causing membrane reconstruction (Wang, et al, 2008) and vesicle instability in solution.

To understand how NPs influence vesicle properties, we have chosen to study how the most commonly engineered NPs, Al_2O_3, TiO_2 and ZnO, interact with LPS and PE lipids. Atomic force microscopy (AFM) is used to probe changes in the vesicle and micelle structures of LPS and PE. The specific objectives in this study were to examine 1) lipid vesicles/micelles morphology changes induced by NPs; 2) vesicle/micelle stability in solution; and 3) the effects of pH, ionic strength and electrolyte type on the interaction between vesicle/micelles and NPs.

4.3 Materials and Methods

4.3.1 Chemicals and Materials

Aluminum oxide (with a mean diameter of 60 nm, and BET surface area of 208 m^2/g), titanium oxide (50 nm, BET surface area 325 m^2/g) and zinc oxide (20 nm, BET surface area 54 m^2/g) NPs were purchased from Zhejiang Hongsheng Material Technology Co., China. The NP powders were dispersed in distilled deionized (DI) water (Millipore, resistivity =18.3 MΩ/cm) to make stock suspensions of 2,000 mg/L. The mica

surface, two-side polished sapphire planar surface (10×10×0.5 mm, MTI Corporation), premium high-resolution tapping mode silicon probes (MPP-11100-10, Veeco) were purchased for AFM scanning.

The LPS used in this study was extracted from *E. coli* O55:B5, and PE was also extracted from *E. coli*. Both were lyophilized powders bought from Sigma Aldrich and used without further purification. LPS was dissolved in DI water to make 2000 mg/L stock solution. To prepare aqueous PE solution, the 200 mg/L PE in DI water was bath-sonicated for 30 min, then diluted to the needed concentration, and bath-sonicated again before measurement/treatment.

4.3.2 AFM Imaging

For AFM studies, freshly cleaved mica or sapphire wafer was vertically placed in LPS/PE solution or their mixtures with NPs for 30 min, to allow the sorption of NPs and biomolecules on the mica surface. Then the mica or sapphire wafer was dipped in DI water several times to remove the weakly sorbed biomolecules or particles, and was then air dried in a dust-free environment. The samples were then examined with a Dimension 3100 AFM instrument (Digital Instruments). Tapping mode AFM measurements were carried out with a silicon cantilever auto-tuned in the 0 to 300 kHz frequency region.

4.3.3 Zeta Potential Measurement

Zeta potentials of 200 mg/L LPS, PE and NPs were measured by a zetasizer (Brookhaven Instrument Ltd.) at 25 °C. For the measurements, LPS was diluted in 0.01 *M* NaCl, PE in DI water, and NPs in both DI water and 0.01 *M* NaCl. Then, each solution

was put into an ultra-sonicated bath to disperse aggregates before measurement. All the samples were divided into aliquots and adjusted to various pH values from 3 to 10 by 0.01 *M* HCl or NaOH solutions. The exact pH values were measured again after zeta potential measurements.

4.3.4 Adsorption and Stability Experiments

The adsorption isotherms of LPS to Al_2O_3 and TiO_2 NPs were obtained using batch experiments at 25 °C and pH 6.5 in 5 mL screw cap vials. Initial LPS concentrations were from 10 to 200 mg/L, using three replicates for each concentration, and the total volume was 4 mL. The adsorbent was 2 mg in each vial and was obtained by adding 1 mL of 2000 mg/L NP stock suspension while stirring. The vials with adsorbates and adsorbents were shaken on a shaker for 24 hours (Preliminary experiment showed the apparent equilibrium was reached before 16 hours). After centrifugation (3000 rpm, 30 min), supernatant was assayed by the phenol-sulfuric acid method (Dubois et al., 1956). Supernatant 1 mL was mixed with 0.5 mL of 5% (w/v) phenol in glass test tubes. Then, 2.5 mL of concentrated H_2SO_4 was added to each tube with slight shaking. Samples were left to stand for 10 min and then were kept at 30 °C for 20 min. The LPS concentration was measured by absorbance at 490 nm. The Freundlich model was employed to fit the experiment data:

$$S = K_f C_e^N$$

where K_f is Freundlich affinity coefficient; N is the Freundlich exponential coefficient; S is Equilibrium solid phase concentration; and C_e is Equilibrium liquid phase concentration.

Estimated model parameters and correlation coefficients (R^2) were determined by OriginPro 8. The initial concentration of 100 mg/L LPS was chosen to evaluate the adsorption at different pH values (4, 6 and 9), ionic strengths (0.01, 0.02 and 0.1 *M* NaCl) and electrolytes compositions (NaCl, $CaCl_2$ and $NaSO_4$).

PE (25 mg/L) was mixed with 50 mg/L Al_2O_3, TiO_2 and ZnO NPs at pHs 4, 6 and 9 to study the effects on PE vesicle stability. After 24 hrs of shaking at 25 °C and centrifugation, the PE concentration in the supernatant was quantified by a total organic carbon analyzer (TOC-5000A, SHIMADZU, Japan).

4.4 Results and Discussion

4.4.1 Effects of Al_2O_3 and TiO_2 NPs on LPS Micelle/Vesicle Structure and LPS Coating Layer on the Particle Surface

As an amphiphilic molecule, LPS forms micelles and vesicles in aqueous solution (Figure 4.2A). AFM images show that the edge of the spherical vesicles is thicker than middle, indicating the intact vesicles are attached on the mica surface (Figure 4.2B). The thicker border is due to more LPS molecules overlapping at the sphere's edge (Figure 4.2B). Vesicle rupture should cause an irregular shape of the LPS layer, and even thickness. The diameter of LPS vesicles is measured to be about 1.5 μm. The sizes of micelles varied from ≤ 100 nm to 300 nm. Previous reports found the diameters of the premicelle oligomers and large aggregates to be 119 and 190 nm respectively (Santos et al, 2003). The smaller "micelles" observed in Figure 4.2A may just be aggregates of several LPS molecules (Figure 4.1D), rather than strictly defined micelles. The comparably larger hydrophilic polysaccharide chain makes smaller aggregates stable in

water, which causes more random LPS aggregate constructions to be observed in solution. Moreover, the LPSs extracted from bacteria are a collection of molecules with different polysaccharide chain length (up to 50 nm) (Jucker et al., 1998), which is another reason for the varied micelle sizes.

Upon adding Al_2O_3 NPs into the LPS solution, a LPS layer is formed around Al_2O_3 NPs (Figure 4.2C), and the large LPS vesicle dissappear. The AFM sections crossing the NPs showed that the LPS layers are between 40 and 100 nm (Figure 4.2D), but the image cross sections cannot indicate if the LPS layers on the Al_2O_3 surface are ordered bilayers or just random LPS molecular/micelle aggregates. It is quite clear, though, that the larger LPS vesicles seen in the pure LPS solution (Figure 4.2A) are absent when the NPs are added (Figure 4.2C), suggesting that the NPs have disrupted the LPS vesicles. The formation of supported LPS bilayers around NPs may be difficult, because LPS O-antigen sugar chains attach to the oxide surface through hydrogen bonds (Jucker et al, 1997) as the supporting surface. Moreover, the heterogeneous length and composition of the LPS sugar chains would likely make it difficult for their lipid A tails to optimally arrange together.

The interactions of TiO_2 NPs with NPs were also studied by AFM. TiO_2 NPs do not readily attach to the negatively-charged mica surface, so a sapphire surface was used for the AFM measurements. Unfortunately LPS vesicles or micelles do not keep their shapes on the sapphire surface (Figure 4.3A), possibly due to stronger interaction between the aluminum oxide and LPS molecules. After mixing a 10 mg/L LPS solution with TiO_2 NPs, large aggregates are formed (Figure 4.3B). These aggregates on the AFM image are a mixture of NPs and LPS molecules, but their shapes and sizes are not

uniform. The large and non-uniform aggregates compared to Al_2O_3 NPs are due to the feature of TiO_2 NP aggregation in suspension (Chapter 2).

4.4.2 LPS-NPs Interactions Evaluated by Adsorption Isotherms

Isotherms can be used to represent the physical characteristics of LPS adsorption on Al_2O_3 and TiO_2 NPs surfaces (Figure 4.4A). The Freundlich equation was used for the isotherm fitting, resulting in the correlation coefficients (R^2) of 0.97 for the adsorption on the two NPs. The Freundlich affinity coefficient (K_f) is 5.128 for Al_2O_3 NPs, and 15.44 for TiO_2 NPs. The Freundlich exponential coefficient (N) for Al_2O_3 NPs is close to 1 (0.928), while it is much lower (0.387) for the TiO_2 NPs. The difference in N values is reflected in the isotherm shape, which is more linear for Al_2O_3 than for the TiO_2 NPs. Generally N decreases as adsorption strength increases (Hyung and Kim, 2008), therefore the adsorption of LPS on TiO_2 is stronger than on Al_2O_3 NPs. The LPS adsorption percentage on Al_2O_3 NPs is around 65% over the measured concentration range, while it decreased from 88% to 17% for the TiO_2 NPs over the same concentration range. In effect, Al_2O_3 NPs adsorbed more LPS than TiO_2 NPs at high C_e values, but less LPS when $C_e \leq 10$ mg/L.

The desorption of LPS from both NPs shows hysteresis. In fact, nearly no LPS desorbs within a 24-hour equilibration time. Such "irreversible" adsorption has been attributed to the multiple hydrogen bonds between LPS sugar chains and the oxide surface (Jucker, 1997, 1998). The longer the LPS O-antigen sugar chain, the more sugar monomer units hydrogen bonded to the surface, and the slower the desorption rates are, which is an idea illustrated schematically in Figure 4.4B. The LPS from *E. coli* O55:B5 is

a “smooth” form and has long polysaccharide chains (Ooi, 1991). The desorption experiments indicate that LPS molecules attach to the NPs very tightly. Such firm attachment may cause dispersion of LPS vesicles, or removal via flocculation of intact micelles/vesicles when the NPs attach to the micelles/vesicles and increase their gravity. Thus, only tiny aggregates remained in LPS solution after adding NPs (Figure 4.2C).

4.4.3 Effect of pH and Electrolyte on LPS-NP Interaction

The effects of pH, ionic strength and electrolyte type on LPS adsorption amount was also investigated. The adsorption on both Al_2O_3 and TiO_2 NPs is decreased under alkaline condition (Figure 4.5 A&B). The possible reasons could be that 1) hydroxyl groups on oxides are deprotonated, thereby diminishing the hydrogen bonding to the oxide surface, and/or 2) the zeta potential of the oxide surface is decreased (Figure 4.5C), changing the interaction force. Both of the factors could inhibit the approach of LPS to the oxide. The zeta potential of LPS nearly constant from pH 4 to 10. The point of zero charge (PZC) of Al_2O_3 NPs is 8.1, while the PZC of TiO_2 NPs is 5.7 in 0.01 *M* NaCl. However, low pH values (i.e. pH 4) do not increase the LPS adsorption amount on TiO_2 NPs even though the surface charge of TiO_2 NPs charges from negative to positive. The reverse of surface charge, which could conceivably cause electrostatic attraction between LPS and the TiO_2 NPs, does not create new adsorption sites.

High ionic strengths reduce LPS adsorption (Figure 4.5A&B), which means at least part of the LPS molecules are adsorbed onto the NPs by an outer-sphere interaction (Hayes et al., 1988). Water layers should exist between LPS and the particles. Compared to Na^+, Ca^{2+} increases the adsorption of LPS on TiO_2 NPs (Figure 4.5B). Calcium may

form a cation bridge between two negatively charged surfaces. The LPS molecules could attach to TiO_2 NPs through a Ca^{2+} cation bridge, and more adsorption sites might be created by the presence of Ca^{2+}. The possible Ca^{2+} cation bridge is not functional on positively charged Al_2O_3 NPs surface (Figure 4.5A). Instead, 0.01 *M* $CaCl_2$ slightly decreases adsorption on Al_2O_3 due to increased ionic strength, which is comparable to the adsorption in 0.02 *M* NaCl. The SO_4^{2-} ions inhibited the adsorption of LPS on both Al_2O_3 and TiO_2 NPs. SO_4^{2-} can adsorb on the positively charged Al_2O_3 surface through electrostatic interactions, thereby competing with the negatively charged LPS molecules. This phenomenon, however, does not explain the decreased adsorption on the negatively-charged TiO_2 surface in the presence of SO_4^{2-}. Presumably, Na_2SO_4 electrolyte decreases the LPS adsorption mainly through increasing ionic strength.

4.4.4 Effect of Al_2O_3, TiO_2 and ZnO NPs on PE Vesicle Structure

PE molecules exist as vesicles in the solution. The zwitterionic head groups of this lipid cause PE to interact with oxide surfaces while maintaining its bilayer structure (Mornet et al, 2005). Usually there is a water layer between the lipid head groups and the oxide surface (Xu et al.; 2009). Phospholipid vesicles in solution, however, were reported to form supported bilayers on mica surfaces (Radler 1995). Indeed, a PE bilayer coating changes the hydrophilic mica surface to hydrophobic (Figure 4.6A). Thus, PE coated mica slides float on water, and drops of water are not dispersed on the PE coated mica, whereas they are on un-coated mica (Figure 4.6A). AFM phase scanning on the PE coated mica showed dark patches with unclear borders (Figure 4.6B). Such patterns are not detectable in height images. The supported PE bilayers are formed from vesicle

deposition (Richter et al., 2006). The PE bilayer thickness is not even because vesicles overlap.

After mixing the PE solution with Al_2O_3, ZnO and TiO_2 NPs, changes are evident (Figure 4.6 B, C and D). Al_2O_3 NP exposure results in large and round vesicles, which can be detected in height images. These observations indicate that multilamellar vesicles form with detectable height on AFM image and that vesicles are not ruptured to form flat phospholipid bilayers. Even small vesicles have the detectable thicknesses. Probably Al_2O_3 NPs are wrapped by PE molecules. Previous work found that multiple supported lipid bilayers are formed on flat quartz, rutile and corundum surfaces (Oleson and Sahai, 2008). Thus, it is possible that similar PE bilayers surround the Al_2O_3 NP core. Forming of multilamellar vesicles or wrapping of the NP core by PE bilayers could accelerate the PE precipitation, which corresponds to the diminished PE concentration in the supernatant upon adding the Al_2O_3 NPs (Figure 4.7A).

The addition of ZnO NPs also changes how PE arranges on mica; very small spherical features are now observed (Figure 4.6D). Such small spots do not appear to have a vesicle-like structure. The work in chapter 3 has demonstrated that ZnO NP can break the phosphodiester bond of PE. After the phosphodiester bond is broken, PE is no longer an amphiphilic molecule and cannot form a bilayer structure. The small features observed in the AFM image might be evidence of this effect.

The addition of TiO_2 NPs results in more defined features on the mica surface (Figure 4.6E). These patterns do not appear on the height image, indicating that the PE is most likely organized as discrete collections of monolayers on the surface. A likely explanation for the change in going from the pure PE sample to the sample with TiO_2

NPs is the removal of some of the PE amount from the supernatant at neutral pH due to precipitation along with the NPs (Figure 4.7A). The reduced PE solution concentration allows the edges of individual PE layers to be seen (Figure 4.6E).

4.4.5 Effect of Al_2O_3, TiO_2 and ZnO NPs to PE Stability in Water

The aqueous stability of PE under different conditions is shown in Figure 4.7A. The original PE concentration was 25 mg/L for each treatment. Centrifugation decreases the supernatant PE amount significantly, even without adding NPs, and this makes sorption experiment difficult to perform. For pure PE and each NP treatment group, a high pH enhances PE's aqueous stability, while a low pH results in more precipitation (Figure 4.7A). The zeta potential of PE vesicles is negative over the entire measured pH range (Figure 4.7B). Thus, the greater PE stability at the high pH is an electrostatic effect – the vesicles electrostatically repel one another, which keeps them from aggregating and precipitating. A low pH has the opposite effect. PE precipitation is also induced by 0.01 *M* NaCl, which indicates that vesicle stability is sensitive to ionic strength. For this reason, all the comparisons were done in DI water. The differences in electrolyte types are not discussed.

All three NPs decrease PE supernatant concentrations at each pH value. These results reflect the interaction between the NPs and PE and possibly explain the vesicle structural changes in the AFM images. Among the three NPs, PE vesicles are more stable with TiO_2 at neutral and alkaline pH because both the vesicles and TiO_2 NPs are negatively charged. This result is consistent with the minimal changes observed to the PE vesicles in the AFM images. Almost no PE is adsorbed to TiO_2 NPs at pH 9. However, at pH 4 the

TiO_2 NPs exposure results in similar PE precipitation as observed with the other two NPs because TiO_2 is positively charged at this lower pH. ZnO NPs partially dissociate in water (Chapter 2), and low pHs can cause increased dissociation. Thus, we did not measure its zeta potential or test its effect on PE below pH 6. At neutral pH some dissociation occurs, and about 2 mg/L of Zn^{2+} can be detected in ZnO NP suspensions (Chapter 2). As indicated above, the phosphodiester bond of PE can be broken by ZnO NPs (Chapter 3), which may explain the lower amount of PE measured in the presence of ZnO particles. Breakage of the phosphodiester bond would result in the formation of an insoluble hydrocarbon chain that would then not be measured using the TOC analyzer. PE precipitation in the presence of the Al_2O_3 NPs is likely explained by the formation of large multilamillar vesicles with higher density (Figure 4.6C). These larger vesicles readily precipitate from solution, thereby lowering the PE concentration in the supernatant.

Besides the effects of ionic strength and chemical structural damage, particle charge is another key factor that can affect PE vesicle stability. PE vesicles can be considered as a particle with certain charges. The positively charged particles (blue circles: Al_2O_3 NP at pH 4 and 6, TiO_2 NP at pH4) cause the lowest PE supernatant concentration (Figure 4.7B). The moderately negatively charged particles ($\geqslant$-30 mV, green circles: Al_2O_3 NP at pH 9, TiO_2 NP at pH 6, and PE vesicle at pH 4) result in higher PE concentrations. The highly negatively charged particles (below -40 mV, red circles: TiO_2 NP at pH 9, PE vesicles at pH 6 and 9) cause most of the PE to remain in the supernatant.

4.4.6 Interaction of NPs to Bacterial Cell Membrane

LPS and PE are key constituents of bacterial cell membranes. The lipid membrane can be viewed as a liquid crystal with the molecules being mobile in the membrane. The fluidity, integrity and lateral organization of the membrane is critical to cell physiological activities. The attachment of NPs to the lipid bilayer can potentially influence membrane fluidity. Anionic NPs were reported to induce local gelation, while cationic NPs were reported to induce local fluidization (Wang, 2008). The phospholipid head group has an electric dipole moment, due to the phosphate and ammonium groups (Figure 4.1B), that lies at an angle relative to the membrane surface. Anionic NPs are attracted the ammonium group and are repelled by the phosphate group. The net effect is to increase the tilt angle of the head group, causing the lipid tails to increase in density. Conversely, cationic NP reduce the tilt angle, reducing the lipid tail density.

Based on the model studies here, interactions with NPs can potentially compromise membrane integrity in several ways. First, the phospholipid chemical structure can be damaged (Chapter 3), resulting in the loss of its amphiphilic properties and destruction of the membrane. In the case of ZnO NP exposure, we found that PE molecules can no longer form vesicles (Figure 4.6D). Second, the firm membrane attachment to NPs and the NP curvature could deform and rupture the bilayer (Morgan, 2008). The large multilamellar vesicles in Figure 4.6C are presumably formed from the rupture of the original single-lamellar vesicles and reconstruction of bilayers forced by interactions with Al_2O_3 NPs. Third, LPS polysaccharide chains could form multiple

hydrogen bonds with the oxide NPs. The firm and almost irreversible binding (Figure 4.4) might extract LPS molecules from the membrane, thereby breaking or dispersing the membrane. Indeed, LPS coatings on Al_2O_3 NPs were observed and the intact LPS vesicles disappeared (Figure 4.2).

Cell membranes are an extremely complex structure of hundreds of different lipids and proteins. The membranes are not laterally homogeneous but contain domains with distinct lipids and proteins. When NPs attach to a membrane, their surface is more attractive to some biomolecules than others, due to the difference in lipid/protein polarity, charge and hydrophobicity. Therefore, certain types of biomolecules could accumulate on certain NPs, which could disturb a cell membrane's lateral organization.

4.5 Conclusions

Oxide NPs can change the assembly of amphiphilic biomolecules in solution. Al_2O_3 and TiO_2 NPs are shown to disrupt LPS vesicles and micelles by adsorption to the polysaccharide chains. LPS molecules form a coating layer on Al_2O_3 NPs, while they form aggregates with TiO_2 NPs. The pH, ionic strength and electrolyte type all can influence LPS adsorption on these NPs. PE vesicle structure is also changed in the presence of NPs. Al_2O_3 NPs induce the formation of multilamillar vesicles, while ZnO NP completely disrupt PE vesicles, presumably by breaking the phosphodiester bond and destroying the amphiphilicity of the PE molecules. In addition, oxide NPs affect PE vesicle stability through adsorption, aggregation, flocculation and the molecular change.

The results obtained with these model systems provide a deeper understanding of the possible effects that NPs can have on cell membranes. The interactions of oxide NPs with

the cell membrane bilayers could possibly influence membrane fluidity, integrity and lateral organization, and therefore impact cell physiological activities. These potential effects could be some of the reasons for NP cytotoxicity. Knowing the potential effects of NPs on cell membranes could be helpful for designing safer nanomaterials for biological applications.

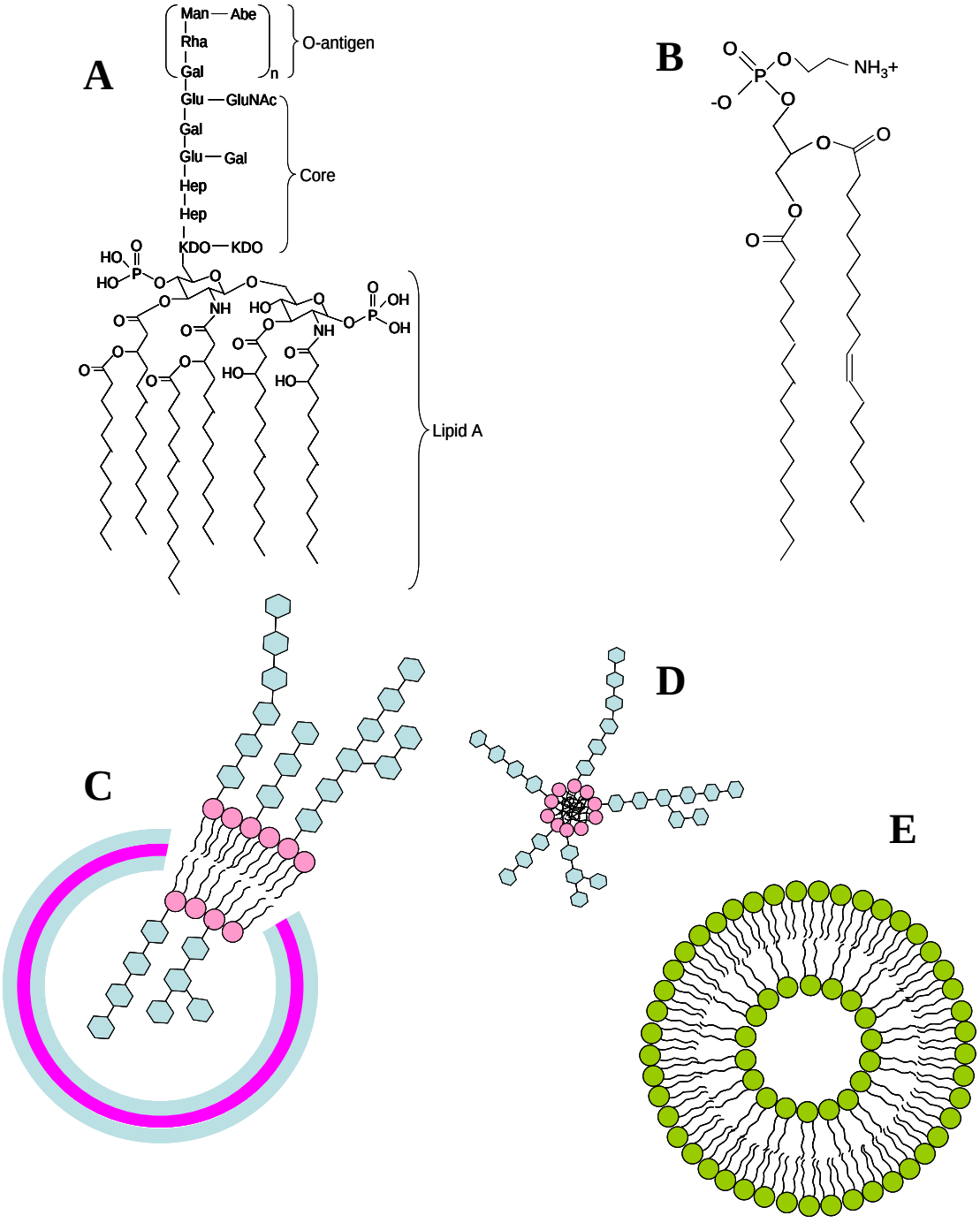

Figure 4.1. Chemical structures of (A) lipopolysaccharide (LPS), (B) L-α-phosphatidyl-ethanolamine (PE), (C) LPS vesicle, (D) LPS micelle or aggregate, (E) PE vesicle.

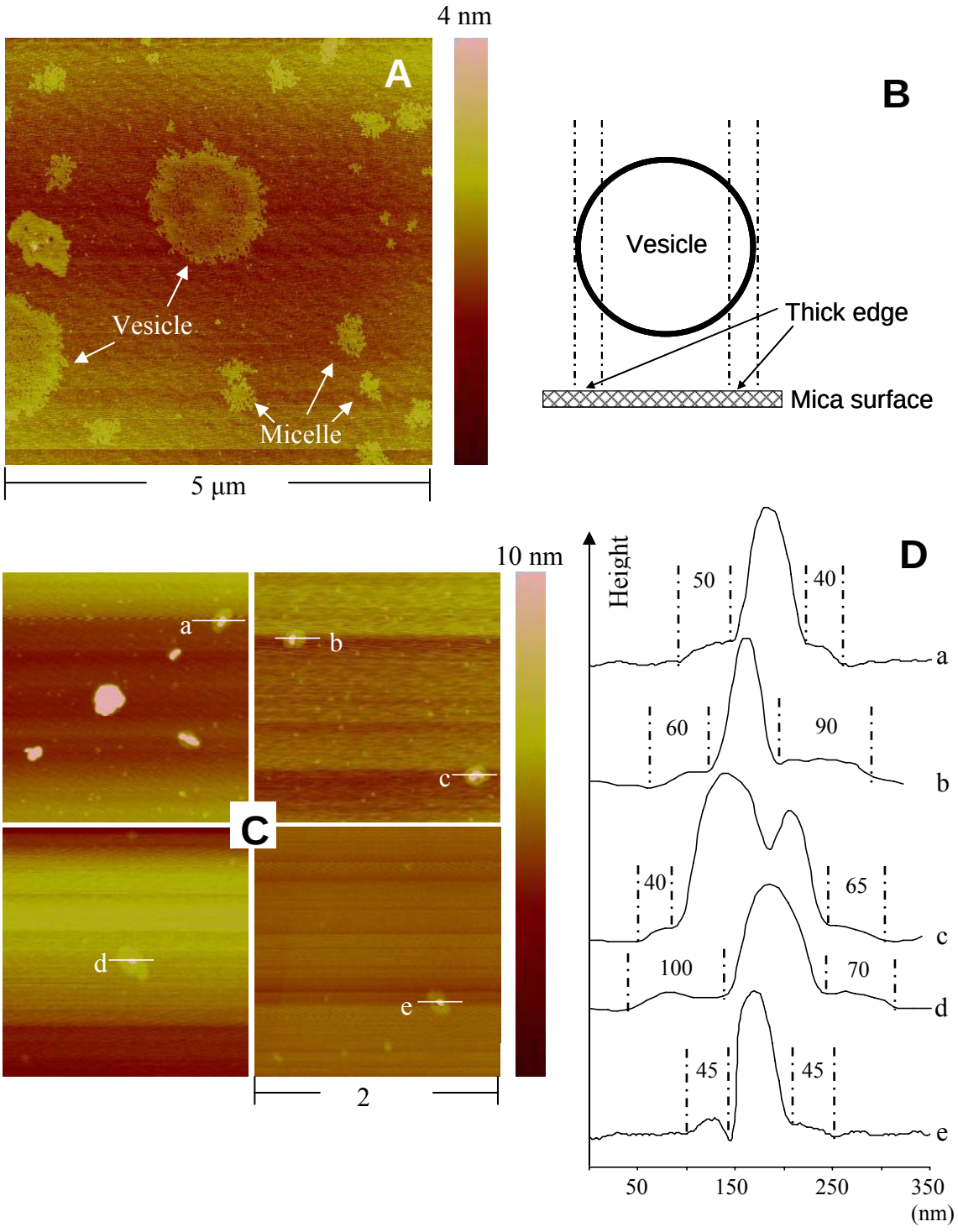

Figure 4.2. LPS solution at 10 mg/L forms micelles and vesicles (A). Vesicle structure formed a round area with thick edge when drying on the mica surface (B). LPS coated on the particle surface when mixing with 5 mg/L Al_2O_3 NPs (C). The thickness of LPS layer surrounding Al_2O_3 NPs (D). a, b, c, d, e were sections across Al_2O_3 NPs and surrounding LPS.

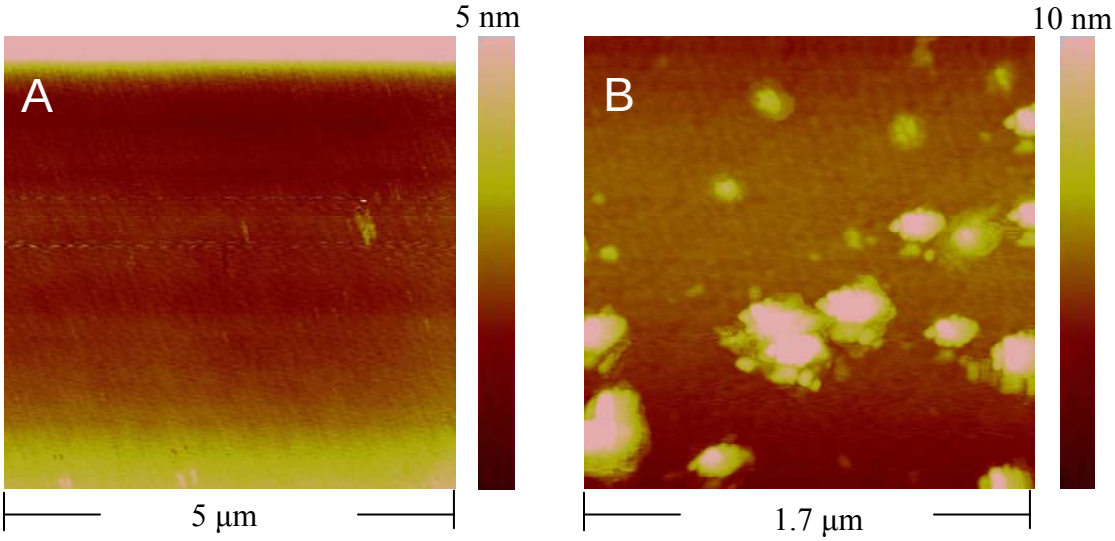

Figure 4.3. LPS 10 mg/L on sapphire Al_2O_3 surface (A). TiO_2 NPs 5 mg/L formed aggregates with LPS (B).

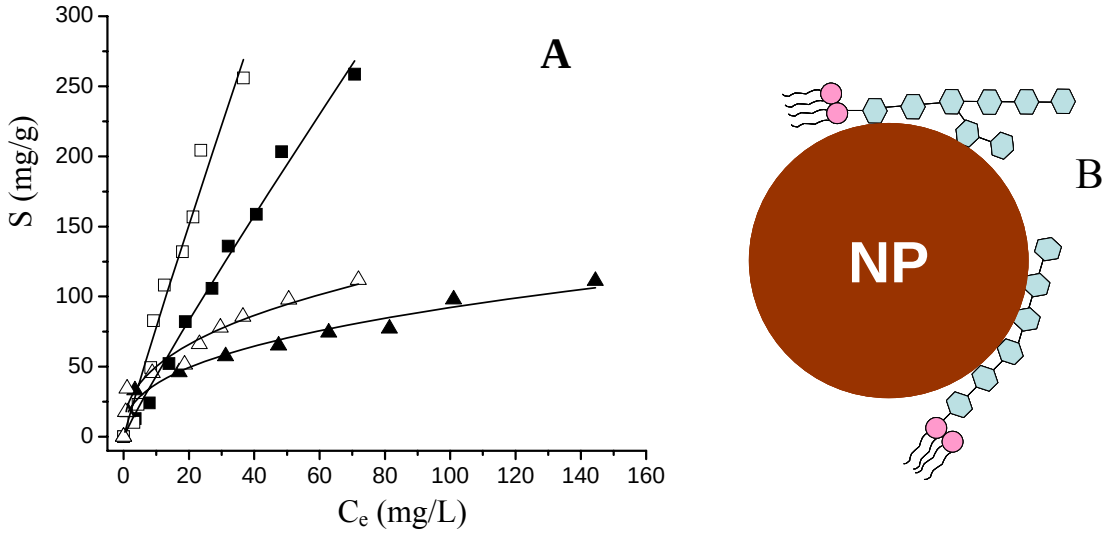

Figure 4.4. Adsorption isotherm of LPS on Al_2O_3 (■) and TiO_2 (▲) NPs.The open symbols represent the LPS desorption from Al_2O_3 (□) and TiO_2 (△) NPs (A). S: LPS concentration on solid phase. C_e: LPS concentration in liquid phase. LPS adsorbed on NPs through polysaccharide chain (B).

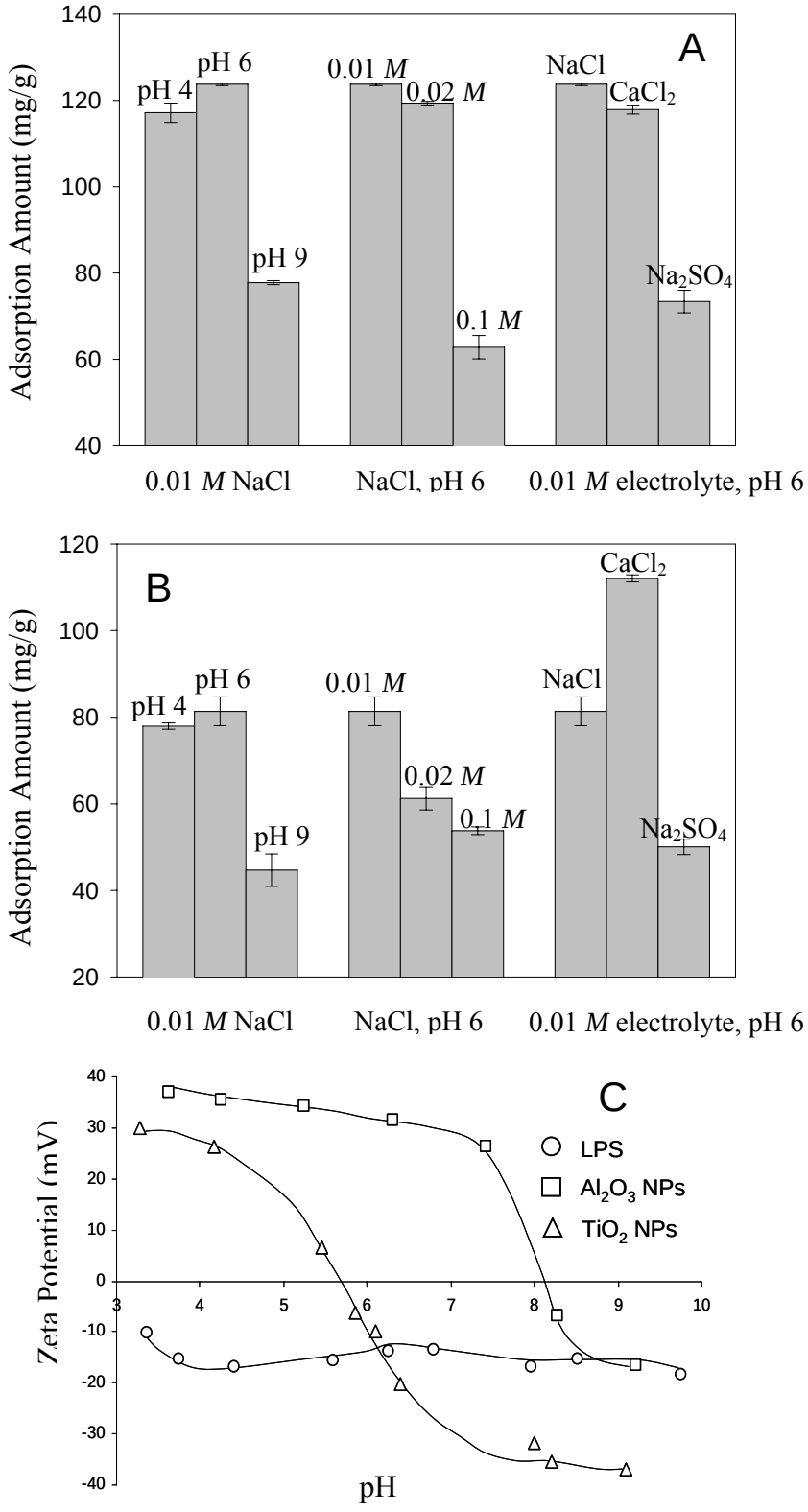

Figure 4.5. The pH, ionic strength and electrolyte type influenced LPS adsorption amount at 100 mg/L on Al_2O_3 NPs (A) and TiO_2 NPs (B). The zeta potential of LPS and the two type of NPs were measured in the pH range 3-10 in 0.01 *M* NaCl.

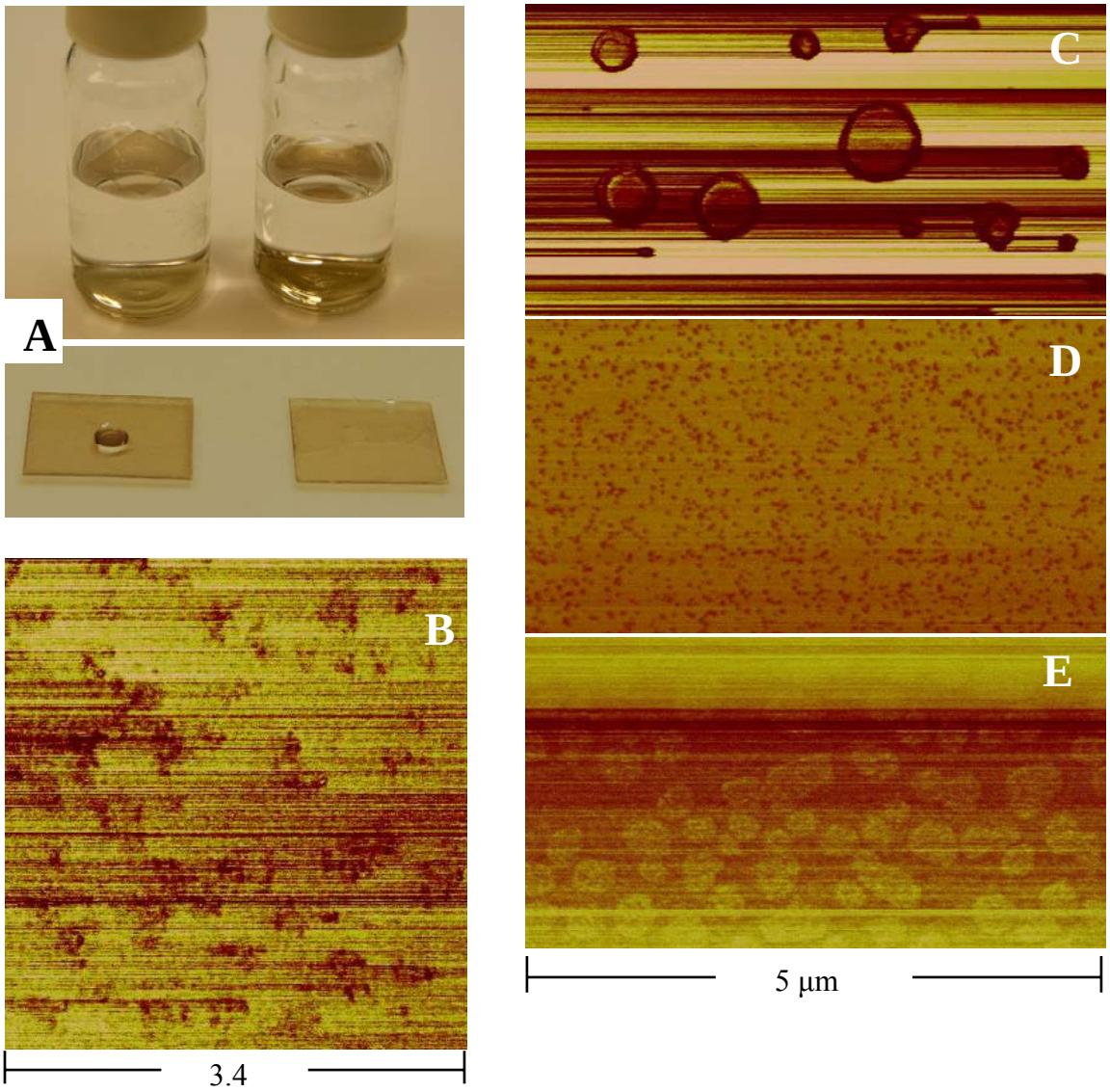

Figure 4.6. PE 20 mg/L coating on mica changed hydrophilic mica surface to hydrophobic. The PE coated mica floated on water surface, and a drop of water kept its shape on the PE coated mica (A, left). Uncoated mica sank to the bottom, and the water drop spread on it (A, right). AFM phase image showed some dark patches on coated mica (B). The morphologies of PE vesicles exposing to 10 mg/L Al_2O_3 (C), ZnO (D) and TiO_2 (E) NPs were also demonstrated by AFM phase images.

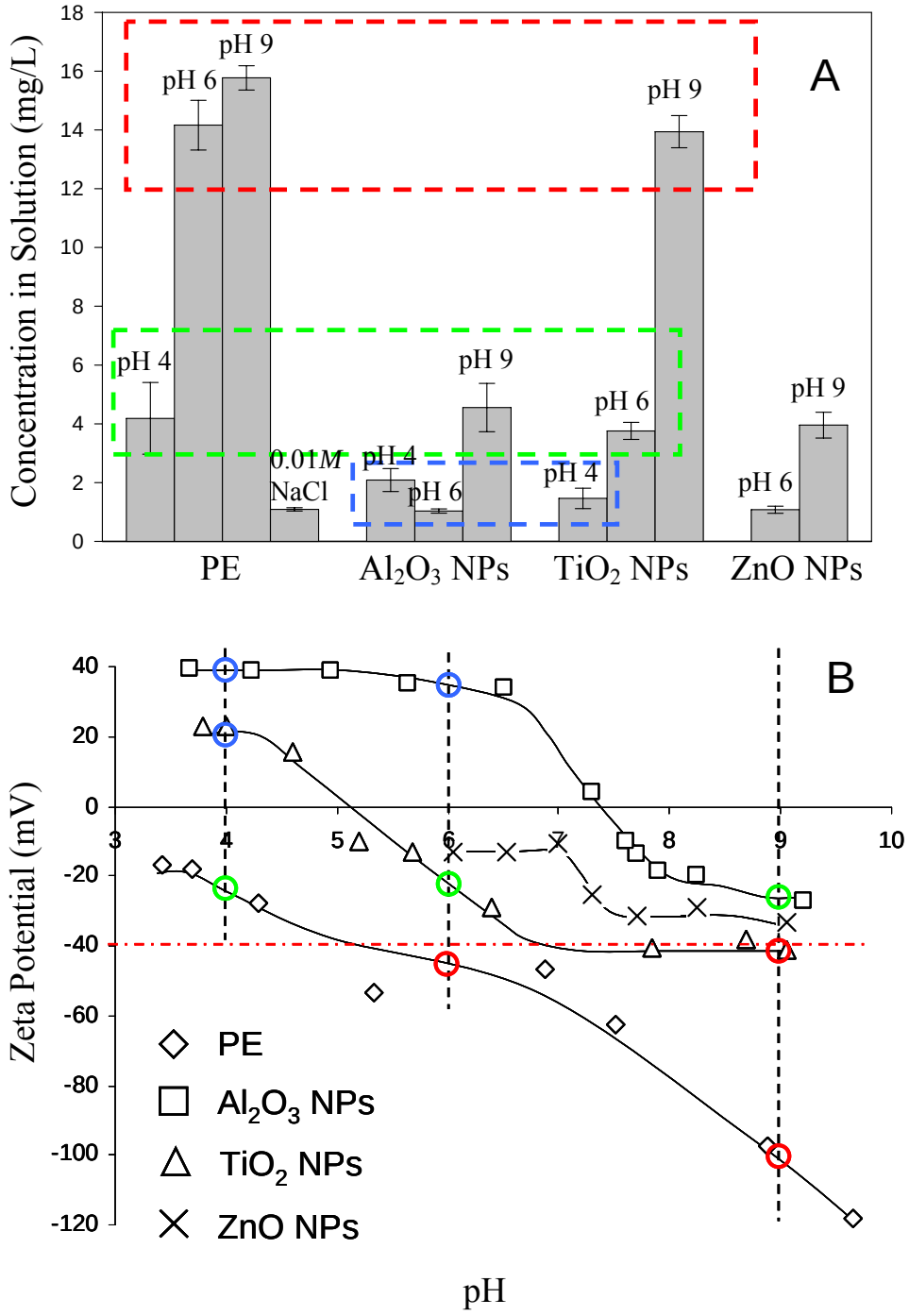

Figure 4.7. Effects of NPs on 25 mg/L PE vesicle stability at different pH (A). The zeta potential of PE vesicle and NPs in the pH range 3-10 (B).

CHAPTER 5

SYNTHESIS AND IMPLICATION

The overall goal of my doctoral research was to evaluate the safety of NPs on the nano-bio interface. Al_2O_3, SiO_2, TiO_2 and ZnO NPs were used and the bacterial cell envelope was the bio-surface studied. The main research objectives were successfully achieved in three connected steps: 1) confirmation of the NP toxicity to bacteria and relationship of toxicity to NP attachment, 2) detection of NP-induced molecular damage of bacterial cell envelope biomolecules, and 3) examination of the structural and morphological changes on lipid membrane.

The first step of research was carried out to better understand if NP toxicity to bacteria was size or composition related. It involved comparing the NPs to their bulk counterparts, and evaluating the contribution of dissolved metal ions to the overall toxicity. All NPs except TiO_2 exhibited signs of toxicity to the tested bacteria compared to the control. Although released metal cations from NPs contributed bacterial mortality, the NP toxicity to bacteria still related to its small size, resulting in higher toxicity of NPs than their bulk counterparts. TEM images confirmed the attachment of Al_2O_3, SiO_2 and ZnO NPs to the surface of bacteria, but the bacteria cells were rarely coated by TiO_2 NPs. Toxicity of NPs seemed to derive from their ability to attach onto the cell envelope. Electrostatic force contributed greatly to the adhesion of positively charged particles (Al_2O_3, SiO_2), and played an important role in repelling negatively charged TiO_2 NPs from the bacterial cell wall as shown by clean cell surface. Bacteria could attract small

aggregates and individual particles from the suspension, moving the NPs aggregation-dispersion equilibrium towards the dispersion direction (Figure 5.1).

The second research part revealed the NP-induced chemical structure changes in bacterial surface biomolecules. Since NP attachment to the cell envelope appeared necessary to their bacterial cytotoxicity, the damage to the structure and change in the physio/chemical properties of surface biomolecules may be a possible reason of NP microbial toxicity. In bacterial cells, lipopolysaccharide (LPS), lipoteichoic acid (LTA), protein and phospholipid would be the major biomolecules possibly interacting with NPs when NPs attach to cell surface. FTIR technique was used to probe the bacteria-oxide interface. All the examined biomolecules showed IR spectral changes after NP exposure. When small particles are attracted to bacteria, LTA or LPS are most likely the first contact with the particles. LTA adsorbed on the NPs by ligand exchange, and LPS adsorbed on the NPs via hydrogen bonding. Such bonding did not seem to damage the biomolecules because this is similar to the way in which bacteria adhere to surfaces through LPS or LTA polymers in the natural environment. The cytotoxicity-related molecular changes most probably depend on damage to proteins and phospholipids. The phospholipid membrane and membrane proteins are protected by cell surface biopolymers and usually do not attach to the particles or surfaces during normal bacterial adhesion processes. Their chances of exposure to NPs may be increased, however, because the small sizes of the NPs enable them to enter the gaps between the long biopolymer chains (Figure 5.2b). The three NPs decreased the intensity ratio of β-sheets/α-helices, indicating protein structure change, which may affect cell physiological activities. The phosphodiester bond of L-α-Phosphatidyl-ethanolamine (PE) was broken

by ZnO NPs (Figure 5.2c), forming phosphate monoesters and resulting in the highly disordered alkyl chain. That possibly caused the rupture of the membrane and the leakage of the periplasm. The cell surface biomolecular changes revealed by FTIR spectra provided a better understanding of the cytotoxicity of oxide NPs.

In the third step, constructional and morphological changes of LPS and PE micelles and vesicles were detected after NP exposure. Lipid vesicles could be a model for studying the cell membrane. LPS vesicles and micelles were dispersed when the sugar chain bonded to the NPs, indicating the bacterial outer membrane integrity possibly was broken through NP attachment. A LPS coating was formed on Al_2O_3 NP surface, while aggregations with TiO_2 NPs were found. Desorption from both of the NPs was hard due to the firm hydrogen bonding. The firm and irreversible bonding of LPS on NPs may pull out the LPS lipid A part from membrane, resulting membrane rupture or dispersion. For PE, Al_2O_3 NPs induced large multilamillar vesicles, while ZnO NP changed vesicles to tiny aggregates due to molecular damage. The large multilamellar vesicles were formed from the rupture of original single-lamellar vesicles and reconstruction of bilayers forced by Al_2O_3 NP attraction. Hence, it was harmful to cells when NP approach and attach on the cell membrane. PE stability in solution was disturbed by adding NPs, but stability was enhanced by increasing pH. The electrostatic interaction was the determinant factor for the vesicle stability. The interaction between NPs and membrane amphiphilic biomolecules may affect membrane fluidity, integrity and lateral organization. Therefore the NP cytotoxicity could happen through the membrane reconstruction without damaging the membrane biomolecules.

These findings have a broad significance both for both NP safety evaluation and new nanomaterial designs. Some types of NPs can release toxic cations, or can damage the biomolecule chemical structure through surface or solution reactions, resulting in high cytotoxicity. The positively charged NPs are more attractive to the cell membrane than negatively charged NPs, and easier to cause membrane to deform, damage or rupture. Engulfing of NPs into cells is not necessary for toxicity generation. Attaching of NPs on cell surface can induce function-involved or devastating changes to proteins and phospholipid. These factors should be considered when selecting/designing safe NPs for biological and biomedical applications. Moreover, the NP difference in bacterial toxicity and the mechanism explanation are important for antimicrobial implications. The interactions between NPs and amphiphilic biomolecules are useful to modify the NPs to achieve the desired properties.

Nano-bio interface interaction is a challenging and promising research area. When we learn something new or even discover some findings in this area, we always find there are more things we do not understand, but we need to know and want to know. This is the amazing part of nano-bio interface research. In this dissertation, the membrane damage was detected after NP exposure, which could explain the NP cytotoxicity. However, the chemical reactions causing molecular damage should be further studied. ZnO NPs broke the phosphodiester bond of phospholipid, but the exact surface reactions are unclear. Understanding the surface chemistry of toxic NPs is helpful to constitute policies to determine their application scope and to protect humans or organisms from the exposure. The NP-induced membrane fluidity, integrity and lateral organization changes are also worth additional study using more in-situ and even real-time methods. Fluorescence

technique is a probably ideal method to record the changes of membrane. We could add fluorescent lipid into phospholipid vesicles to make the vesicle shape change visible under fluorescence microscopy. Then the membrane deformation, rupture and reconstruction process will be detectable. We also can use special fluorescent dye to reveal membrane gelation and fluidity after NP attachment. Forster resonance energy transfer (FRET) technique may be used to show the biomolecule approaching to the NPs and the induced membrane lateral organization changes. Results of these works will help us to better understand the NP behavior on the bio-surface.

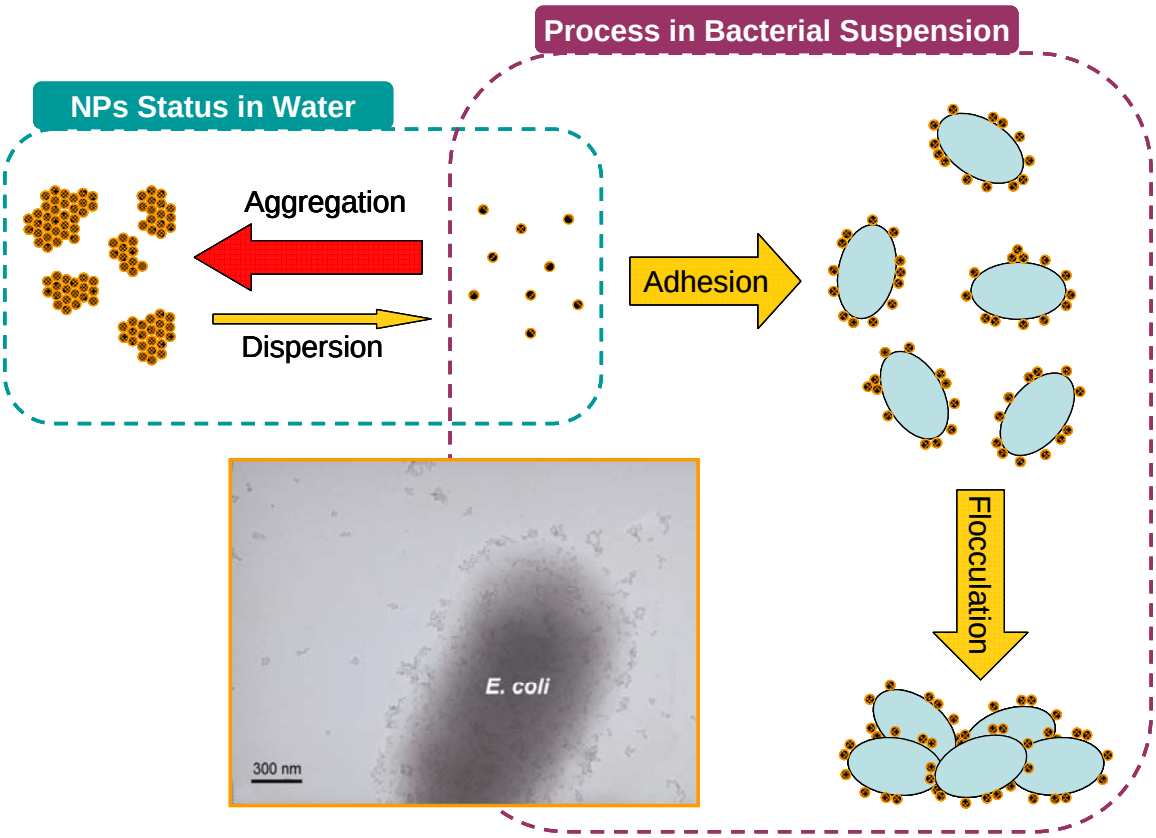

Figure 5.1 Bacteria could attract small aggregates and individual particles from the suspension, moving the NPs aggregation-dispersion equilibrium towards the dispersion direction.

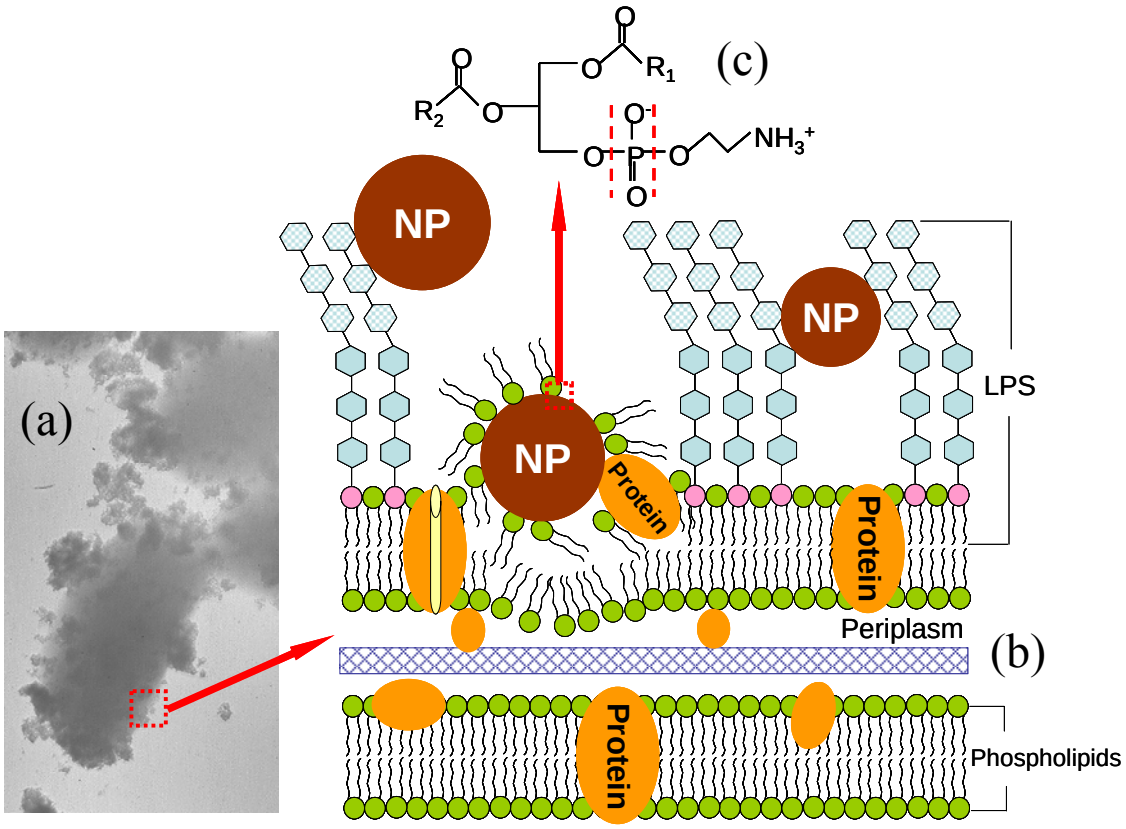

Figure 5.2. TEM image showing the attachment of NPs to bacterial surfaces (a). Schematic illustration of NPs approaching to the bacterial cell surface and causing damage to cell envelope (b). Enlarged PE chemical structure, showing the potential damage caused by the NP surface as revealed by FTIR (c).

BIBLIOGRAPHY

Abachin, E., Poyart, C., Pellegrini E., Milohanic, E., Fiedler, F., Berche. P., Trieu-Cuot, P., 2002. Formation of D-alanyl-lipoteichoic acid is required for adhesion and virulence of Listeria monocytogenes, *Molelular Microbiology* 43, 1-14.

Adams, L.K., Lyon, D.Y., Alvarez, P.J.J., 2006. Comparative eco-toxicity of nanoscale TiO_2, SiO_2, and ZnO water suspensions. *Water Research* 40, 3527-3532.

Araki Y., Ito E., 1989. Linkage units in cell walls of gram-positive bacteria. *Critical Reviews in Microbiology* 17, 121–35

Arredondo, R., Garcia, A., Jerez, C. A., 1994. Partial removal of lipopolysaccharide from *Thiobacillus ferrooxidans* affect its adhesion to solids. *Applied and Environmental Microbiology* 60 (8), 2846-2851.

Badireddy, A. R., Korpol, B. R., Chellam, S., Gassman, P. L., Engelhard M. H., Lea A. S., Rosso K. M., 2008. Spectroscopy characterization of extracellular polymeric substance from *Escherichia coli* and *Serratia marcescens*: Suppression using sub-inhibitory concentrations of bismuth thiols. *Biomacromolecules* 8, 3079-3089.

Bainbridge, W. S., Mihail, C. R., 2001. "Societal Implications of Nanoscience and Nanotechnology." NSET.

Bartl, F., Urjasz, H., Brzezinski, B., 1998. FT-IR study of pyridoxal phosphate. *Journal of Molecular Structure* 441, 77-81.

Baun, A., Hartmann, N. B., Grieger, K., Kusk K. O., 2008. Ecotoxicity of engineered nanoparticles to aquatic invertebrates: a brief review and recommendations for future toxicity testing. *Ecotoxicology*, 17, 387-395.

Bellamy, L. J., 1975. *The Infra-red Spectra of Complex Molecules.* Eds.: John Wiley and Sons: New York.

Benz, R., 1988. Structure and function of porins from Gram-negative bacteria. *Annual Reviews of Microbiology* 42, 359-393.

Berveridge, T. J., 1981. Ultrastructure, chemistry, and function of the bacterial wall. *International Review of Cytology* 72, 229-317.

Bihan, O. L., Bonnafous P., Marak L., Bickel T., Trepout S., Mornet S., Haas F. D., Talbot H., Taveau J., Lambert O., 2009. Cryo-electron tomography of nanoparticle transmigration into liposome. *Journal of Structural Biology* 168, 419-425.

Bitton, G., Marshall, K. C., 1980. *Adsorption of microorganisms to surfaces.* John Wiley & sons, Inc.

Branan, N., Wells, T. A., 2007. Microorganism characterization using ATR-FTIR on an ultrathin polystyrene layer. *Vibrational Spectroscopy* 44, 192-196.

Brandenburg, K.; Kusumoto, S.; Seydel, U., 1997. Conformational studies of synthetic lipid A analogues and partial structures by infrared spectroscopy. *Biochimica et Biophysica Acta* 1329, 183-201.

Brandenburg, K.; Seydel, U., 1996. In *Infrared Spectroscopy of Biomolecules*: Mantsch, H. H.; Chapman, D. Eds.: John Wiley and Sons: New York, pp 203-237.

Brayner, R., Ferrari-Lliou, R., Brivois, N., Djediat, S., Bebedetti, M. F., Fievet, F., 2006. Toxicology impact studies based on *Escherichia coli* bacteria in ultrafine ZnO nanoparticles colloidal medium. *Nano letters* 6, 866-870.

Brunner, T .J., Wick, P., Manser, P., Spohn, P., Grass, R. N., Limbach, L. K., Bruinink, A., Stark, W.J., 2006. In vitro cytotoxicity of oxide nanoparticles: comparison to asbestos, silica, and the effect of particle solubility. *Environmental Science and Technology* 40, 4374-4381.

Buijs J., Norde W., 1996. Changes in the second structure of adsorbed IgG and F(ab')2 studied by FTIR spectroscopy. *Langmuir* 12, 1605-1613.

Carter, D. C., Ho, J. X., 1994. Structure of serum-albumin. *Advances in Protein Chemistry* 45, 153-203.

Cascone, A., Eerola, S., Ritieni, A., Rizzo A., 2006. Development of analytical procedures to study changes in the composition of meat phospholipids caused by induced oxidation. *Journal of Chromatography A* 1120, 211-220.

Chang, J.S., Chang, K., Liang, B., Hwang, D.F. and Kong, Z.L., 2007. In vitro cytotoxicity of silica nanoparticles at high concentrations strongly depends on the metabolic activity type of the cell line. *Environmental Science and Technology* 41, 2064-2068.

Choi, O., Hu, Z., 2008. Size dependent and reactive oxygen species related nanosilver toxicity to nitrifying bacteria. *Environmental Science and Technology* 42, 4583-4588.

Cieslik-Boczula, K., Czarnik-Matusewicz, B., Perevozkina, M., Filarowski, A., Boens, N., De Borggraeve, W. M, Koll, A., 2008. ATR-IR spectroscopic study of the structural changes in the hydrophobic region of ICPAN/DPPC bilayers. *Journal of Molecular Structure* 878, 162-168.

Cravatt, E., 2005. Nuclear magnetic resonance spectroscopic studies of lipoteichoic acid adhesion on biomaterials. *Ethnicity and Disease* 15, 96-97.

Creighton, T. E., 1993. *Proteins*. W. H. Freeman and Co., New York, 2nd edn.

Daoud, W. A., Xin, J. H., Zhang, Y-H, 2005. Surface functionalization of cellulose fibers with titanium dioxide nanoparticles and their combined bactericidal activities. *Surface Science* 599, 69-75.

Derfus, A.M., Chan, W.C., Bhatia, S.N., 2004. Probing the cytotoxicity of semiconductor quantum dots. *Nano letter* 4, 11-18.

Deo, M., Natarajan, K.A., Somasundaran, P., 2001. Mechanisms of adhesion of Paenibacillus polymyxa onto hematite, corundum and quartz. *International Journal of Mineral Processing* 62, 27-39.

Dubois, M., Gilles, K. A., Hamilton, J. K., Rebers, P. A., Smith, F., 1956. Colorimetric method for determination of sugars and related substances. *Analytical Chemistry* 28, 350-356.

Fang J., Lyon D. Y., Dong J., Alvarez P. J. J., 2007. Effect of a fullerene water suspension on bacterial phospholipids and membrane phase behavior. *Environmental Science and Technology* 41, 2636–2642

Fortunelli, A.; Monti, S. Simulations of Lipid Adsorption on TiO_2 Surfaces in Solution. *Langmuir* 2008, 24, 10145-10154.

Franklin, N.M., Rogers, N.J., Apte, S.C., Batley, G.E., Gadd, G.E., Casey, P.S., 2007. Comparative toxicity of nanopartulate ZnO, bulk ZnO, and $ZnCl_2$ to a freshwater microalga (*Pseudokirchneriella subcapitata*): the importance of particle solubility. *Environmental Science and Technology* 41, 8484-8490.

Fu, G., Vary, P. S., Lin, C. T., 2005. Anatase TiO_2 nanocomposites for antimicrobial coatings. *The Journal of Physical Chemistry B* 109, 8889-8898.

Galle, T., Van Lagen, B., Kurtenbach, A., Bierl, R., 2004. An FTIR-DRIFT study on river sediment particle structure: Implications for biofilm dynamics and pollutant binding. *Environmental Science and Technology* 38, 4496-4502.

Gao, X., Metge, D. W., Ray, C., Harvey, R. W., Chorover, J., 2009. Surface complexation of carboxylate adheres cryptosporidium parvum oocysts to the hematite-water interface *Environmental Science and Technology* 43, 7423-7429.

Ghosh, S., Mashayekhi, H., Pan, B., Bhowmik, P., Xing B., 2008. Colloidal behavior of aluminum oxide nanoparticles as affected by pH and natural organic matter. *Langmuir* 24, 12385-12391.

Ghuysen, J. M., Hakenbeck, R., 1994. *Bacterial Cell Wall.* Elsevier Science B. V., Amsterdam, The Netherland.

Giacomelli, C. E.; Bremer, M. G. E. G.; Norde, W., 1999. ATR-FTIR study of IgG adsorbed on different silica surfaces. *Journal of Colloid and Interface Scence* 220, 13-23.

Glenn, A. R., 1976. Production of extracellular proteins by bacteria. *Annual Review of Microbiology* 30, 41-62

Gomez-Suarez, C., Pasma, J., Van Der Borden, A. J., Wingender, J., Flemming, H. C., Busscher, H. J., Van Der Mei, H. C., 2002. Influence of extracellular polymeric substances on deposition and redeposition of *Pseudomonas aeruginosa* to surfaces. *Microbiology* 148, 1161.

Goward, C. R., Irons, L. I., Murphy, J. P., Atkinson, T. 1991. The secondary structure of protein-G *Biochemistry Journal* 274, 503-507.

Green, M., Howman, E., 2005. Semiconductor quantum dots and free radical induced DNA nicking. *Chemical Communications*, 121-123.

Greenhall, M. H., Yarwood, J., Brown, R., Swart, R. M., 1998. Spectroscopic studies of model biological membranes in vesicles and Langmuir-Blodgett films *Langmuir* 14, 2619-2626.

Griffitt, R. J., Weil, R., Hyndman, K. A., Denslow, N. D., Powers, K., Taylor, D., Barber, D. S., 2007. Exposure to copper nanoparticles causes gill injury and acute lethality in Zebrafish (Danio rerio). *Environmental Science and Technology* 41, 8178-8186.

Grit, M., Crommelin, D., Liang, J., 1991. Determination of phosphatidylcholine, phosphatidylglycerol and their lyso forms from liposome dispersions by high-

performance liquid chromatography using high-sensitivity refractive index detection. *Journal of Chromatography A* 585, 239-246.

Gue, M., Dupont, V., Dufour, A., Sire, O., 2001. Bacterial swarming: A biochemical time-resolved FTIR study of *Proteus mirabilis* swarm-cell differentiation. *Biochemistry* 40, 11938-11945.

Han, Z.T., Zhang, F., Lin, D.H., Xing, B., 2008. Clay minerals affect the stability of surfactant-facilitated carbon nanotube suspensions. *Environmental Science and Technology* 42, 6869-6875.

Harrick, N. J., 1967. *Internal reflection spectroscopy*. New York: John Wiley.

Hayes, K. F., Papelis, C., Leckie, J. O., 1988. Modeling ionic-strength effects on anion adsorption at hydrous oxide solution interfaces. *Journal of Colloid and Interface Science* 125, 717-726.

Heinlaan, M., Ivask, A., Blinova, I., Bubourguier, H., Kahru, A., 2008. Toxicity of nanosized and bulk ZnO, CuO and TiO2 to bacteria *Vibrio fischeri* and crustacean *Daphnia magna* and *Thamnocephalus platyurus*. Chemosphere 71, 1308-1316.

Huang, Z., Zheng, X., Yan, D., Yin, G., Liao, X., Kang, Y., Yao, Y., Huang, D., Hao, B., 2008. Toxicological effect of ZnO nanoparticles based on bacteria. *Langmuir* 24, 4140-4144.

Hussain, S.M., Hess, K. L., Gearhart, J.M., Geiss, K. T., Schlager, J. J, 2005. In vitro toxicity of nanoparticles in BRL 3A rat liver cells. *Toxcology in Vitro* 19, 975-983.

Hyung, H.; Kim, J., 2008. Natural organic matter (NOM) adsorption to multi-walled carbon nanotubes: Effect of NOM characteristics and water quality parameters. *Environmantal Science and Technology* 42, 4416-4421.

Iorio, M., Pan, B., Capasso, R., Xing, B., 2008. Sorption of phenanthrene by dissolved organic matter and its complex with aluminum oxide nanoparticles. *Environmental Pollution* 156, 1021-1029.

Israelachvili, J., 1992. "Intermolecular and Surface Forces," 2nd ed., Academic Press, London.

Jackson, M.; Mantsch, H. H., 1991. Protein secondary structure from FT-IR spectroscopy – Correlation with dihedral angles from 3-dimensional ramachandran plots. *Canadian Journal of Chemistry* 69, 1639-1642.

Jaiswal, J.K.; Simon, S.M., 2004. Potentials and pitfalls of fluorescent quantum dots for biological imaging. *Trends in Cell Biology* 14 (9), 497-504.

Jiang, W., Saxena, A., Song, B., Ward, B. B., Beveridge, T. J., Myneni, S. C. B., 2004. Elucidation of functional groups on Gram-positive and Gram-negative bacterial surfaces using infrared spectroscopy. *Langmuir* 20, 11433-11442.

Jucker, B., Harms, H., Hug, S. J., Zehnder, A. J. B., 1997. Adsorption of bacteria surface polysaccharides on mineral oxides is mediated by hydrogen bonds. *Colloids and Surfaces B: Biointerfaces* 9, 331-343.

Jucker, B., Zehnder, A. J. B., Harms, H., 1998. Quantification of polymer interactions in bacterial adhesion. *Environmental Science and Technology* 32, 2909-2915.

Kang, S., Mauter, M. S., Elimelech, M, 2009. Microbial cytotoxicity of carbon-based nanomaterials: Implications for river water and wastewater effluent. *Environmental Science and Technology* 43, 2648-2653.

Kang, S., Xing, B., 2007. Adsorption of dicarboxylic acids by clay minerals as examined by in situ ATR-FTIR and ex situ DRIFT. *Langmuir* 23, 7024-7031.

Kang, S., Xing, B., 2008. Humic acid fractionation upon sequential adsorption onto goethite. *Langmuir* 24, 2525-2531.

Kaufmann, S., Tanaka, M., 2003. Cell adhesion onto highly curved surfaces: One-step immobilization of human erythrocyte membranes on silica beads. *Chemphyschem* 4, 699-704.

Keren, S., Zavaleta, C., Cheng, Z., de la Zerda, A., Gheysens, O., Gambhir, S. S., 2008. Noninvasive molecular imaging of small living subjects using Raman spectroscopy. *Proceedings of the National Academy of Sciences of the United States of America* 105, 5844-5849.

Kim, J., Kim, G., Cremer, P. S., 2001. Investigations of water structure at the solid/liquid interface in the presence of supported lipid bilayers by vibrational sum frequency spectroscopy. *Langmuir* 17, 7255-7260.

Kinder, R., Ziegler, C., Wessels, J. M., 1997. Gamma-Irradiation and UV-C light-induced lipid peroxidation: A Fourier transform-infrared absorption spectroscopic study *International Journal of Radiation. Biology* 71, 561-571.

Kiwi, J., Nadtochenko, V., 2005. Evidence for the mechanism of photocatalytic degradation of the bacterial wall membrane at the TiO_2 interface by ATR-FTIR and laser kinetic spectroscopy. *Langmuir* 21, 4631-4641.

Laurencin, M.; Georgelin, T.; Malezieux, B.; Siaugue, J.; Menager, C., 2010. Interactions between giant unilamellar vesicles and charged core-shell magnetic nanoparticles. *Langmuir* 26, 16025-16030.

Lewis, R. N. A. H.; McElhaney, R. N.; Monck, M. A.; Cullis, P. R., 1994. Studies of highly asymmetric mixed-chain diacyl phosphatidylcholines that form mixed-interdigitated gel phases – Fourier transformed infrared and H-2 NMR spectroscopic studies of hydrocarbon chain conformation and orientational order in the liquid-crystalline state. *Biophysical Journal* 67, 197-207.

Lewis, R. N. A. H.; McElhaney, R. N., 1996. In *Infrared Spectroscopy of Biomolecules:* Mantsch, H. H., Chapman, D., Eds.: John Wiley and Sons: New York, pp 159-202.

Lewis, R. N. A. H.; McElhaney, R. N., 1998. The structure and organization of phospholipid bilayers as revealed by infrared spectroscopy *Chemistry and Physics of Lipids* 96, 9-21.

Liang, J. K., 1991. Quantitative determination of cholesterol in liposome drug products and raw materials by high-performance liquid chromatography. *Journal of Chromatography A* 507, 157-163.

Leone, L., Ferri, D., Manfredi, C., Persson, P., Shchukarev, A., Sjoberg, S., Loring, J., 2007. Modeling the acid-base properties of bacterial surfaces: A combined spectroscopic and potentiometric study of the Gram-positive bacterium *Bacillus subtilis*. *Environmental Science and Technology* 41, 6465-6471.

Lin, D., Xing, B., 2007. Phytotoxicity of nanoparticles: Inhibition of seed germination and root growth. *Environmental Pollution* 150, 243-250.

Lin, D., Xing, B., 2008. Root uptake and phytotoxicity of ZnO nanoparticles. *Environmental Science and Technology* 42, 5580-5585.

Lok, C.N., Ho, C.M., Chen, R., He, Q.Y., Yu, W.Y., Sun, H., Tam, P.K.H., Chiu, J.F., Che, C.M., 2007. Silver nanoparticles: partial oxidation and antibacterial activities. *Journal of Biological Inorganic Chemistry* 12, 527-534.

Long, T.C., Saleh, N., Tilton, R.D., Lower, G.V., Veronesi, B., 2006. Titanium Dioxide (P25) produces reaction oxygen species in immortalized brain microglia (BV2):

implications for nanoparticle neurotoxicity. *Environmental Science and Technology* 40, 4346-4352.

Lovern, S.B., Strickler, J. R., Klaper, R., 2007. Behavioral and physiological changes in Daphnia magna when exposed to nanoparticle suspensions (titanium dioxide, nano-C_{60}, and $C_{60}HxC_{70}Hx$). *Environmental Science and Technology* 4, 4465-4470.

Lyon, D. Y., Adams, L. K., Falkner, J. C., Alvarez, P. J. J, 2006. Antibacterial activity of fullerene water suspensions: effects of preparation method and particle size. *Environmental Science and Technology* 40, 4360-4366.

Makin, S. A., Beveridge, T. J., 1996. *Microbiology* –UK 142, 299.

Maroncelli, M., Qi, S. P., Straus, H. L, Snyder, R. G., 1982. Nonplanar conformers and the phase-behavior of solid normal-alkanes. *Journal of the American Chemical Society* 104, 6237-6247.

McWhirter, M.J., McQuillan, A.J., Bremer, P.J., 2002. Influence of ionic strength and pH on the first 60 min of *Pseudomonas aeruginosa* attachment to ZnSe and to TiO_2 monitored by ATR-IR spectroscopy. *Colloid and surfaces B: Biointerfaces* 26, 365-372.

Mitchell, M. B., 1993. Fundamentals and applications of diffuse-reflectance infrared fourier-transform (DRIFT) spectroscopy. *Advances in Chemistry Series* 236, 351-375.

Mager, M. D.; Almquist, B.; Melosh, N. A. Formation and characterization of fluid lipid bilayers on alumina. *Langmuir* 2008, 24, 12734-12737.

Mornet, S., Lambert, O., Duguet, E., Brission, A., 2005. The formation of supported ;ipid bilayers on silica nanoparticles revealed by cryoelectron microscopy. *Nano Letters* 5, 281-285.

Nadtochenko, V. A., Rincon, A. G., Stanca, S. E., Kiwi, J., 2005. Dynamics of *E. coli* membrane cell peroxidation during TiO_2 photocatalysis studies by ATR-FTIR spectroscopy and AFM microscopy. *Journal of photochemistry and photobiology A: Chemistry* 169, 131-137.

Naumann, D., Schultz, C. P., Helm, D., 1996. In *Infrared Spectroscopy of Biomolecules:* Mantsch, H. H.; Chapman, D. Eds.: John Wiley and Sons: New York, pp 279-310.

Neal, A.L., 2008. What can be inferred from bacteria-nanoparticle interactions about the potential consequences of environmental exposure to nanoparticles? *Ecotoxicology* 17, 362-371.

Nel, A., Xia, T., Madler, L., Li, N., 2006. Toxic potential of materials at nanolevel. *Science* 311, 622-627.

Nel, A. E., Madler, L., Velegol, D., Xia, T., Hoek, E. M. V., Somasundaran, P., Klaessig, F., Castranova, V., Thompson, M., 2009. Understanding biophysicochemical interactions at the nano-bio interface. *Nature Materials* 8, 543-557.

Neu, T., Marshall, K., 1990. Bacterial Polymers: Physicochemical Aspects of Their Interactions at Interfaces. *Journal of Biomaterials Applications* 5, 107-133.

Neuhaus, F. C., Baddiley, J., 2003. A continuum of anionic charge: structures and functions of D-alanyl-teichoic acid in Gram-positive bacteria, *Microbiology and Molecular Biology Reviews* 67, 686-723.

Nowack, B., Bucheli, T.D., 2007. Occurrence, behavior and effects of nanoparticles in the environment. *Environmental Pollution* 150, 5-22.

Oberdorster, E., 2004. Manufactured nanomaterials (fullerenes, C_{60}) induce oxidative stress in the brain of juvenile Largemouth Bass. *Environmental Health Perspectives* 112, 1058-1062.

Ojeda, J. J., Romero-Gonzalez, M. E., Bachmann, R. T., Edyvean, R. G. J., Banwart, S. A., 2008. Characterization of cell surface and cell wall chemistry of drinking water bacteria by combining XPS, FTIR spectroscopy, modeling, and potentiometric titrations. *Langmuir* 24, 4032-4040.

Oleson, T., Sahai, N., 2008. Oxide-dependent adsorption of a model membrane phospholipid, dipalmitoylphosphatidylcholine: Bulk adsorption isotherms. *Langmuir* 24, 4865-4873.

Omoike, A., Chorover, J., 2004. Spectroscopic study of extracellular polymeric substances from Bacillus subtilis: Aqueous chemistry and adsorption effects. *Biomacromolecules* 5, 1219-1230.

Omoike, A., Chorover, J., Kwon, K. D., Kubicki, J. D., 2004. Adhension of bacterial exopolymers to α-FeOOH: Inner-sphere complexation of phosphodiester groups. *Langmuir* 20, 11108-11114.

Ooi, C. E., Weiss, J., Deorfler, M. E., Elsbach, P., 1991. Endotoxin-neutralizing properties of the 25-KD N-terminal fragment and a newly isolated 30-KD C-terminal fragment of the 55-60-KD bactericidal permeability-increasing protein of human neutrophils. *Journal of Exeperimental Medicine* 1991, 174, 3, 649-655.

Pal, S., Tak, Y. K., Song, J. M., 2007. Does the antibacterial activity of silver nanoparticles depend upon the shape of the nanoparticle? A study of the Gram-negative bacterium *Escherichia coli*. *Applied and Environmental Microbiology* 73, 1712–1720.

Parikh, S.J., Chorover, J., 2005. FTIR spectroscopic study of biogenic Mn-Oxide formation by *Pseudomonas putida* GB-1. *Geomicrobiology Journal* 22, 207-218.

Parikh, S.J., Chorover, J., 2006. ATR-FTIR spectroscopy reveal bond formation during bacteria adhesion to iron oxide. *Langmuir* 22, 8492-8500.

Parikh, S.J., Chorover, J., 2007. Infrared spectroscopy studies of cation effects on lipopolysaccharides in aqueous solution. *Colloids and Surfurface B* 55, 241.

Parikh, S.J., Chorover, J., 2008. ATR-FTIR study of lipopolysaccharide at mineral surfaces. *Colloids and Surfaces B: Biointerfaces* 62 188-198.

Peters, T., 1996. *All About Albumin: Biochemistry, Genetics, and Medical Applications*. Academic Press.

Persson, P., Nilsson, N., Sjoberg, S., 1996. Structure and bonding of orthophosphate ions at the iron oxide aqueous interface. *Journal of Colloid and Interface Science* 177, 263-275.

Pollard, T. D., Earnshaw, W. C., 2004. *Cell Biology*. Saunders, Philadelphia, Pennsylvania.

Qian, X., Peng, X., Ansari, D. O., Yin-Goen, Q., Chen, G. Z., Shin, D. M., Yang, L., Young, A. N., Wang, M. D., Nie, S., 2008. In vivo tumor targeting and spectroscopy detection with surface-enhanced Raman nanoprticle tags. *Nature Biotechnology* 26, 83-90.

Raeze, C. R. H., Dowhan, W., 1990. Biosynthesis and function of phospholipids in *Escherichia coli*. *The Journal of Biological Chemistry* 265, 1235-1238.

Radler, J., Strey, H., Sackmann, E., 1995. Phenomenology and kinetics of lipid bilayer spreading on hydrophilic surfaces. *Langmuir* 11, 4539-4548.

Rapuano, R., Carmona-Ribeiro, A. M., 1997. Physical adsorption of bilayer membranes on silica. *Journal of Colloid and Interface Science* 193, 104-111.

Reimhult, E., Hook, F., Kasemo, B., 2002. Vesicle adsorption on SiO_2 and TiO_2: Dependence on vesicle size. *Journal of Chemical Physics* 117, 7401-7404.

Reimhult, E., Hook, F., Kasemo, B., 2003. Intact Vesicle Adsorption and Supported Biomembrane Formation from Vesicles in Solution: Influence of Surface Chemistry, Vesicle Size, Temperature, and Osmotic Pressure. *Langmuir* 19, 1681-1691.

Rice, C. V., Wickham, J. R., 2004. Heterogeneous binding of lipoteichoic acid to the surface of titanium dioxide as determined with ^{31}P solid-state NMR spectroscopy. *Journal of American Chemical Society* 127, 856-857.

Richer, R. P., Berat, R., Brission, A. R. Formation of solid-supported lipid bilayers: An integrated view. *Langmuir* 2006, 22, 3497-3505.

Rietschel, E.T., 1982. Bacterial endotoxins: chemical structure, biological activity and role in septicaemia. *Scandinavian Journal of Infectious Disease* 31, 8-21.

Roberts, I. S., 1996. The biochemistry and genetics of capsular polysaccharide production in bacteria. *Annual Review of Microbiology* 50, 285–315.

Roberts, A. P., Mount, A. S., Seda, B., Souther, J., Qiao, R., Lin, S., Ke, P.H., Rao, A.M., Klaine, S. J., 2007. In vivo biomodification of lipid-coated carbon nanotubes by Daphnia Magna. *Environmental Science and Technology* 41, 3025-3029.

Rothen-Rutishauser, B. M., Schurch, S., Haenni, B., Kapp, N., Gehr, P., 2006. Interaction of fine particles and nanoparticles with red blood cells with advanced microscopic techniques. *Environmental Science and Technology* 40, 4353-4359.

Sahai, N., 2002. Biomembrane Phospholipid–Oxide Surface Interactions: Crystal chemical and thermodynamic basis. *Journal of Colloid and Interface Science* 252, 309–319.

Salata, OV., 2004. Applications of nanoparticles in biology and medicine. *Journal of Nanobiotechnology* 2.

Santos, N. C., Silva, A. C., Castanho, M. A. R. B., Matins-Silva, J., Saldanha, C., 2003. Evaluation of lipopolysaccharide aggregation by light scattering spectroscopy *Chembiochem* 4, 96-100.

Scheuring, S., Levy, D., Rigaud, J., 2005. Watching the components of photosynthetic bacterial membranes and their in situ organization by atomic force microscopy. *Biochimica et Biophysica Acta* 1712, 109-127.

Schmitt, J., Flemming, H. C., 1998. FTIR-spectroscopy in microbial and material analysis. *International Biodeterioration and Biodegradation* 41, 1-11.

Scott J. R., Barnett, T. C., 2006. Surface proteins of Gram-positive bacteria and how they get there. *Annual Review Microbiology* 60, 397-423.

Seifert, U., 1997. Configuration of fruit membranes and vesicles. *Advances in Physics* 46, 13-137.

Seifert, U., Lipowsky, R., 1990. Adhesion of vesicles. *Physical Review A* 42, 4768–4771.

Singleton, P., 1997. *Bacteria: In biology, biotechnology and medicine.* John Wiley & Sons Ltd, West Sussex, England.

Smith, C. J., Shaw, B.J., Handy, R.D., 2007. Toxicity of single walled carbon nanotubes on rainbow trout, (Oncorhynchus mykiss): respiratory toxicity, organ pathologies, and other physiological effects. *Aquatic Toxicology* 82, 94-109.

Socrates, G., 2001. *Infrared and Raman Characteristic Group Frequencies: Table and Chart.* Eds.: John Wiley and Sons.

Stephen, D. J., Allen, V. J., 2003. Light microscopy techniques for live cell imaging. *Science* 300, 82-86.

Stoimenov, P. K, Klinger, R. L., Marchin, G. L., Klabunde, K. J., 2002. Metal oxide nanoparticles as bactericidal agents. *Langmuir* 18, 6679–6686.

Strehle, M. A., Rosch, P., Petry, R., Hauck, A., Thull, R., Kieferc, W., Popp, J., 2004. A Raman spectroscopic study of the adsorption of fibronectin and fibrinogen on titanium dioxide nanoparticles . *Physical Chemistry Chemical Physics* 6, 5232-5236,

Surewicz, W. K., Mantsch, H. H., Chapman, D., 1993. Determination of protein secondary structure by Fourier transform infrared spectroscopy: a critical assessment. *Biochemistry* 32, 389-394.

Thill, A., Zeyons, O., Spalla, O., Chauvat, F., Rose, J., Auffan, M., Flank, A. M., 2006. Cytotoxicity of CeO_2 nanoparticles for *Escherichia coli*. Physico-chemical insight of the cytotoxicity mechanism. *Environmental Science and Technology* 40, 6151-6156.

Torii, H., Tasumi, M., 1996. In *Infrared Spectroscopy of Biomolecules:* Mantsch, H. H.; Chapman, D. Eds.: John Wiley and Sons: New York, pp 1-18.

Vance, D. E., Vance, J. E., 1991. *Biochemistry of Lipids, Lipoproteins and Membranes*. Elsevier Science Publishers B. V., Amsterdam, The Netherland.

Vedantham, G., Sparks, H. G., Sane, S. U., Tzannis, S., Przybycien, T. M., 2000. A holistic approach for protein secondary structure estimation from infrared spectra in H_2O solutions. *Analytical Biochemistry* 285, 33-49.

Verma, A., Stellacci, F., 2010. Effect of surface properties on nanoparticle-cell interactions. *Small* 6, 12-21.

Vertegel, A. A., Siegel, R. W., Dordick, J. S., 2004. Silica nanoparticle size influences the structure and enzymatic activity of adsorbed lysozyme. *Langmuir* 20, 6800-6807.

Wang, B., Zhang, L., Bae, S. C., Granick, S., 2008. Nanoparticle-induced surface reconstruction of phospholipid membranes. *Proceedings of the National Academy of Sciences of the United States of America* 105, 18171-18175.

Wang, H.H., Wick, R.L., Xing, B.S., 2009. Toxicity of nanoparticulate and bulk ZnO, Al_2O_3 and TiO_2 to the nematode *Caenorhabditis elegans*. *Environmental Pollution* 157, 1171-1177.

Wang, X.L., Lu, J.L., Xu, M., Xing, B., 2008. Sorption of pyrene by regular and nanoscaled metal oxide particles: Influence of adsorbed organic matter. *Environmental Science and Technology* 42, 7267-7272.

Wang, J.X., Zhou, G.Q., Chen, C.Y., Yu, H.W., Wang, T.C., Ma, Y.M., Jia, G., Gao, Y.X., Li, B., Sun, J., Li, Y. F., Jiao, F., Zhao, Y.L., Chai, Z.F., 2007. Acute toxicity and biodistribution of different sized titanium dioxide particles in mice after oral administration. *Toxicology Letters* 168,176-185.

Wickham, J. R., Rice C. V., 2008. Solid-state NMR studies of bacterial lipoteichoic acid adsorption on different surfaces. *Solid State Nuclear Magnetic Resonance* 34, 154-161

Wong, P. T. T., Papavassiliou, E. D., Rigas, B., 1991. Phosphodiester stretching bands in the infrared-spectra of human tissues and cultured-cells. *Applied Spectroscopy* 45, 1563-1567.

Worle-Knirsch, J. M., Kern, K., Schleh, C., Adelhelm, C., Feldmann, C., Krug, H.F., 2007. Nanoparticulate vanadium oxide potentiated vanadium toxicity in human lung cells. *Environmental Science and Technology* 41, 331-336.

Wu, X., Narsimhan, G., 2008. Characterization of secondary and tertiary conformational changes of beta-lactoglobulin adsorbed on silica nanoparticle surfaces. *Langmuir* 24, 4989-4998.

Xu, J., Stevens, M. J., Oleson, T. A., Last, J. A., Sahai, N., 2009. Role of oxide surface chemistry and phospholipid phase on adsorption and self-assembly: Isotherms and atomic force microscopy. The Journal of Physical Chemistry C 113, 2187-2196.

Yang, K., Lin, D., Xing, B., 2009. Interactions of humic acid with nanosized inorganic oxides. *Langmuir* 25, 3571-3576.

Yuan, C., Zhao, D., Liu, A., Ni, J., 1995. A NMR study of the interaction of silica with dipalmitoylphosphatidylcholine liposome. *Journal of Colloid and Interface Science* 172, 536-538.

Zhdanov, V., Kasemo, B., 2001. Comments on rupture of adsorbed vesicles. *Langmuir* 17, 3518-3521.

Zhu, M., Feng, W., Wang, Y., Wang, B., Wang, M., Ouyang, H., Zhao, Y., Chai, Z., 2009a. Particokinetics and extrapulmonary translocation of intratracheally instilled ferric oxide nanoparticles in rats and the potential health risk assessment. *Toxicological Sciences* 107, 342–351.

Zhu, X., Zhu, L., Chen, Y., Tian, S., 2009b. Acute toxicities of six manufactured nanomaterial Suspensions to *Daphnia magna*. J*ournal of nanoparticle research* 11, 67-75.